This is to certify that the

dissertation entitled

FRICTION-INDUCED VIBRATION IN LINEAR ELASTIC MEDIA
WITH DISTRIBUTED CONTACTS

presented by

Choong-Min Jung

has been accepted towards fulfillment
of the requirements for

Ph.D. degree in Mechanical Engineering

Major professor

Date 12/2/99

FRICTION-INDUCED VIBRATION IN LINEAR ELASTIC MEDIA WITH DISTRIBUTED CONTACTS

By

Choong-Min Jung

A DISSERTATION

Submitted to
Michigan State University
in partial fulfillment of the requirements
for the degree of

DOCTOR OF PHILOSOPHY

Department of Mechanical Engineering

1999

ABSTRACT

FRICTION-INDUCED VIBRATION IN LINEAR ELASTIC MEDIA WITH DISTRIBUTED CONTACTS

By

Choong-Min Jung

When there is friction between two parts in contact relative motions may generate vibrations and noise which can cause serious problems in applications. In this study friction-induced vibrations in elastic media subjected to distributed contacts are investigated in order to understand mechanisms responsible for generations of noise and vibrations. We investigated system stability and stick-slip oscillations to explain friction-induced vibration in linear elastic media with distributed contacts.

A one-dimensional elastic media with fixed-end boundary conditions are investigated. The system is marginally stable when the coefficient of friction is a constant. Under fixed-end boundary conditions distributed friction leads to a non-self-adjoint system. A non-self-adjoint eigenvalue problem and an eigenvalue problem based on a proper inner product are reviewed as alternative methods in handling non-self-adjoint systems. A contradictory result between the exact and an assumed mode projection based on the non-self-adjoint formulation is presented as a cautionary example.

Under periodic boundary conditions the one-dimensional system is destabilized with a constant coefficient of friction. The destabilizing phenomena occur in the form of unstable traveling waves propagating in the direction of the slider velocity. External and internal damping play stabilizing roles in system stability. By constructing a discretized lumped-parameter model, the non-symmetric eigenvalue problem is studied. A negative-slope in friction-velocity curve destabilizes the system.

Stick-slip oscillations are analyzed with the lumped-parameter discretized model. An algorithm for handling nonlinear stick-slip oscillations is presented. Series of detachments over whole domains and localized small-grouped stick-slip oscillations are observed. Effects of system parameters on stick-slip oscillations are considered as well. Under high normal loads, the frequency of the series of detachments is lowered and frequency of small-grouped motions is increased. Sustained stick-slip oscillations are observed when the friction-velocity curve is discontinuous ($\mu_s > \mu_k$) and the system is linearly unstable. With the help of finite element analysis dynamic behaviors of one- and two-dimensional linear elastic systems are investigated.

To my God and family

ACKNOWLEDGMENTS

This research was possible with the help of many individuals, most notably my advisor, Dr. Brian Feeny. I would like to express my sincere gratitude to him for his patience and encouragement. Thanks also goes to the members of my dissertation committee: Drs. Steven Shaw, Alan Haddow, and Charles MacCluer for their many valuable suggestions to my research work.

I would also acknowledge all professors who taught me the knowledge in engineering and mathematics. Professors Brian Feeny, Steven Shaw, Ronald Rosenberg, Clark Radcliffe, Hassan Khalil, Byron Drachman, Richard Phillips, Jerry Schuur of Michigan State University, Professors Dae-Gab Gweon of KAIST, and Chang-seop Song of Hanyang University in Korea deserve thanks for their enthusiastic lectures. I also appreciate the help of Dr. Farhang Pourboghrat for conversations about my research, and Dr. David Wiggert and Mr. Nevin Leder for corrections in my dissertation. A special appreciation goes to Dr. Jen Her of the Ford Motor Co., who provided partial support and motivation to the topic of this research.

Chris Hause, Polarit Apiwattanalunggarn, Reimund Keiser, Mark Berry, Yi Wu, Ming Liao, and Brian Olson were a great team in the Dynamics and Vibrations Laboratory. I would also like to thank Pastor Jung Kee Lee, who inspired me spiritually.

Special thanks to my mother, who always prays for me, and to all family members who always encouraged me. My wife, Yoonkoum Ji, who dedicated herself in supporting my study and taking care of my son, Jin Hong, deserves thanks for this accomplishment.

Thank you, God.

TABLE OF CONTENTS

LIST OF TABLES

LIST OF FIGURES

CHAPTER 1

INTRODUCTION

1.1 Motivation

It is well known that troublesome noise and oscillations occur in systems subjected to frictional contact. Friction-induced vibrations and accompanying noise are serious problems in many industrial applications, for example brake systems in automobiles, wheel and rail systems in trains, water-lubricated bearing systems in ships, robot joint systems, and machine-tool/work-piece systems in manufacturing. These various forms of vibrations are undesirable not only because of their detrimental effects on the performance of the mechanical systems, but also as sources of discomfort in operating environments.

Consider the example of frictional slip and stick-slip vibrations in the stabilizer bar of automobile suspension systems. Figure 1.1 shows a simplified schematic model of the elements in the squeak system. The clamped rubber bushing is represented as the annulus. The outer surface of the annulus is fixed, and there is frictional con-

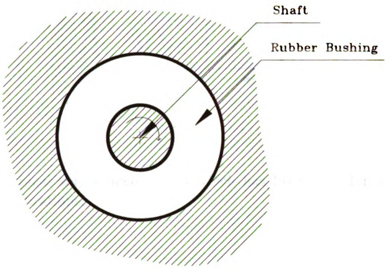

Figure 1.1. A schematic diagram for the bushing squeaking noise problem in an automotive suspension system. Squeaking noise is generated on the contact surface between the rotating shaft and the rubber bushing material.

tact between the rotating shaft and the rubber bushing at the interface. Under some circumstances, the rubber-on-steel contact between the bushing and the shaft generates an annoying, high-frequency, frictional squeaking noise. Such noise problems motivate us to study vibrations and dynamics of the bushing system.

Previous studies which related how the friction generates such unwanted noise and vibrations have shown that causes of friction-induced vibrations and noise depend on numerous factors including:

- Friction force characteristics with respect to relative sliding speed
- Clamping torque producing normal contact pressure
- Humidity and heat generation on the contact surface

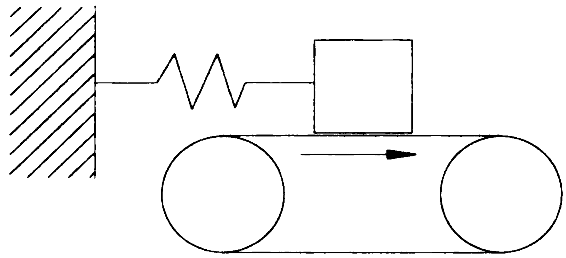

Figure 1.2. A typical spring-mass model which has been used for explanations of friction-induced vibrations.

- Random roughness on the contact surface

- Material nonlinearities

- Modal coupling effects in frictional steady sliding

In order to understand the dynamic system behavior of the elastic medium, which results from self-excited vibrations and stick-slip oscillations, an appropriate mathematical model which explains the distributed friction effect is required. However, only a limited number of studies have considered the influence of distributed friction contact on system behavior. Most of the mathematical models in previous studies have been based on simplified, discretized, low-degree-of-freedom models. For a basic example, a spring-mass on a frictional moving belt model (Figure 1.2) has been used to explain friction-induced vibrations in previous studies. Such a model has limitations, and cannot describe the dynamics of a continuum subjected to distributed frictional contacts.

One of the particular phenomena occurring in a frictionally excited elastic media is the vibration in the form of waves. According to research on deformable elastic materials, oscillations in the form of waves are generated by distributed friction (Schallamach [26], Martins *et al.* [25], and Adams [23, 24]) and some of waves can destabilize the overall system. Therefore, an investigation on frictional waves in an elastic medium is required to understand the generating mechanisms of the noise and vibrations caused by distributed friction.

Furthermore, when stick-slip oscillations occur over distributed contact surfaces, stick-slip motions can be observed at the interface. This means that within the system domain, micro-scale stick and slip regions are observed on the contact surface of the continuum. This produces difficulties in defining the system configurations and leads to complicated responses in the continuous elastic medium. The experimental investigations by De Togni *et al.* [99] and Vallett and Gollub [101], who dealt with the distributed friction contacts, revealed mechanisms responsible for friction-induced vibrations including the stick-slip responses. However, there have been few analytic investigations regarding stick-slip oscillations in a continuum and detailed system behaviors that lead to vibrations and noise in a continuum have not been investigated.

Possible mechanisms for generating vibration and noise are hypothesized to be linear instability and nonlinear limit cycles. For linear instability we look for eigenvalues of a system under a steady sliding condition and identify criteria for instability by varying system parameters. Such instability means growth in vibration and is usually expected to lead to stick-slip limit cycle behaviors. It is possible that a linearly stable system can have a stable stick-slip limit cycle. Thus by setting initial conditions representing the bushing system we seek the possibility of sustained stick-slip limit cycle behaviors.

The primary concerns of this study are determining the mechanisms that can generate noise and vibrations in distributed friction systems, and understanding the dynamic behaviors of the system.

Emphasizing the structural stability, several issues regarding system properties are considered in this study. System properties which are introduced by distributed friction contact are investigated. Effects of damping and boundary conditions on system stability are considered in this investigation.

1.2 Literature Review

1.2.1 Dynamic Instability due to Friction

Experimental and analytical investigations for noise and vibrations induced by friction have shown that numerous system parameters have influenced on dynamic system instability, which may result in chattering, squeaking, squealing noise. Although it is not easy to distinguish system parameters as independent factors influencing system stability, categorizations based on their functions will show several primary parameters responsible for friction-induced vibrations and noise.

Crucial parameters which dominate system stability are friction force characteristics with respect to relative speed, dependency of normal loads, coordinate couplings by friction contact, random roughness of contact surface, temperature and humidity around the contact surface, transient or time-dependent state variables, geometric nonlinearities, frictionally destabilized waves on elastic materials, boundary conditions and so on. In this section, previous studies related to dynamic stability are organized and presented in order to understand principal mechanisms of friction-induced vibrations and noise.

Characteristics of friction-speed relation

One of the main parameters which affects system stability is the slope of the friction-speed relation. Brockley *et al.* [65] investigated fundamental mechanisms of friction-induced vibrations of a system composed with a spring-damper-mass on a frictional moving belt. The results suggested a critical sliding belt speed must be exceeded in order to attenuate oscillations induced by friction. The operating under the critical sliding speed, which depends on damping, normal loads, system stiffness, and friction force characteristics, limited an incidence of vibrations and reduced the amplitude of oscillations. They emphasized that the friction-speed curve plays an important and crucial role in an occurrence of self-excited vibrations. Experimental verifications were also conducted by Brockley and Ko [66].

Moreover, variations of the friction characteristics also effect stability. Cockerham [67] presented analyses of stick-slip and sliding stability by using a discontinuous friction model which consist of different coefficients of friction in acceleration and deceleration. Additionally, nonlinear variations in coefficients of friction during oscillation cycles were analyzed by Antoniou *et al.* [47]. Some researchers included ideas of the discontinuous properties of static and kinetic frictional coefficients associated with time dependency in modeling processes (Brockley [65], Gao *et al.* [45, 46], Tworzydlo *et al.* [52]). For example, experimental studies by Gao *et al.* [45, 46] showed that the rate of increase in static friction coefficient on sticking time is a crucial parameter in addition to friction-speed effects on stick-slip and steady sliding motions.

Such friction-speed relations, sometimes with time-dependent forms, have influenced the effective system damping and destabilized systems in many applications, e.g., brake systems (Friesen [69], Abdelhamid [70], Black [71]), bearing systems (Bhusha [73] Simpson and Ibrahim [74], Krauter [75]), and manufacturing systems (Ulsoy [59], Palmov [31], Paslay [34], Dareing [33], Dawson [35], Belyaev [32]).

In the study by Krauter [75], unstable high-frequency vibrations, which result in as squealing noise, were originated from the growth of unstable vibration modes. The quantity most affected the onset of instability was the slope of friction-speed relation and effective modal structural damping. In the research on water-lubricated compliant rubber bearings (Bhusha [73] and Simpson and Ibrahim [74]), experimental and analytical approaches by modeling of the system ascertained that instability mainly depends on the negative slopes of friction properties. Stability analysis for machining systems in manufacturing industries have confirmed the importance of friction-speed relations on system stability as well (band saw system (Ulsoy [59]), drilling process (Palmov [31], Paslay [34], Dareing [33], Dawson [35], Belyaev [32]), musical instrument analysis (Schelleng [92]), audio system (Majewski [68]), and turbine blades systems (Pfeiffer [91]).

Detailed explanations about dynamic stability by the effects of friction-speed relations have been summarized in works by Nakai and Yokoi [72] and Ibrahim [93, 94].

Coupling instability associated with normal loads

Observations of experimental phenomena for friction-induced vibrations of multi-degree-of-freedom systems have provided another significant mechanism responsible for system instability: a coupling instability associated with normal loads.

Tolstoi [48] investigated experimental kinetic friction systems in the presence of vibrations and informed that negative friction-speed slopes and frictional self-excited vibrations are closely associated with the freedom of normal displacement of the slider. Later, several researchers have confirmed that the self-excited oscillations were accompanied by normal displacement of sliding elements (Aronov *et al.* [61], Sakamoto [49, 50], Tworzydlo *et al.*[51, 52] and Dweib and D'Souza [55, 56]).

By using experimental works, Aronov *et al.* [61] showed when the normal load reaches a critical value, which depends on the system rigidity, high frequency self-excited vibrations are generated. These oscillations exhibited coupling between a lateral and a normal degree of freedom. In their series of works (Aronov *et al.* [62, 63, 64]), stiffness couplings have significant effects on the normal load at which a transition takes place from mild to severe friction and wear.

Further investigations related to coupled self-excited vibrations were performed by Dweib and D'Souza [55, 56]. They determined four different friction regions, such as linear, nonlinear, transient, and self-excited vibration region, as the normal load increases. The self-excited vibrations occurred under high normal loads and a small equivalent kinetic coefficient of friction. By using the linear stability theory the conditions which caused the steady state sliding motions to become unstable oscillations were presented.

A numerical study by Tworzydlo *et al.* [52] has confirmed that coupling between the rotational and normal modes was the primary mechanism responsible for self-excited oscillations. Oscillations with high-frequency stick-slip motions produced significant reductions of the apparent kinetic coefficients of friction (Sakamoto [49, 50], Gao *et al.* [45, 46]).

Coordinate coupling instabilities have been found in many applications as well. Nakai and Yokoi [72, 57] investigated the squeal mechanisms of band brakes in order to develop effective treatments of reduction or elimination of squealing noise. They showed that squealing noise caused by frictional forces were originated from the coupling between two modes of the brake band. Experimental studies on the disc brake squeal (Ichiba and Nagasawa [54]) and multiple modes coupling effects have been found in several applications as well (Hulten [58], Abdelhamid [70], Sherif [60]).

Surface roughness and other environmental effects

The dependence of surface treatment and environmental conditions on system stability have been investigated by several researchers who were interested in dynamic behaviors with tribological effects. Surface roughness allowed the interlocking between two contacted bodies and also promoted the normal vibrations of the slider in real situations. Soom *et al.* [42, 43] investigated the oscillations caused by the interactions of normal and frictional forces when surface roughness is considered. The normal oscillating forces were generated due to the surface irregularities being swept through the contact region during sliding, and destabilized the system (Soom and

Chen [41], Hess and Soom [40]).

Environmental conditions, such as temperature and humidity of the contact also contributed to the system stability. Bhushan [73] investigated basic phenomena for frictional sliding and stick-slip oscillations of the water-lubricated rubber bearing in ships. The mechanism for noise generation was stick-slip motions of rubber at the interface. Generated noise was closely related contact conditions, such as roughness, temperature, and humidity. In humid conditions some dry spots developed during sliding, which would make nonuniform friction forces over the surface. This caused the bearing to undergo stick-slip oscillations, resulting in chattering and squealing noise. From an experimental study by Nakai and Yokoi [57] conditions for generating the screaming noise were changed by the surface treatment and temperature of interfacial surfaces. At high temperatures, slopes in the friction-speed curves became more negative than at the ordinary operating temperature condition and resulted in severe noise and vibrations. Stick-slip amplitudes by the effect of humidity showed that in high humidity condition the stick-slip oscillations are apt to occur (Gao *et al.* [45, 46]).

1.2.2 Stick-Slip Oscillations induced by Friction

When elastic systems are driven by friction forces, the motions of the elastic body may not continuous, but may be intermittent and proceed by processes of stick-slip oscillations. The occurrences of stick-slip motions are unpredictable and system behaviors including chattering, squealing, squeaking noise and even chaotic phenomena are expected.

The analytical approaches for stick-slip behaviors have been performed by many researchers. The periodically forced, single-degree-of-freedom system was considered by Den Hartog [102]. He has made the exact solutions for the systematic steady state responses. Later, Hundal [104] studied the analytical solutions in closed form of continuous sliding and stick-slip motions. Dynamic responses and stability of a system having discontinuous static and kinetic coefficients of friction were investigated by Shaw [105].

Some simple deterministic systems are chaotic when they subjected to friction forces. Feeny [106] and Feeny and Moon [107] provided chaotic motions in a harmonically forced spring-mass-damper system. They used different friction law models and showed the system dynamics in terms of maps for non-smooth systems. The extended analyses associated with phase space reconstructions (Feeny and Liang [108]) and a wavelet analysis in low dimensional characteristics (Liang and Feeny [109]) were conducted as well. Other investigations related to two-degree-of-freedom frictional systems were found in several works (Yeh [103], Pratt and Williams [110]).

Meanwhile, for investigations of non-periodic forcing systems, a mass on a frictional moving belt has been used as a typical model for explaining stick-slip motions. (Refer to Figure 1.2 for system configuration.) The analytical solutions and experimental data were given by Banerjee [83] and Bo and Pavelescu [82] for influences of kinetic friction on stick-slip motions. Additionally, the influence of friction-speed relation in the stick-slip motions were investigated by You and Hsia [80] and Capone *et al.* [81] with graphical techniques.

Nonlinear phenomena introduced by stick-slip motions were investigated by several researchers. Stelter and Sextro [85] and Popp and Stelter [78] investigated the frictional system characterizations with one- and two-degree-of-freedom systems and provided the bifurcation behaviors of deterministic systems. Period doubling and Hopf bifurcations were observed in parameter variations and a jump phenomenon in amplitude of responses of frictional systems was founded. Later, Galvalnetto *et al.* [86, 87] investigated the stick-slip vibration with a two-degree-of-freedom mechanical system and the global dynamics was characterized by using a Poincaré map.

Dynamics in two-degree-of-freedom stick-slip oscillations were studied by Awrejcewicz and Delfs [89, 90]. They showed the qualitative changes in equilibria by changing system parameters along with integration techniques for stick-slip motions in numerical aspects. In addition, Pfeiffer [91] studied dynamics of turbine blades as a multi-dimensional stick-slip system. Studies for self-excited and stick-slip motions have been found in several works (Popp and Stelter [78], Popp [79], Hinrichs *et al.* [84]).

Most of the previous research has dealt with low-degree-of-freedom systems, which did not include distributed friction effects. However, real systems always have areas of contact and sometimes that could have major influences on dynamic characteristics. The model consist of blocks of masses have been used to describe the dynamics for multi-dimensional systems and also used for earthquake fault analysis (Carlson and Langer [97, 98], Carlson *et al.* [96], Takayasu [95]). Carlson and Langer [97, 98] have investigated global stick-slip behaviors of a multi-degree-of-freedom system. They also provided the system slipping instability and analyzed earthquake events.

Vallette and Gollub [101] studied the stick-slip motions with spatiotemporal dynamic systems and explained the experimental behaviors of stick-slip motions in terms of propagating waves. The instability occurred as consequences of Schallamach waves [26] of detachment. Studies on the elastomeric friction system were found in the works by De Togni *et al.* [99] and Rorrer [100].

Analysis related to the stick-slip oscillations in elastic systems, especially for elastic continua, is difficult since stick-slip motions are unpredictable and generate variable-degree-of-freedom systems. In this study, a discretized lumped-parameter model is established and its stability is analyzed (Chapter 4). Dynamic system behaviors including the stick-slip motions are numerically performed with various system parameters (Chapter 5).

1.2.3 Destabilized Waves due to Friction

When an elastic continuum is subjected to specific boundary conditions, materials have been known to generate troublesome noise and vibrations. Such noise and vibrations are originated from unstable motions around a contact surface. In steady frictional sliding, unstable friction-induced waves have been reported.

For semi-infinite, homogeneous, isotropic, materials having free surface, waves propagating around surface, known as Rayleigh waves, were observed in elastic materials. The Rayleigh wave, which has an exponentially decaying amplitude with the distance from the free surface, propagates along the free surface of the elastic body (Fung [37]). On the other hand, when two different materials bonded together, there are waves between the bonded interfaces, called Stoneley waves [30], which are similar in nature to Rayleigh waves. Barnett *et al.* [29] investigated a variant of the Stoneley wave, namely a slip wave between two anisotropic elastic half-spaces in sliding contact. Surface waves involving interface separation and unbonded interface were investigated by Comninou and Dundurs [28].

When elastic media were subjected to distributed friction it was reported that entire systems were destabilized due to unstable waves. In experimental works with a continuous system, such as rubber on a moving rigid body, the unstable wave, called a Schallamach wave, has been observed by Schallamach [26] and Best *et al.* [27]. The unstable motions caused by static instability in the vicinity of the front part of contact propagates as a wave of detachment sequence by the effect of static buckling.

Recently, Martins *et al.* [25] and Adams [23] investigated the wave propagation in distributed friction contact in two-dimensional systems by analytic methods. A mathematical model for a infinite compressed elastic medium was established and unstable waves were found under a condition of a constant coefficient of friction. Adams [24] studied a tensioned beam subjected to friction and found unstable solutions in sliding contact as a one-dimensional system. These works showed that under a constant coefficient of friction two sliding materials caused unstable oscillations, which travel from front to rear in presence of friction. They found that the solutions have properties of non-symmetry by the effect of friction and instabilities are caused by the coupling of various degrees of freedom in the form of waves.

Togni *et al.* [99], Rorrer *et al.* [100], Vallette *et al.* [101] experimented on continuous materials in contact. Rorrer *et al.* [100] experimented with elastomer on a sliding body and revealed four different frequency regimes of sliding, such as steady state sliding, low frequency self-excited motions, high frequency motions and stick-slip motions. He showed that the stick-slip motion did not require a negative slope in the friction-velocity curve. Vallette *et al.* [101] also investigated the unstable phenomena using the stretched latex membranes in contact with a translating rod. He claimed that the instability can occur even without a negative slope in friction-speed relation as a consequence of wave of detachment, known as Schallamach waves [26].

In this thesis, friction-induced waves in an elastic medium are investigated in Chapter 3. Instability mechanisms in the presence of friction are presented in terms of the traveling wave mechanics.

1.2.4 System Properties related to Friction

Elastic systems subjected to nonconservative forces, such as friction forces or follower-type traction forces, become unstable either statically or dynamically (Ziegler [17], Beda [14]). Those instabilities also can be found in the area of aero-elasticity systems (Dowell [8], Higuchi [9, 10]), friction involved systems [25], and some specific boundary conditioned systems (Meirovitch and Hagerdorn [2], Meirovitch and Kwak[1]). Unlike conservative systems, nonconservative systems can have dynamic instability called flutter instability. The flutter destabilizing phenomena were investigated by Herrmann and Bungay [11] and Herrmann and Jong [12]. Plaut [15] and Seyranian and Pedersen [13] showed theoretical investigations about nonconservative instabilities including system properties. Plaut [15] and Beta [14] formulated the material stability conditions and classified the generic loss of stability scenarios in dynamic systems as fundamental researches.

By dealing such system stability which typically described by partial differential equations (PDEs), evaluations of such system stability have primarily depends on system eigenvalues, which can be evaluated after the model reduction. Due to infinite dimensionality of partial differential equations, continuous systems are generally difficult to analyze. Moreover the system subjected to specific boundary conditions sometimes does not admit closed form solutions. These difficulties can be avoided when the system is approximated by eliminating the spatial dependence through discretization in space. There are two major classes of approximated discretization procedures—one based on expansion of the solution in finite series of given functions, and the other is consisting of simply lumping the system properties. Galerkin's method is the most appealing and reduces a continuous system to n-degree-of-freedom system by assuming the solution with series of assumed functions.

However in applying the approximate method (Galerkin's method), careful attentions should be needed in handling eigenvalue problems. Based on the previous studies (Prasad and Herrmann [4], Meirovitch [2]), the Galerkin's approximate method does not provide an estimated magnitude of the error involved, nor does it, in general, guarantee convergence for non-self-adjoint systems. That statement about non-convergence has been proved by Bolotin's works [16]. Bolotin [16] investigated the membrane exposed to a flow in research of aero-elasticity and showed that the non-convergence of Galerkin's method to that particular system. He showed that the example of "flutter paradox" in the membrane flow and gave the range of application for its method in order to reduce its dimension.

Diprima and Sani [6] studied for the convergence of the Galerkin's method for the beam subjected to the non-conservative forces and Prasad and Herrman [4] and Pedersen and Seyranian [5] investigated the general non-self-adjoint problem. The proof of convergence for the non-self-adjoint system can be found in few simple problems (Kantorovich [7], Diprima [6]). Several recent studies have investigated the convergence of non-self-adjoint systems by using modified candidate functions (Meirovitch [1, 2], Hagedorn [3]).

1.3 Proposed Research

The goal of this study is to investigate the dynamics of friction-induced vibrations in a continuous elastic medium subjected to distributed frictional contact.

In order to understand dynamic stability and system behaviors by effects of friction, a mathematical model for a continuous elastic medium subjected to distributed friction is established. The non-self adjointedness, which is the intrinsic property introduced by friction, is shown in this study and the eigenvalue problem associated with the non-symmetric property is investigated. In order to show the feasibility for applying approximate discretization methods the exact and approximate eigenvalues are compared.

Wave dynamics involving friction effect in one- and two-dimensional continuous elastic medium are shown by imposing periodic boundary conditions. Stability analyses including external, internal, and frictional damping, are performed with the lumped-parameter model.

Stick-slip oscillations dependent on spatial and temporal motions are analyzed numerically. Visual presentations of stick-slip oscillations of the elastic system are provided and mechanisms related to generating noise are explained with various system parameters. The numerical results of stick-slip oscillations are verified by finite element analysis.

1.4 Contributions

The chief contribution of this study is the dynamic analysis of an elastic medium which are subjected to distributed frictional contact. Summaries of contributions are as follows.

- The construction of a mathematical model of continuous system with driving friction can extend the scope of research from discretized systems to continuous systems. Most of the previous work has focused on discrete, low-degree-of-freedom systems. With the aid of modeling work, a mathematical description of continuous elastic system subjected to friction can be established.

- Using the established model, parameter effects on system stability can be analyzed in order to show the mechanisms how friction generates noise and vibration.

- The validity of a discretization method—Galerkin's method—is examined. A non-convergence of Galerkin's projection in calculating eigenvalues in this study provides a cautionary example on the blind application of projection method.

- It has been known that the system stability closely depends on its boundary conditions. The wave dynamics for one- and two-dimensional periodic boundary condition models are provided to show the possible causes of unstable waves in presence of friction.

- Stick-slip motions of the space and time dependent system explain how the distributed friction generates noise and vibration in an elastic medium. Visualizations of stick-slip motions in high-dimension are shown.

- Verification by finite element analysis assures the validity of this study.

1.5 Thesis Organization

The remainder of this dissertation is organized as follows. Chapter 2 covers fundamental topics basic to the thesis. A mathematical model of a one-dimensional elastic medium subjected to distributed frictional contact is derived. The exact solution of the partial differential equation is obtained. The eigenvalue problem is non-self-adjoint, and the self-adjoint transformation method is given as an alternative. An approximate discretization method is applied to show the validity of Galerkin's method to this problem.

In Chapter 3, mathematical models of frictional slip waves in one- and two-dimensional systems are provided with periodic boundary conditions. System stability, including the effects of general damping, is determined to explain the existence of unstable traveling slip waves in elastic systems.

In Chapter 4, a lumped-parameter model is established and its pure-sliding frictional stability is obtained. By including general damping effects and nonlinear friction characteristics the system instability which initiates self-excited motion is evaluated.

In Chapter 5, using the model developed in the previous chapters, stick-slip vibration is simulated and then interpreted in terms of mechanisms of noise and vibration. The numerical algorithms which deal with state-dependent boundary conditions are explained and the visual presentations of stick-slip vibrations are shown. The trends of behavior due to changing parameters are considered.

In Chapter 6, the stick-slip vibrations are simulated by using finite element analysis. The numerical algorithms used in the finite element analysis are given and the comparisons between the approximate and exact solution are made. Numerical results for one- and two-dimensional elastic systems with parameter effects are provided as well.

In Chapter 7, the conclusion and summaries of the research conducted, lessons learned and directions for the future works are presented.

CHAPTER 2

FRICTIONAL SLIDING IN A ONE-DIMENSIONAL MEDIUM

2.1 Introduction

In most of the previous research related to friction-induced vibrations, low-degree-of-freedom, discretized models have been used in order to explain dynamic stability of frictional sliding and stick-slip vibrations. For example, a simple model composed a spring-damper-mass on a moving rigid body has usually been used. Despite its simplicity in modeling and analysis, such a system may have limitations in showing characteristic features of an elastic medium subject to distributed friction. Especially, in order to investigate a continuum in contact with a large area, such as in the suspension bushing that motivates this study, a proper continuous model which can capture dynamic features is required. In order to understand dynamic behaviors of a continuous system a one-dimensional continuous system under fixed boundary conditions is investigated in this chapter.

This chapter is organized as follows. A mathematical model for a one-dimensional elastic material subjected to distributed friction contact is established. Because of the friction the boundary value problem is non-self-adjoint. The system properties related to non-self-adjointness are presented, and the general eigenvalue problem, which covers the non-self-adjoint eigenvalue problem, is explained. Using a proper inner product, the transformation from a non-self-adjoint problem to a self-adjoint problem is shown in this chapter. A cautionary example in applying an approximate discretization method for finding the system eigenvalue is presented as well. The effect of distributed friction on the system stability is explained based on the system eigenvalues.

2.2 Equation of Motion

Consider a system shown in Figure 2.1. A linear elastic medium, placed between a moving belt (a moving rigid body) and a frictionless linear bearing, represents a one-dimensional, undamped, continuous system in distributed sliding contact. The friction coefficient is considered as a constant. Although a non-linear coefficient of friction has been known to be one of the crucial factors for system stability, the friction coefficient is assumed to be a constant with respect to relative speed. (Non-linear friction coefficient effects on dynamic stability are mainly discussed in Chapter 4.) In addition, any parameters having random properties, such as roughness of contact surface, are not included in this development in order to emphasize on dynamic

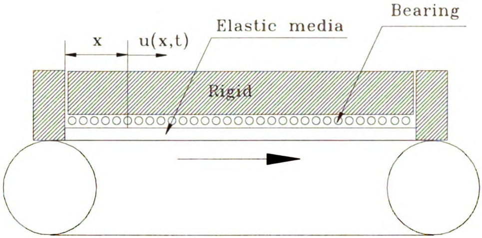

Figure 2.1. A schematic diagram for a one-dimensional elastic medium subjected to distributed friction. Friction between a moving belt (a moving rigid body) and an elastic medium induces vibrations and noise. A medium is under a fixed boundary condition. A frictionless linear bearing is installed on top of a medium so as to allow axial motions of an elastic medium.

stability by effects of uniform properties of materials. Moreover, any non-uniform motions, such as stick-slip motion or loss of contacts are not included in this development. (Demonstrations of stick-slip motions by using a lumped-parameter model are presented in Chapter 5.)

A system composed of a linear elastic medium undergoes a axial sliding. An equation of axial motion for undamped elastic medium is

$$A(x)\frac{\partial \sigma_x(x,t)}{\partial x} + f(x,t) = \rho \frac{\partial^2 u}{\partial x^2}, \tag{2.1}$$

where $A(x)$ is a cross sectional area of elastic medium, ρ is a mass density of elastic material, $\sigma_x(x,t)$ is a stress over the cross section, $u(x,t)$ is an axial displacement, and $f(x,t)$ is a friction force per unit length. Applying linear stress-strain relation, stress is expressed as $\sigma_x(x,t) = E\ \epsilon_x(x,t)$, where E is Young's modulus of the material.

The friction force including Poisson's ratio effect per unit length is given by

$$f(x,t) = -\mu\sigma_y(x,t) = -\mu\{\sigma_0 + \nu\sigma_x(x,t)\}, \tag{2.2}$$

where μ is a friction coefficient, $\sigma_y(x,t)$ is a contact normal stress, and σ_0 is a preloaded normal stress per unit length, which should be always less than zero (compression) to generate friction force and maintain contact to the sliding rigid body.

By considering the linear strain-displacement relation, $\epsilon_x(x,t) = \frac{\partial u(x,t)}{\partial x}$, a non-dimensional equation of motion is obtained by

$$\frac{\partial^2 u}{\partial {x^*}^2} - \alpha\frac{\partial u}{\partial x^*} + \alpha\beta = \frac{\partial^2 u}{\partial {t^*}^2}. \tag{2.3}$$

The dimensionless parameters used in equation (2.3) are $\alpha = \frac{\mu\nu l}{A}, \beta = -\frac{\sigma_0 l}{\nu E}, x^* = \frac{x}{l}$, and $t^* = \frac{t}{\sqrt{\frac{\rho l^2}{AE}}}$, where l denotes contact length and x^* and t^* are the dimensionless coordinate and time, respectively. For the sake of simplicity, the notation $*$ will be neglected in the following development.

The boundary conditions are

$$u(0,t) = u(1,t) = 0. \tag{2.4}$$

For a typical system subjected to distributed friction contact a fixed boundary condition is selected. Stability analyses with a different boundary condition, e.g., a periodic boundary condition, are analyzed in Chapter 3.

2.3 Exact Solution

The exact solution for the equation (2.3) satisfying the boundary condition (2.4) is obtained by using the separation of variables method. Consequently, the exact solution, $u(x,t)$, which is composed with the static solution $u_s(x)$ and dynamic solution $u_d(x,t)$, is

$$u(x,t) = u_s(x) + u_d(x,t), \tag{2.5}$$

in which

$$u_s(x) = -\frac{\beta l}{(e^{\alpha l} - 1)}(e^{\alpha l x} - 1) + \beta l x, \tag{2.6}$$

and

$$u_d(x,t) = \sum_{j=1}^{\infty} \sqrt{2} e^{\frac{\alpha}{2}x} \sin(j\pi x) \, \{a_j \cos(\omega_j t) + b_j \sin(\omega_j t)\}, \tag{2.7}$$

where natural frequencies of $\omega_j = \sqrt{(j\pi)^2 + \frac{\alpha^2}{4}}$, and a_j, b_j are constants determined by initial conditions.

The exact static solution in equation (2.6) by changing β and α are shown in Figure 2.2 and Figure 2.3, respectively. Figure 2.2 depicts the variation in the static solution $u_s(x)$ for β in the range of 0.1 to 1.0 with increments of 0.1 under a condition of $\alpha = 4.0$. As β increases, i.e., as normal loads and contact length increase, or Young's modulus decreases, the non-symmetric static solution along the x axis gets

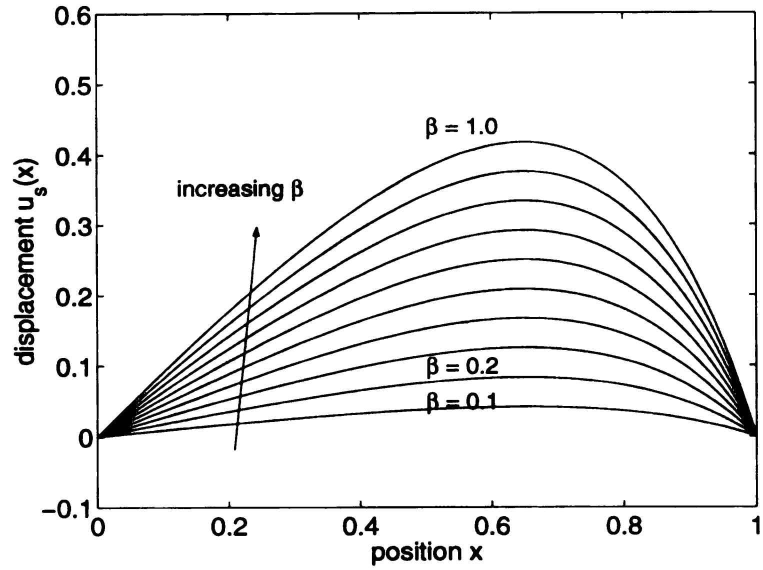

Figure 2.2. The exact static solution $u_s(x)$ by changing β in the one-dimensional system. Here β is in the range of 0.1 to 1.0 with increments of 0.1. In this example $\alpha = 4.0$.

larger. Figure 2.3 provides the trends of static solutions under variations in α from 1.0 to 10.0 with increments 1.0 with $\beta = 1.0$. α influences the asymmetry of $u_s(x)$.

Static strain distributions, defined by $\frac{du_s(x)}{dx}$, under changes β and α are shown in Figure 2.4 and Figure 2.5, respectively. The static strains are increased by increasing β and α. High tensile regions are observed at the front, while high compressive regions are located at the rear on the x axis. Moreover, a sensitivity on the variation of the parameters is clearly shown. In the compressive region, i.e., where $\frac{du_s(x)}{dx} < 0$, stress variations for varying β are larger than those of the tensile region because of the existence of Poisson's ratio.

Importances of the strain and stress in elastic material have been found by Schallamach [26] and Krauter [75] through their experimental and theoretical studies. The

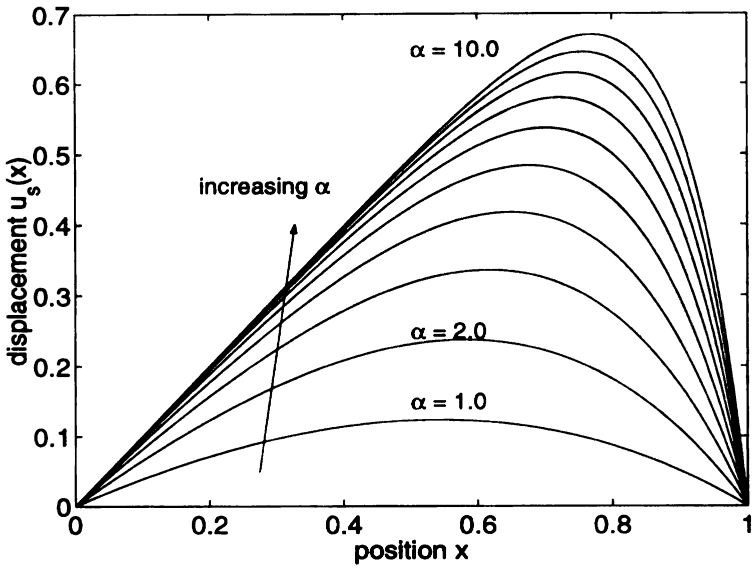

Figure 2.3. The exact static solution $u_s(x)$ by changing α in the one-dimensional system. Here α is in the range of 1.0 to 10.0 with increments of 1.0. In this example $\beta = 1.0$.

expectation of buckling by the effects of tangential stress has been found to be the source of wave propagations in elastic materials. Detailed works related to stick-slip motion are presented in Chapter 5.

The first three exact modes shapes, which depend on parameter α in equation (2.7), are shown in Figure 2.6. Increasing α influences the shapes of the free-vibration unsymmetric eigenfunctions. However, it does not destabilize system. In other words, α determines the modes shapes, which are non-symmetric along the x axis, and α affects the natural frequencies in equation (2.7). This is a conservative system when α is a constant. It should be noted variations of α do not destabilize the dynamic system under fixed boundary conditions with a constant coefficient of friction.

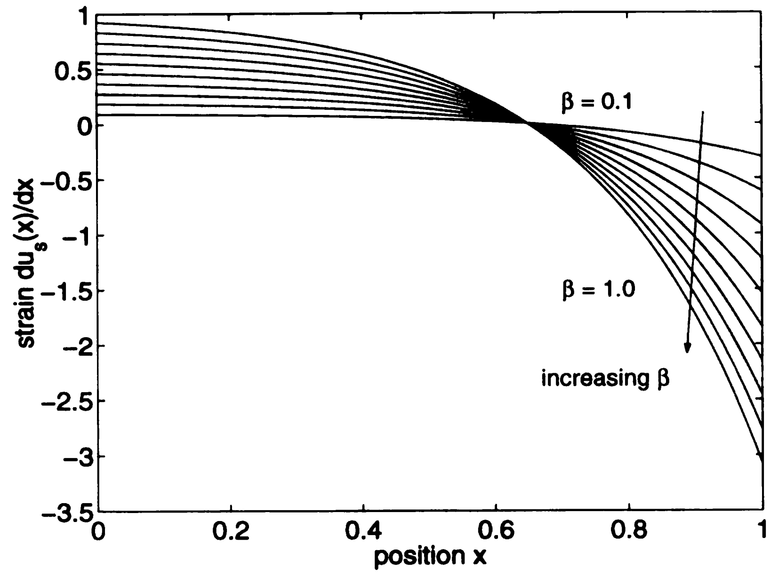

Figure 2.4. The exact static strain solution $\frac{du_s(x)}{dx}$ by changing β in the one-dimensional system. Here β is in the range of 0.1 to 1.0 with increments of 0.1. In this example $\alpha = 4.0$.

2.4 The Non-Self-Adjoint Eigenvalue Problem

Numerous systems encountered in structural dynamics are belonging to distinct eigenvalues and self-adjoint. This means that such systems have symmetric properties. When a system is self-adjoint eigenvalues and eigenfunctions are real quantities. Moreover, the eigenfunctions are orthogonal to each other. However, structural systems which endure aerodynamic forces, friction forces, and follower forces have been reported to lose their symmetries and have non-self-adjoint properties (Meirovitch [18], Martins *et al.* [25], Dowell [8], Higuchi [9, 10]). The orthogonal relations and the expansion theorem which have been developed on the bases of self-adjoint properties are no longer applicable to the non-self-adjoint systems.

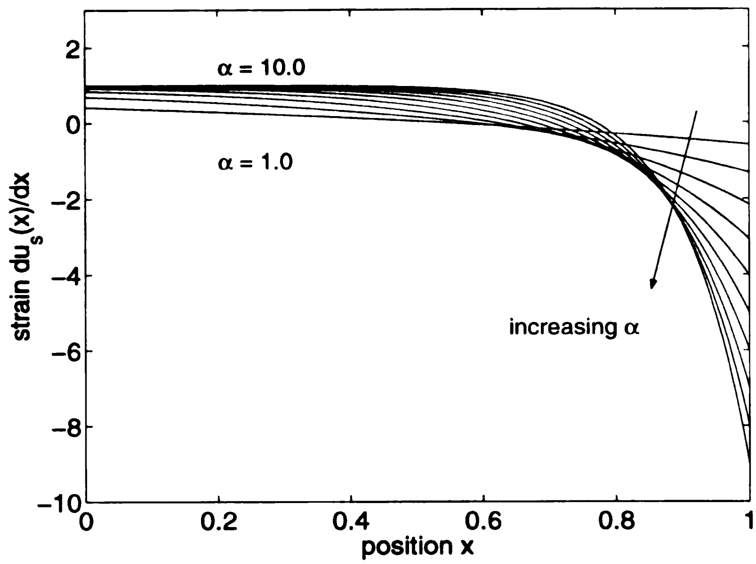

Figure 2.5. The exact static strain solution $\frac{du_s(x)}{dx}$ by changing α in the one-dimensional system. Here α is in the range of 1.0 to 10.0 with increments of 1.0. In this example $\beta = 1.0$.

Although non-self-adjoint systems can be transformed to self-adjoint systems by defining a proper inner product, the problem of non-self-adjointedness can also be handled through similar procedures of the self-adjoint cases (MacCluer [20], Hochstadt [21]). (The techniques associated with transformations of system properties are presented in the next section.)

Let us review the general eigenvalue problem, which includes non-self adjoint problems. Suppose that a solution $u(x,t)$ is represented as equation (2.5). Then the term $\alpha\beta$ in equation (2.3) is eliminated by static solution $u_s(x)$ in equation (2.6), and a dynamic equation of motion in terms of $u_d(x,t)$ is obtained as

$$\frac{\partial^2 u_d}{\partial x^2} - \alpha\frac{\partial u_d}{\partial x} = \frac{\partial^2 u_d}{\partial t^2}. \tag{2.8}$$

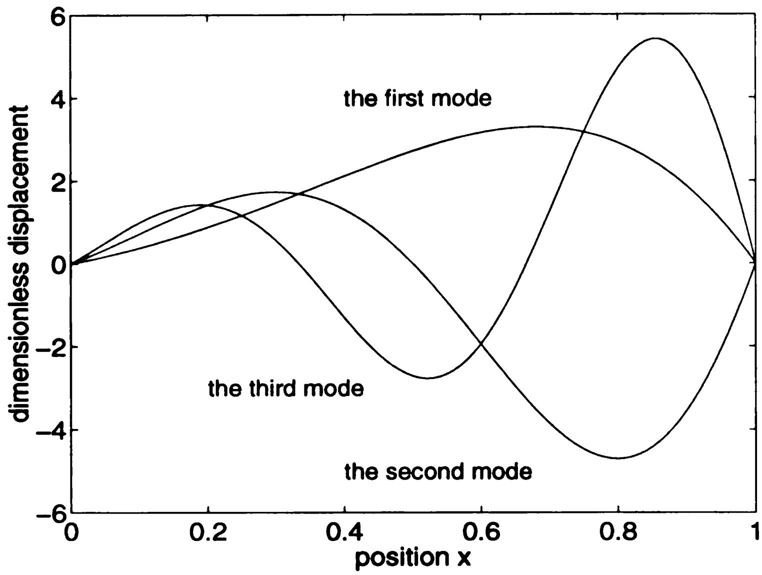

Figure 2.6. The first three eigenfunctions in the dynamic solution. ($e^{\frac{\alpha}{2}x}\sin(j\pi x)$, where $j = 1, 2, 3$ with $\alpha = 4.0$.)

Let the dynamic solution of equation (2.8) can be represented in the form, $u_d(x,t) = \Phi(x)Q(t)$. Then the eigenvalue problem is given by

$$-\frac{\partial^2\Phi}{\partial x^2} + \alpha\frac{\partial\Phi}{\partial x} = \lambda\Phi, \tag{2.9}$$

with the boundary conditions of

$$\Phi(0) = \Phi(1) = 0. \tag{2.10}$$

The eigenvalue problem represented with system operator L is

$$L\Phi = \lambda\Phi, \tag{2.11}$$

where the linear operator in equation (2.11) is defined by

$$L \stackrel{\text{def}}{=} -\frac{d^2}{dx^2} + \alpha\frac{d}{dx}. \tag{2.12}$$

We introduce the classical definition of an inner product of

$$< f, g > \stackrel{\text{def}}{=} \int f(x)g(x)\, dx. \tag{2.13}$$

Then, the operator L has always an adjoint operator L^* defined by

$$< \Psi, L\Phi > = < L^*\Psi, \Phi > . \tag{2.14}$$

And the original system and its adjoint system can be written as

$$L\phi_i = \lambda_i\phi_i, \tag{2.15}$$

$$L^*\psi_j = \lambda_j^*\psi_j, \tag{2.16}$$

where λ_i and λ_j^* are real or complex eigenvalues corresponding to L and L^*, respectively. The operator L^* is called as the adjoint operator of L and the set of eigenfunctions ψ_j $(j = 1, 2, \ldots)$ is said to be adjoint to the set of eigenfunction ϕ_i $(i = 1, 2, \ldots)$ over the defined classical inner product (2.13).

A large class of structural dynamic systems with conservative forces are *self-adjoint*, which means that the two operators L and L^* are identical, $L = L^*$, and the two sets of eigenfunctions are the same for the corresponding eigenvalues. In such case orthogonality is expressed as

$$<\phi_i, \phi_j> = \int_D \phi_i \phi_j dx = 0, \quad i \neq j \quad i,j = 1,2,\ldots\infty. \tag{2.17}$$

By using the orthogonality, coefficients of any function $w(x,t) = \sum_{j=1}^{\infty} \phi_j(x) q_j(t)$ can be written as

$$q_i = <\phi_i, w> = <\phi_i, \sum_{j=1}^{\infty} \phi_j q_j> . \tag{2.18}$$

This is called as the *expansion theorem* for self-adjoint system.

However, if the linear operator L is not the same to the adjoint operator L^*, $L \neq L^*$, the system is non-self-adjoint, and the orthogonality in equation (2.17) does not hold. For the case in which $L \neq L^*$, multiplying equation (2.15) by ψ_j, and equation (2.16) by ϕ_i, and then integrating over the interval D yields

$$\begin{aligned} <\psi_j, L\phi_i> &= \int_D \psi_j L\phi_i dx = \lambda_i \int_D \psi_j \phi_i dx, \\ <\phi_i, L^*\psi_j> &= \int_D \phi_i L^* \psi_j dx = \lambda_j^* \int_D \phi_i \psi_j dx. \end{aligned} \tag{2.19}$$

Subtracting equations (2.19) leads to

$$(\lambda_i - \lambda_j^*) \int_D \phi_i \psi_j dx = 0. \tag{2.20}$$

Hence, if $\lambda_i \neq \lambda_j^*$

$$< \phi_i, \psi_j >= \int_D \phi_i \psi_j dx = 0, \quad i \neq j \;\; i,j = 1,2,\ldots\infty. \tag{2.21}$$

This is the *biorthogonality* of eigenfunctions ϕ_i and ψ_j, which means an eigenfunction of L corresponding to an eigenvalue λ_i is orthogonal to an eigenfunction of L^* corresponding to λ_j^*, where the λ_i is distinct from λ_j^*. The non-self-adjoint operator L has the same eigenvalues as the operator L^*. The general expansion theorem related to non-self-adjoint systems, called the dual-expansion theorem, is presented in the works by Meirovitch [18] and MacCluer [20].

Let us return to the problem of interest. In order to seek the adjoint operator L^* of this study, we examine the adjoint operator L^* defined in the equation (2.14):

$$\begin{aligned}
\int_0^1 \Psi\ L\Phi\ dx &= \int_0^1 \Psi(-\frac{d^2}{dx^2} + \alpha\frac{d}{dx})\Phi dx \qquad (2.22)\\
&= \Psi(-\frac{d\Phi}{dx} + \alpha\Phi)\ |_0^1 + \int_0^1 (\frac{d\Phi}{dx} + \alpha\Phi)\frac{d\Psi}{dx}dx \\
&= \Psi(-\frac{d\Phi}{dx} + \alpha\Phi)\ |_0^1 + \Phi\frac{d\Psi}{dx}\ |_0^1 - \int_0^1 \alpha\Phi\frac{d\Psi}{dx}dx - \int_0^1 \Phi\frac{d^2\Psi}{dx^2}dx \\
&= \int_0^1 \Phi(-\frac{d^2\Psi}{dx^2} - \alpha\frac{d\Psi}{dx})dx \\
&= \int_0^1 \Phi\ L^*\Psi\ dx,
\end{aligned}$$

where the boundary conditions of equation (2.4) have been accounted for. Thus the adjoint operator of this study is

$$L^* \stackrel{\text{def}}{=} -\frac{d^2}{dx^2} - \alpha\frac{d}{dx} \tag{2.23}$$

with zero boundary conditions. Note that the adjoint operator L^* in equation (2.23) is not identical to the operator L in equation (2.12). Assuming that dynamic solutions of this study can be represented by

$$u_d(x,t) = \sum_{j=1}^{\infty} \phi_j(x)\, q_j(t) \tag{2.24}$$

then, by multiplying adjoint eigenfunction ψ_i, and using biorthogonality in equation (2.21), coefficients $q_j(t)$ are obtained as

$$q_j(t) =< \psi_i, u_d >=< \psi_i, \sum_{j=1}^{\infty} \phi_j(x)\, q_j(t) > . \tag{2.25}$$

Thus the biorthonormal relations of the eigenfunctions are

$$\int_0^1 \psi_i(x)\, \phi_j(x) dx = \delta_{ij}, \tag{2.26}$$

where

$$\begin{aligned} \psi_i(x) &= \sqrt{2} e^{-\frac{\alpha}{2}x} \sin(i\pi x), \\ \phi_j(x) &= \sqrt{2} e^{\frac{\alpha}{2}x} \sin(j\pi x), \quad i,j = 1,2,\ldots,\infty. \end{aligned} \tag{2.27}$$

By multiplying the normalized adjoint eigenfunction, $\psi_i(x)$, with equation (2.9) and integrating from 0 to 1, an infinite set of decoupled ordinary differential equations is obtained by

$$\sum_{j=1}^{\infty} m_{ij}\ddot{q}_j + \sum_{j=1}^{\infty} k_{ij}q_j = 0, \qquad i = 1, 2, \ldots, \infty, \tag{2.28}$$

where

$$\begin{aligned} m_{ij} &= <\psi_i, \phi_j> = \int_0^1 \psi_i \phi_j dx = \delta_{ij}, \qquad (2.29) \\ k_{ij} &= <\psi_i, L\phi_j> = \int_0^1 \psi_i L\phi_j dx = {\omega_j}^2 \delta_{ij} = (j\pi)^2 + \alpha^2/4, \quad i, j = 1, 2, \ldots, \infty. \end{aligned}$$

Consequently, the projection by using the adjoint eigenfunctions in the non-self-adjoint system yields the set of decoupled ordinary differential equations. In addition, it is verified that eigenvalues derived from general eigenvalue problems are the same as the exact solutions derived in the previous section.

2.5 Eigenvalue Problem based on a Proper Inner Product

The eigenfunctions derived in the previous section are not mutually orthogonal since the system has a non-self-adjoint operator. However, it is folklore that such a non-self-adjoint problem can be cast as self-adjoint by using a proper inner product (MacCluer [20]). In this section, the method for choosing a proper inner product which enables the system to be self-adjoint is reviewed. Then this method is applied to the problem of interest in order to suggest an alternative way in solving the general eigenvalue problem.

The general second order partial differential equation in the form of

$$p_0(x)\frac{d^2y}{dx^2} + p_1(x)\frac{dy}{dx} + p_2(x)y + \lambda p_3(x)y = 0, \tag{2.30}$$

with the auxiliary homogeneous boundary conditions

$$\begin{aligned} a_0y(x_0) + a_1\frac{dy(x_0)}{dx} + a_2y(x_1) + a_3\frac{dy(x_1)}{dx} &= 0, \\ b_0y(x_0) + b_1\frac{dy(x_0)}{dx} + b_2y(x_1) + b_3\frac{dy(x_1)}{dx} &= 0 \end{aligned} \tag{2.31}$$

is defined on the interval (x_0, x_1). This is the Sturm-Liouville problem subject to homogeneous boundary conditions (Hochstadt [21], Powers [22]). Suppose that the coefficients $p_0(x)$ and $p_3(x)$ are positive and the $p_0(x), p_1(x)$, and $p_3(x)$ are twice differentiable. Let

$$p(x) = e^{\int_{x_0}^{x} \frac{p_1(x)}{p_0(x)}dx}, \quad q(x) = \frac{p_2(x)p(x)}{p_0(x)}, \quad g(x) = \frac{p_3(x)p(x)}{p_0(x)}, \tag{2.32}$$

and multiply equation (2.30) by weighting function $\frac{p(x)}{p_0(x)}$. Then

$$\frac{d}{dx}\{p(x)\frac{dy}{dx}\} + \{q(x) + \lambda g(x)\}y = 0, \tag{2.33}$$

which is a more convenient self-adjoint form. Thus by multiplying equation (2.30) by the weight function $\frac{p(x)}{p_0(x)}$, the system is shown to be self-adjoint.

Consider the problem of interest in equation (2.9) again. According to the self-adjoint transform in equation (2.33), the equation of motion (2.9) can be transformed to self-adjoint system by using the weight function $e^{-\alpha x}$.

Thus the eigenvalue problem in self-adjoint form is given by

$$-\frac{d}{dx}\{e^{-\alpha x}\frac{d\Phi}{dx}\} = \lambda\{e^{-\alpha x}\}\Phi. \tag{2.34}$$

The eigenvalue problem represented with self-adjoint operator $\tilde{L}$ and a weight function $w(x) = e^{-\alpha x}$ is

$$\tilde{L}\Phi = \lambda w(x)\Phi, \tag{2.35}$$

where the self-adjoint linear operator $\tilde{L}$ is defined by

$$\tilde{L} \stackrel{\text{def}}{=} -\frac{d}{dx}\{e^{-\alpha x}\frac{d}{dx}\}. \tag{2.36}$$

The self-adjointness of operator $\tilde{L}$ is verified by taking the classical inner product (2.13) and integrating by parts, such that

$$\begin{aligned} <\Psi, \tilde{L}\Phi> &= -\int_0^1 \Psi\frac{d}{dx}\{e^{-\alpha x}\frac{d\Phi}{dx}\}dx \\ &= -e^{-\alpha x}\frac{d\Phi}{dx}\Psi \,|_0^1 + \int_0^1 e^{-\alpha x}\frac{d\Phi}{dx}\frac{d\Psi}{dx}dx \\ &= \int_0^1 e^{-\alpha x}\frac{d\Phi}{dx}\frac{d\Psi}{dx}dx \\ &= <\Phi, \tilde{L}\Psi>. \end{aligned} \tag{2.37}$$

In addition, the positive definiteness also can be shown from the fact that

$$
\begin{aligned}
<\Phi, \tilde{L}\Phi> &= -\int_0^1 \Phi \frac{d}{dx}\{e^{-\alpha x}\frac{d\Phi}{dx}\}dx \\
&= -e^{-\alpha x}\frac{d\Phi}{dx}\Phi \mid_0^1 + \int_0^1 e^{-\alpha x}\{\frac{d\Phi}{dx}\}^2 dx \\
&= \int_0^1 e^{-\alpha x}\{\frac{d\Phi}{dx}\}^2 dx \geq 0
\end{aligned} \tag{2.38}
$$

is always nonnegative. It is equal to zero only if $\Phi(x)$ is a constant throughout the domain. Because of the boundary condition (2.4), however, this constant must be zero, which would imply a trivial solution. It follows that the operator $\tilde{L}$ in equation (2.36) is positive definite. Therefore, the non-self-adjoint operator L described in equation (2.12) is transformed to the self-adjoint positive definite operator $\tilde{L}$ in equation (2.36) by taking the weight function $e^{-\alpha x}$.

Identical results are also obtained by taking the weighted inner product which defined as

$$
<f, g>_w \stackrel{\text{def}}{=} \int f(x)g(x)w(x)\, dx, \tag{2.39}
$$

where $w(x)$ is weight function. By choosing a weight function $w(x) = e^{-\alpha x}$, we can verify the self-adjointedness with respect to the weighted inner product as

$$
<\Phi, L\Psi>_w = <\Psi, L\Phi>_w, \tag{2.40}
$$

where the operator L is defined in (2.12).

The equation of motion in equation (2.34) is identical to the equation of axial free motion for an elastic rod having varying stiffness $e^{-\alpha x}$ and varying mass distribution $e^{-\alpha x}$ without friction.

The discretized equation of motion can be presented by taking the Lagrange formula. Suppose that the solution $u_d(x,t)$ can be written as a series:

$$u_d(x,t) = \sum_{j=1}^{\infty} \phi_j(x)\; r_j(t), \tag{2.41}$$

where $\phi_j(x)$ can be any admissible function without loss of generosity. The kinetic and potential energies of a continuous system have integral expressions. The kinetic energy can be written in the familiar form of

$$T(t) = \frac{1}{2}\int_0^1 e^{-\alpha x}\{\frac{\partial u_d(x,t)}{\partial t}\}^2 dx. \tag{2.42}$$

In the similar expression, the potential energy can be written as

$$V(t) = \frac{1}{2}\int_0^1 e^{-\alpha x}\{\frac{\partial u_d(x,t)}{\partial x}\}^2 dx. \tag{2.43}$$

The natural boundary conditions are of no concern here because they are automatically accounted for in the kinetic and potential energies. Consider Lagrange's equations for conservative systems, namely,

$$\frac{d}{dt}(\frac{\partial T}{\partial \dot{r}_j}) - \frac{\partial T}{\partial r_j} + \frac{\partial V}{\partial r_j} = 0, \quad j = 1, 2, \ldots, \infty. \tag{2.44}$$

The equation of motion in discretized form is obtained by

$$\sum_{j=1}^{\infty} m_{ij}\frac{d^2 r_j(t)}{dt^2} + \sum_{j=1}^{\infty} k_{ij} r_j(t) = 0, \tag{2.45}$$

where

$$\begin{aligned} m_{ij} &= \int_0^1 e^{-\alpha x}\phi_i(x)\phi_j(x)dx, \\ k_{ij} &= \int_0^1 e^{-\alpha x}\frac{d\phi_i(x)}{dx}\frac{d\phi_j(x)}{dx}dx, \quad i,j = 1,2,\ldots,\infty. \end{aligned} \tag{2.46}$$

By selecting the set of $\phi_j(x)$ as normalized eigenfunction in equation (2.46), i.e., $\phi_j(x) = \sqrt{2}e^{\frac{\alpha}{2}x}\sin(j\pi x)$ from the results of the previous section, the discretized equations of motion are obtained. The eigenvalues for this system, which are $\lambda_j = (j\pi)^2 + \frac{\alpha^2}{4}$, are identical to the exact solution (2.7). Thus, it is verified that the system having a form of non-orthogonality in its eigenfunctions is a minor matter, and it is correctable by projecting under the proper inner product.

2.6 Nonconvergence of Galerkin's Method

The exact solution from the previous section shows that this system's dynamic stability is not dependent on the system parameters. The system is neutrally stable, behaving like an undamped vibration system with natural frequencies of $\omega_j = \sqrt{(j\pi)^2 + \frac{\alpha^2}{4}}$. The natural frequencies depend on the parameter, α, but stability does not depend on it. The effect of β changes the system's static solution and has no influence on the linear stability. With the addition of modal damping, the eigenvalues will have negative real parts and steady sliding is expected to be asymptotically stable.

In this section the assumed mode projection—Galerkin's projection—is applied in the evaluation of system stability in order to verify a feasibility for applying an approximate method. Even though the exact eigenvalue solutions have been obtained already in the previous sections, an application of an approximate discretization method may provides a cautionary example for its use.

Apply the assumed mode method to recast equation (2.3) to ordinary differential equations. It should be noted that the equation (2.3) is cast as non-self-adjoint in equation (2.9). Assuming that $u_d(x,t)$ can be represented with assumed modes satisfying the geometric boundary conditions and p derivative in the partial differential equation of order 2 p, where $p = 1$, such an approximate mode can be accepted as one of the candidates. Thus the solutions are expressed by possible assumed modes. Then

$$u_d(x,t) \;=\; \sum_{j=1}^{\infty} \hat{\phi}_j(x) a_j(t), \tag{2.47}$$

where $\hat{\phi}_j(x) = \sqrt{2}\sin(j\pi x)$ is chosen as an approximate mode. After projecting with these assumed modes, an approximate ordinary different equation of motion is

$$\sum_{j=1}^{\infty} m_{ij}\frac{d^2 a_j}{dt^2} + \sum_{j=1}^{\infty} k_{ij} a_j = f_i, \quad i \;=\; 1, 2, \ldots \infty, \tag{2.48}$$

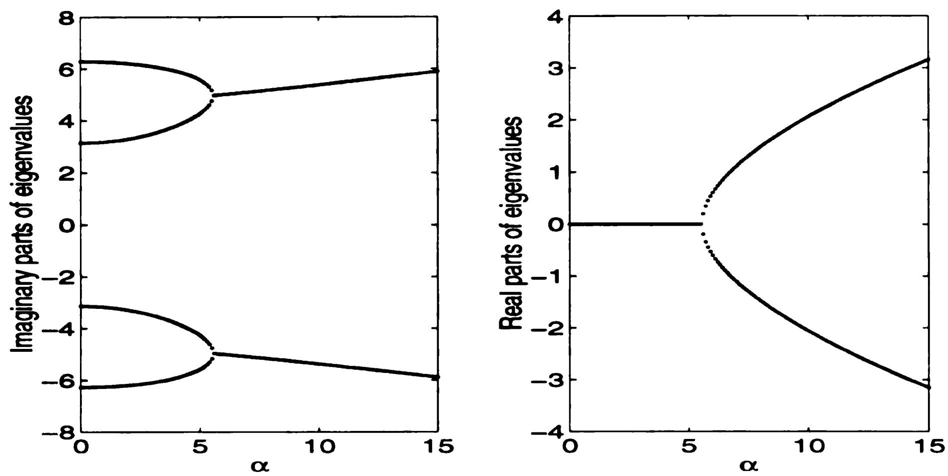

(a) (b)

Figure 2.7. A contradictory result: Eigenvalue trajectories versus α in the one-dimensional friction system by applying the assumed mode method with two modes included. (a) Imaginary and (b) real parts of the eigenvalues versus α are shown. The selected assumed modes are $\hat{\phi}_j(x) = \sqrt{2}\sin(j\pi x)$ for $j = 1, 2$.

where

$$\begin{aligned} m_{ij} &= \delta_{ij}, \quad k_{ij} = k^S_{ij} + k^A_{ij} \\ k^S_{ij} &= (j\pi)^2\delta_{ij} \\ k^A_{ij} &= \begin{cases} \frac{4\alpha ij}{i^2-j^2} & |i-j| = \text{odd}, \\ 0 & \text{otherwise}, \end{cases} \\ f_i &= \begin{cases} \frac{2\sqrt{2}\alpha\beta}{i\pi} & i = \text{odd}, \\ 0 & \text{otherwise}. \end{cases} \end{aligned} \tag{2.49}$$

where k^S and k^A are symmetric and anti-symmetric stiffness matrix, respectively.

Focusing on the low-dimensional dynamics, the system can be approximated with

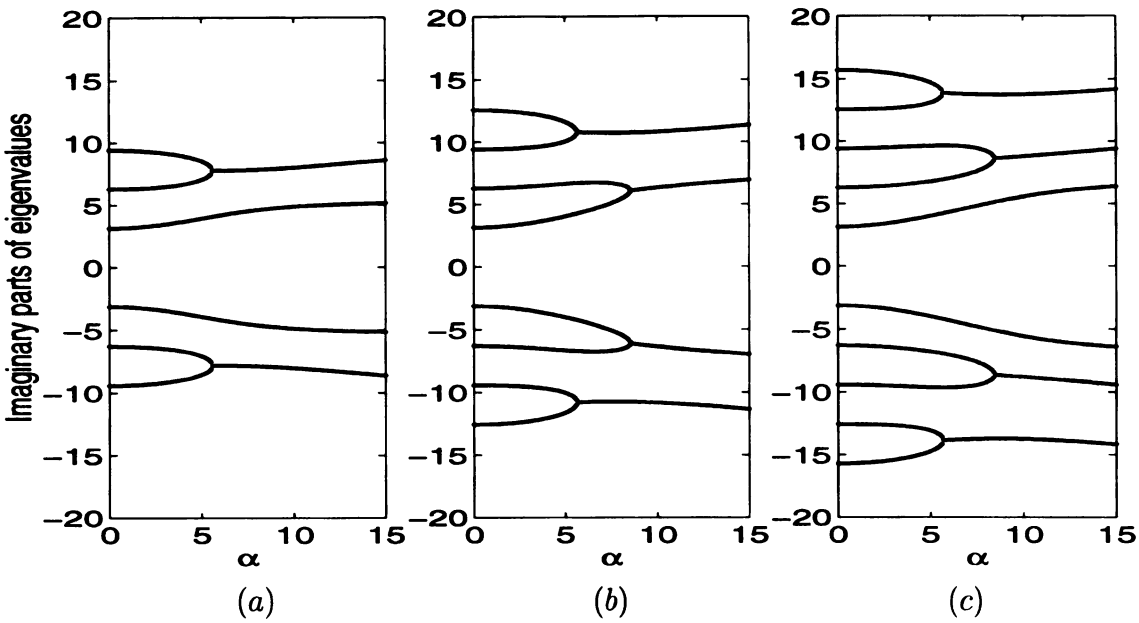

Figure 2.8. A contradictory result: Imaginary parts of the eigenvalues versus α by applying the assumed mode method in the one-dimensional friction system. (a) 3 modes, (b) 4 modes, and (c) 5 modes are included. The selected assumed modes are $\hat{\phi}_j(x) = \sqrt{2}\sin(j\pi x)$.

n-coupled ordinary differential equations. The real parts of the eigenvalues of this system indicate predicted stability characteristics. The dependency of eigenvalues on parameters by including two modes are shown in Figure 2.7. Instability apparently occurs when the real part of an eigenvalue is positive at the critical condition $\alpha = 5.7$ by a collision between two frequencies. This instability mechanism resembles flutter, and has been seen as one of possible instability mechanisms, e.g, flow induced vibrations (Bolotin [16]) and friction induced vibrations (Nakai [57]).

However, these results contradict the exact solution since it has no instability mechanism in the exact solution by parameter α based on the results in the previous

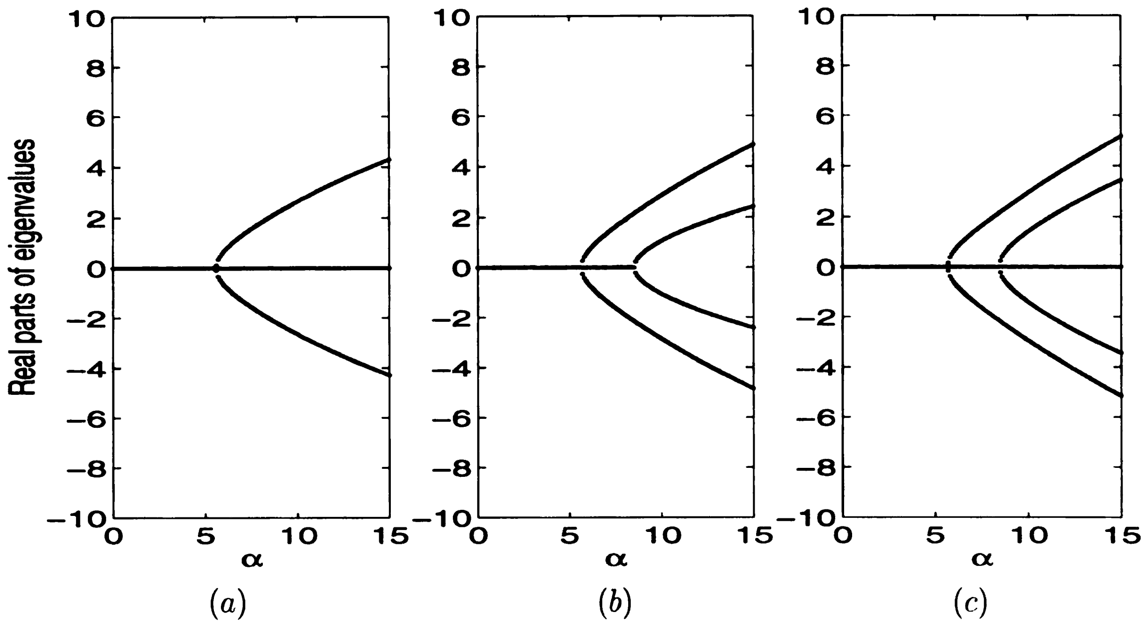

Figure 2.9. A contradictory result: Real parts of the eigenvalues versus α by applying the assumed mode method in the one-dimensional friction system. (a) 3 modes, (b) 4 modes, and (c) 5 modes are included. The selected assumed modes are $\hat{\phi}_j(x) = \sqrt{2}\sin(j\pi x)$.

section. Bolotin [16] had investigated this "paradox" for flow across a membrane. The work showed non-convergent characteristics in the assumed mode projections, and gave a theoretical criterion for convergence based on the linear operator. According to those results, conservative systems with second order operators are not guaranteed to converge in assumed mode approximations.

Nonconvergence of this eigenvalue problem can be demonstrated by increasing the number of assumed modes. Figure 2.8 and Figure 2.9 show the imaginary and real part eigenvalues for 3 to 5 modes, respectively. Considering Figure 2.7 also, the two lowest-frequency modes interact at $\alpha = 5.7$, and $\alpha = 9.0$ for two- and four-mode including approximations, but do not interact for three- and five-mode approximations. This shows that the approximated solution by using assumed mode methods for finding the smallest interaction value α diverges as increasing the modal coordinates. This hints at faulty results when applying the assumed mode method to this problem.

The proof of nonconvergence has been shown by checking the matrix determinant by Bolotin [16]. Consider the convergence of determinant in equation (2.48). The equation (2.48) can be written as

$$\frac{d^2 a_i}{dt^2} + \Omega_i^2 a_i + \eta \sum_{j=1}^{\infty} b_{ij} a_j = 0, \quad i = 1, 2, \ldots, \infty. \tag{2.50}$$

And the characteristic determinant becomes

$$\mid (\Omega_i^2 - \lambda)\delta_{ij} + \eta b_{ij} \mid = 0. \tag{2.51}$$

Dividing the i_{th} row by Ω_i and the j_{th} column by Ω_j, determinant Δ can be expressed in the form of

$$\Delta = \mid \delta_{ij} + c_{ij} \mid . \tag{2.52}$$

According to the works of Bolotin [16] and Kantorovich and Krylov [7], the infinite determinant converges if the double series

$$\sum_{i=1}^{\infty} \sum_{j=1}^{\infty} \mid c_{ij} \mid \tag{2.53}$$

converges. The determinant is described as normal when it satisfies this condition (2.53). By checking the determinant of the equation (2.48), it diverges as taking infinite modes. Thus this series diverge and is not a normal determinant at all.

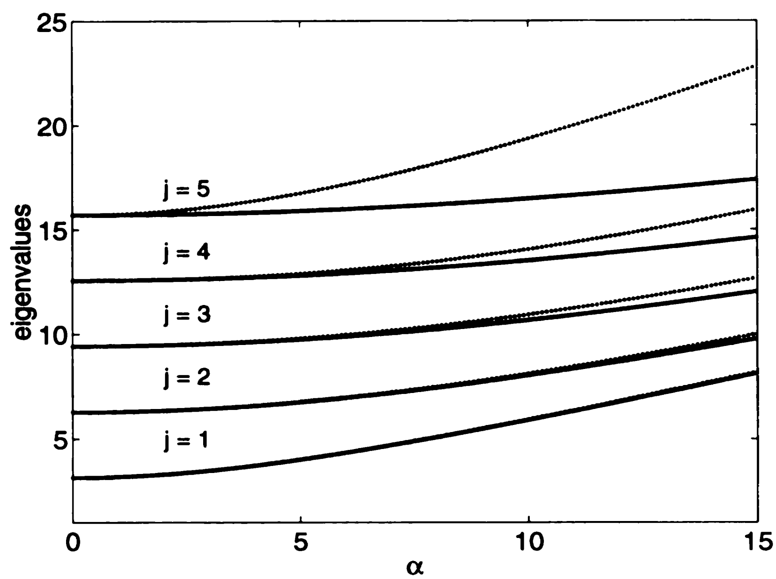

Figure 2.10. Comparison between the exact and approximate eigenvalues: The square roots of the exact eigenvalues, $\sqrt{\lambda_j} = \sqrt{(j\pi)^2 + \frac{\alpha^2}{4}}$, are shown with the solid lines. The mode projected approximate eigenvalues obtained from a self-adjoint system are shown with dotted line. The selected assumed modes are $\hat{\phi}_j(x) = \sqrt{2}\sin(j\pi x)$ for $j = 1, 2, 3, 4, 5$.

For verification, we apply the same assumed mode projection in (2.47) to the equation of motion (2.46), which has the self-adjoint form derived in the previous section by taking the proper inner product. Applying the assumed mode, $\sqrt{2}\sin(i\pi x)$, to the equation of motion (2.46) and using the proper inner product, the approximate eigenvalues have been numerically calculated by parameter α.

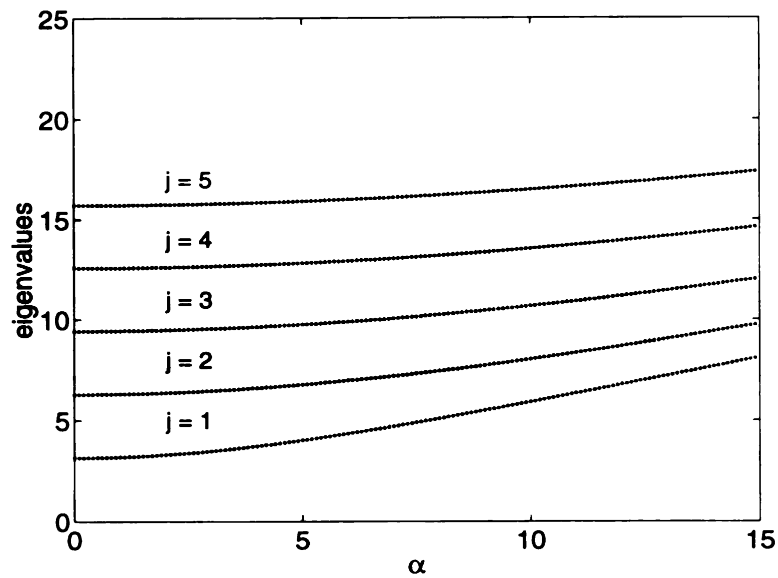

Figure 2.11. Eigenvalues obtained from the non-self-adjoint system by projecting the exact eigenfunctions $\phi_j(x) = \sqrt{2}e^{\frac{\alpha}{2}x}\sin(j\pi x)$.

In this example, five modes are selected for the discretized system. Figure 2.10 presents the exact and approximate eigenvalues based on the proper inner product versus α. The low frequency approximation has good accuracy in eigenvalues calculation. Though there are still slight deviations from the exact solution in high frequency eigenvalue approximations, a more accurate approximation is expected by including more modes. Consequently, a contradictory result has been avoided in evaluating the eigenvalue for self-adjoint system. (When we use the exact eigenfunctions, $\phi_j(x) = e^{\frac{\alpha}{2}x}\sin(j\pi x)$, on the non-self-adjoint system (2.9) and project with the exact eigenfunctions, $\phi_i(x) = e^{\frac{\alpha}{2}x}\sin(i\pi x)$, we have eigenvalues which are identical to the exact eigenvalues, shown in Figure 2.11.)

There are investigations into the approximation of non-self-adjoint systems.

Meirovitch and Hagedorn [2] investigated the modeling of distributed non-self-adjoint systems, such as damped boundary condition models. In using the method of weighted residuals to produce the approximate solution to the eigenvalue problem, the displacement of a non-self-adjoint system is ordinarily represented by a linear combination of comparison functions, i.e., the functions that satisfy all the boundary conditions. Because of difficulties in finding comparison functions the more feasible approach consists of the construction of an approximate solution by using combinations of admissible functions, called quasi-comparison functions, capable of satisfying all the boundary conditions of the problem [2]. The similar approaches for solving the approximate solutions have been found in some literatures by Meirovich and Kwak [1] and Hagedorn [3]. The proof of Galerkin's method for non-self-adjoint boundary value problems has been given by Diprima and Sani [6] and a sensitivity analysis in the non-conservative problem by using adjoint variational method are presented by Prasad and Herrmann [4] and Pedersen and Seyranian [5].

2.7 Conclusion

A one-dimensional continuous system with distributed sliding contact was investigated in order to study the dynamic instability caused by friction. A partial differential equation of motion was established and its exact solution was presented. An eigenvalue problem in this non-self-adjoint system was shown and its solution was provided with a different approach: using the proper inner product and a transformation to a self-adjoint system. A technique for choosing a proper inner product which switches the system properties from non-self-adjoint to self-adjoint was reviewed. The system can overcome the difficulties in evaluating the approximate eigenvalues with the help of the proper inner product.

A contradictory result between the exact solution and the assumed modes approximation in evaluating the eigenvalues was shown as a cautionary example. In this case, non-convergence of the assumed modes method can be easily detected.

The exact solution shows the undamped system is neutrally stable for all parameter values. The constant coefficient of friction does not cause an instability. Boundary conditions and non-linear friction force contributions to the system stability are investigated in Chapter 3 and Chapter 4, respectively.

CHAPTER 3

FRICTIONAL SLIP WAVES IN AN ELASTIC MEDIUM

3.1 Introduction

In the previous chapter, we saw that a one-dimensional elastic material with fixed end points under distributed friction did not undergo an instability when the friction coefficient is a constant. However, the fixed end points may not be representative of our motivational annular system. A first correction might be to implement periodic boundary conditions, which may enable traveling waves to exist.

The structural stability of waves generated in an elastic medium has been an interesting topic for scientists and engineers. When there is contact between two materials, waves, which are generated around the contact area, contain properties of dynamic stability. Such dynamic stabilities have been used to explain the friction-induced vibrations in an elastic medium, which are associated with chattering, squeaking, squealing noise, and stick-slip oscillations.

In classical interpretations of causes for the noise and vibrations, analyses dealing with discretized mathematical models have prevailed (Brockley *et al.*[65], Sakamoto [49, 50]). Moreover, most of the causes cited for steady sliding instabilities have been based on friction-speed relations: a decreasing coefficient of friction in sliding speed has played a primary role in instability of the system based on linear stability criteria (Simpson [74], Nakai and Yokoi [72], Krauter [75]).

Experimental and analytical studies associated with elastic continua have shown that systems have various elastic waves (Stoneley [30], Barnett *et al.* [29], Dundurs [28]) and some of the waves destabilize the systems when elastic materials were subjected to distributed friction forces (Schallamach [26], Martins[25], Adams [23, 24]).

Observations of destabilized waves in elastic continua were performed by Schallamach [26]. Experimentally, he observed that the relative motions between two frictional members are due to waves of detachment crossing the contact area at high speed, and that waves appear as moving folds or wrinkles on the surface of rubber. When the tangential compressive stress reached a buckling state, the buckling of the front edge induced detachment waves, known as Schallamach waves, which travel from the front to rear.

Extended studies of occurrence conditions of such waves were investigated by Best *et al.* [27], Martins *et al.* [25] and Adams [23, 24]. According to experimental studies by Martins *et al.* [25], De Togni *et al.* [99], Rorrer *et al.* [100], and Vallette and Gollub [101], dynamic instabilities can occur even in a condition with no decreasing characteristics in friction-speed relations. For example, Vallette and Gollub [101] measured spatiotemporal internal displacements of an elastic continuum subjected to friction contact and proved that unstable traveling waves can occur even without a decreasing friction coefficient in sliding speed.

Using analytical approaches, the existence of destabilized waves in the presence of friction was confirmed by Martins [25] and Adams [23, 24]. Martins *et al.* [25] showed that the intrinsic non-symmetry of Coulomb's friction contributions to equations of motion and couplings of various degree-of-freedom play an important role in generations of dynamic instabilities. Under a condition of large couplings in spatial coordinates caused by friction stresses, steady sliding motions are dynamically unstable even in a constant coefficient of friction. It is also claimed that a decrease of coefficient of friction with sliding speed is not a necessary condition for the occurrence of unstable elastic waves. The developed studies were found in the works by Adams [23, 24] for one- and two-dimensional elastic medium in contact. He determined the existence of unstable waves by using a one-dimensional model composed of a beam-on-elastic foundation. A beam placed on a series of springs was used as a qualitative model for two bodies in sliding contact. This analysis indicated that steady state solutions are dynamically unstable for any finite sliding speed even with a constant coefficient of friction, due to interactions of complex modes of vibrations.

In this chapter investigations on the stability of waves of an elastic medium on the condition under frictional steady sliding are presented in order to understand the mechanisms which cause vibrations and noise. For a one-dimensional elastic system, the presence of unstable waves in a continuum is investigated via the mathematical model developed in the previous chapter. The fact that the system's stability dependent on the boundary condition is emphasized in this study. Through evaluations of characteristic solutions of waves, explanations for instabilities under a condition of a constant coefficient of friction are provided. In addition, the effects of external and internal damping on overall system stability are analyzed. For a two-dimensional elastic system, a mathematical model of semi-infinite, isotropic, linear material with a periodic boundary condition is presented and its characteristic solution is investigated. Effects of system parameters, such as Poisson's ratio and a friction coefficient, on dynamic stability are shown.

3.2 One-Dimensional Elastic System

3.2.1 Stability Analysis of Elastic Waves

Unstable waves in elastic materials yield non-uniform motions, such as micro scale stick-slip oscillations, or cause to loss of contact at the contact surface. Prior to investigations of the nature of the non-uniform motions (discussed in Chapter 5 in this study), primary causes for dynamic instability are investigated from a wave dynamics point of view.

Consider the one-dimensional, undamped, elastic system developed in the previous chapter. The dynamic equation of motion in the self-adjoint form is

$$\frac{\partial}{\partial x}\{e^{-\alpha x}\frac{\partial u}{\partial x}\} = e^{-\alpha x}\frac{\partial^2 u}{\partial t^2}. \tag{3.1}$$

However, these time periodic boundary conditions

$$\begin{aligned} u(0,t) &= u(1,t), \\ \frac{du(0,t)}{dx} &= \frac{du(1,t)}{dx}, \end{aligned} \tag{3.2}$$

are considered. Note that the system parameter α $(= \mu\nu)$ in equation (3.1) is a constant value, which represents a fixed coefficient of friction and Poisson's ratio. Considering periodic boundary conditions (3.2), solutions are assumed to have the form

$$u(x,t) = \text{Real}\{e^{i2\pi k(x-ct)}\}, \tag{3.3}$$

where k is a positive real number representing the angular frequency of solutions along the x axis, as the term $\frac{1}{k}$ shows the wave periods along the x axis. (See Figure 2.1 for the system configuration. We will use the notation in equation (3.3) in this chapter since references from wave dynamics in continua have used such notation in their studies.)

Generally, c can be a complex value and plays an important role in dynamic system stability. In the case of a real value of c, pure waves of constant shape are expected. This implies that conservative non-dispersing waves exist in the elastic medium and the system is in a neutrally stable state without damping. On the other hand, a complex value of c contains information about the characteristics of the waves. This can be easily expressed by $c = R + Ii$, i.e., c composed with a real component R and a imaginary component I. Thus the equation (3.3) can be rewritten as

$$u(x,t) = \text{Real}\{e^{i2\pi k(x-Rt)}e^{2\pi kIt}\}. \tag{3.4}$$

A positive R indicates that there is a wave propagating toward the positive direction and a positive I indicates that there is an unstable wave which increases its motion exponentially in time. On the other hand, a negative R indicates that there is a wave propagating toward the negative direction and a negative I indicates that there is a stable wave which decreases its motion exponentially in time. Thereby, the imaginary component of the characteristic solutions represents the stability of the wave.

A characteristic equation of c obtained by substituting the equation (3.3) into equation (3.1) is

$$c^2 - (1 + \frac{\alpha}{2\pi k}i) = 0. \tag{3.5}$$

The imaginary and real parts of the characteristic solution are

$$\begin{aligned} R &= \pm\sqrt{\frac{1+\sqrt{1+(\alpha/2\pi k)^2}}{2}}, \\ I &= \frac{\alpha}{4\pi kR} = \pm\frac{\alpha}{4\pi k\sqrt{\frac{1+\sqrt{1+(\alpha/2\pi k)^2}}{2}}}. \end{aligned} \tag{3.6}$$

It is clear that without friction—the condition in which α equals zero—the characteristic solution has pure real solutions for c and the traveling waves which keep their wave shapes in time are pure sinusoidal functions.

When friction is considered, however, the characteristic equation yields general, complex conjugate solutions for c. From the result in equation (3.6), the waves propagating toward the positive x axis, which are represented by a positive value R, are unstable waves. In other words, the amplitude of the propagating waves increases in time. On the other hand, when the waves propagate toward the negative x axis they are stable since they have negative imaginary components in the characteristic solutions.

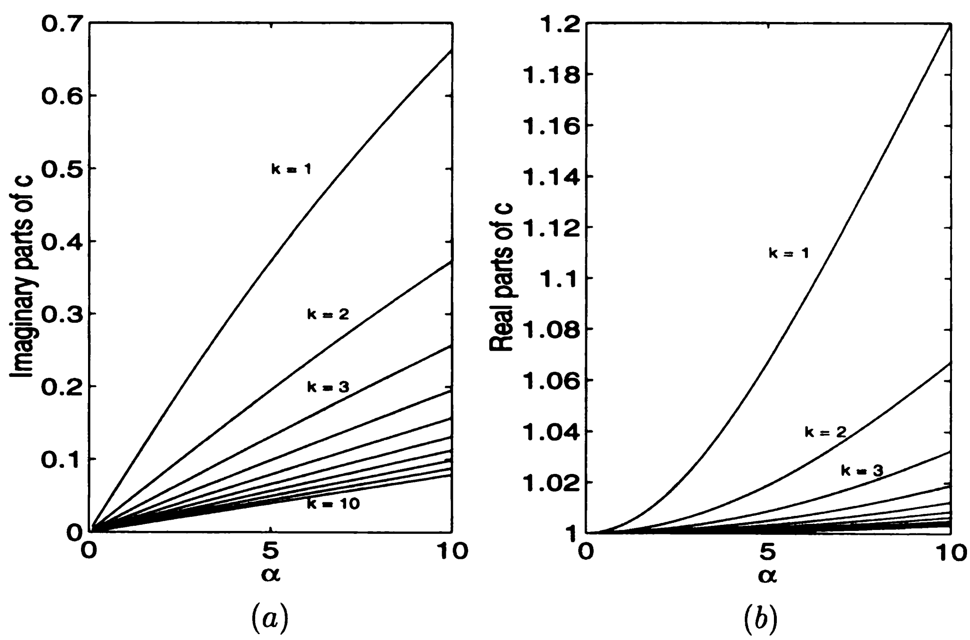

Figure 3.1. The unstable characteristic solutions for the undamped, periodic boundary conditioned model. (a) Imaginary and (b) real parts of the characteristic solution versus α are shown.

Figure 3.1 shows the imaginary and real parts of the characteristic solution corresponding to an unstable wave by increasing the parameter α. Those solutions are presented with various undetermined frequency factors k. As α increases, i.e., as the coefficient of friction or Poisson's ratio increases, waves traveling toward the positive x direction (the direction of the moving rigid body) are increasingly unstable in any finite sliding velocity. Clearly, waves traveling toward the negative x direction (not shown in Figure 3.1) are stable waves.

Similar trends associated with such unstable traveling waves were found in previous studies. Regarding the traveling direction of unstable waves, the direction of the moving rigid body indicates the direction of the unstable waves (Martins *et al.* [25], Adams [23, 24]). In addition the traveling unstable waves make whole systems unstable even if the coefficient of friction is constant. By considering a beam subjected to distributed friction, which was modeled mathematically as a fourth order partial differential equation, Adams [24] proved that one-dimensional traveling waves make whole systems unstable. He included random properties representing the roughness of the contact surface in his modeling.

With the aid of this study, it has been analytically shown that elastic systems subjected to distributed friction can also be unstable in the presence of a constant coefficient of friction, without including any random properties. As described earlier, it is expected that a destabilizing wave phenomenon is one of the possible causes for unstable motions. In real situations, such unstable waves are expected to yield non-uniform motions, such as stick-slip oscillations or loss of contact in materials.

3.2.2 Addition of External Damping

An undamped elastic continuum subject to distributed friction is considered in the previous section. In this section, effects of external damping on system stability are considered. (External damping is defined as a relative dissipation between an elastic material and a ground.) An equation of motion including an external damping coefficient d is

$$\frac{\partial}{\partial x}\{e^{-\alpha x}\frac{\partial u}{\partial x}\} = e^{-\alpha x}\{\frac{\partial^2 u}{\partial t^2} + d\frac{\partial u}{\partial t}\}. \tag{3.7}$$

Applying the periodic boundary condition (3.2) again, the characteristic equation is

$$c^2 + \frac{di}{2\pi k}c - (1 + \frac{\alpha i}{2\pi k}) = 0. \tag{3.8}$$

A search for analytical solutions of quadratic equation (3.8) with complex coefficients is not an easy job, so we apply numerical method in searching for solutions.

Since unstable waves affected by external damping are primary concerns of this study, consider only the maximum value of imaginary parts in the characteristic equation (3.8). The maximum value of imaginary components determines the whole system stability. Remember that a positive imaginary component indicates an unstable traveling wave.

Figure 3.2 and Figure 3.3 provide the imaginary and real parts of equation (3.8) on the parameter domains α and d, respectively. In Figure 3.2, the maximum imaginary part is decreased by decreasing α or increasing d. In other words, a reduction of

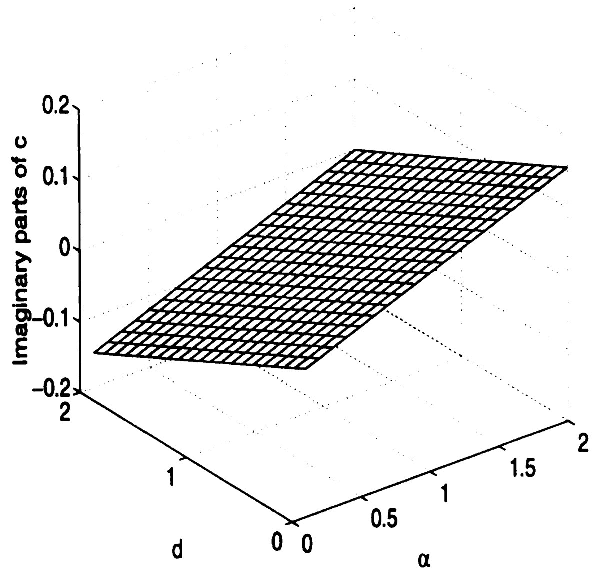

Figure 3.2. The imaginary parts of the characteristic solutions including the external damping coefficient d. The maximum value of the imaginary parts is presented in the parameter domains α and d. In this example $k = 1$.

friction, or an increase in external damping is required to stabilize the system. The traveling speeds of waves, which are represented as the real parts of the characteristic solution, are influenced by α and d as shown in Figure 3.3. The speeds of waves corresponding to the unstable ones are decreased by decreasing α or increasing d.

Figure 3.4 depicts trajectories of imaginary parts of c under variations in d for several frequencies k. In this example, the overall system, which was unstable by having complex conjugate pairs in imaginary characteristic solutions when $d = 0.0$, becomes a stable system with sufficiently large external damping d. The solutions of c no longer have complex conjugate imaginary pairs when d is not equal to zero. Beyond the point $d = 1.0$, all characteristic solutions can have negative imaginary parts, which implies the system is fully stable. Low frequency terms, such as $k = 1$,

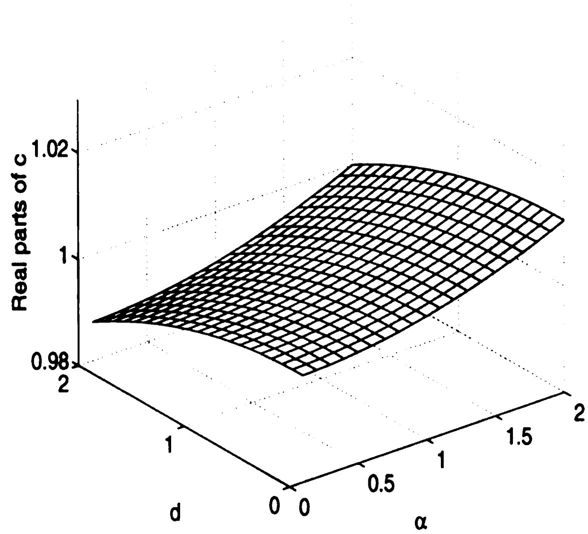

Figure 3.3. The real parts of the characteristic solutions including the external damping coefficient d. The real parts of the characteristic solution corresponding to the maximum imaginary value is presented in the parameter domains α and d. In this example $k = 1$.

are easily stabilized by increasing d, as indicated by the steep downward slopes with increasing d in Figure 3.4.

Based on this interpretation, the system can undergo under an unstable condition; a condition that the system has some stable and unstable eigenvalues in its parameters. (For example, the range $0 < d < 1.0$ in Figure 3.4). Under such condition, responses corresponding to the stable eigenvalues are damped out in time, but responses corresponding to unstable eigenvalues can dominate the whole system responses, generating squeaking or squealing noise and vibrations in experiments.

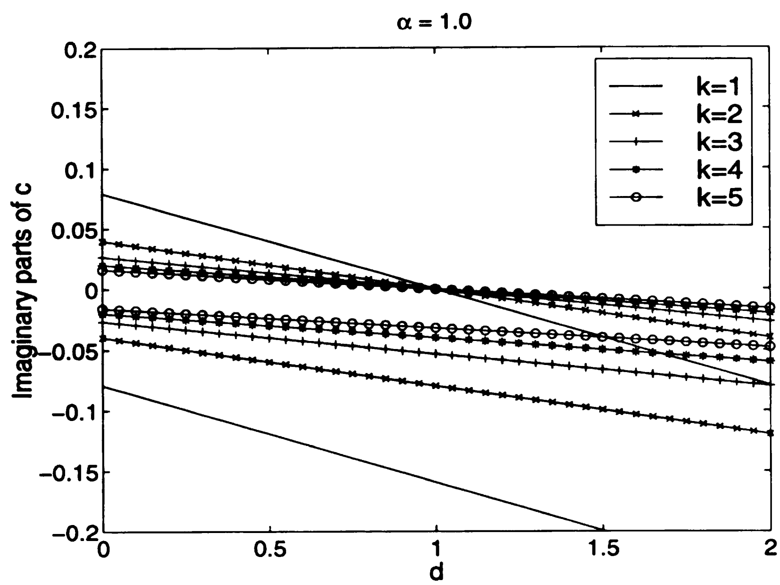

Figure 3.4. The imaginary parts of the characteristic solutions including the external damping coefficient d. In this example $\alpha = 1.0$.

3.2.3 Addition of Internal Damping

Elastic materials such as rubber contain considerable internal damping. (Internal damping is defined as a relative dissipation of strain energy in the materials.) Usually internal damping is stabilizing, but under some conditions, especially when there are non-conservative forces, such internal damping is able to destabilize systems (Bolotin [16], Hendricks [38], Shaw and Shaw [39], and Higuchi and Dowell [10]). Effects of internal damping on the system being studied are not clear. In this section, the effects of internal damping, referred to as structural damping, on system stability are considered.

A stress-strain relation including internal damping is given by

$$\sigma_x(x,t) \quad = \quad E\epsilon + V\dot{\epsilon} = E\frac{\partial u}{\partial x} + V\frac{\partial \dot{u}}{\partial x}, \tag{3.9}$$

where E is the modulus of elasticity and V is the modulus of viscosity of the material. Applying equation (3.9) to equations (2.1) and (2.2), an equation of motion including internal damping γ is given by

$$\frac{\partial}{\partial x}\{e^{-\alpha x}\frac{\partial u}{\partial x}\} + \gamma\frac{\partial}{\partial x}\{e^{-\alpha x}\frac{\partial^2 u}{\partial x \partial t}\} = e^{-\alpha x}\frac{\partial^2 u}{\partial t^2}, \tag{3.10}$$

where γ is an internal damping coefficient defined as V/AE. A characteristic equation obtained by substituting the periodic boundary condition is

$$c^2 + \gamma(2\pi k i - \alpha)c - (1 + \frac{\alpha i}{2\pi k}) = 0. \tag{3.11}$$

Figures 3.5 and 3.6 show the imaginary and real parts of the characteristic solution corresponding to the maximum imaginary value in the parameter domains α and γ, respectively. The imaginary parts attain negative values when increasing γ or decreasing α, as shown in Figure 3.5. Internal damping in elastic materials stabilize the system as the external damping does. The speed of waves versus γ and α is shown in Figure 3.6. From these results, it is concluded that the system is stabilized by increasing internal damping.

Figure 3.7 shows trajectories of imaginary parts of c under variations in γ for several frequencies k. Like external damping does, the system is stabilized beyond

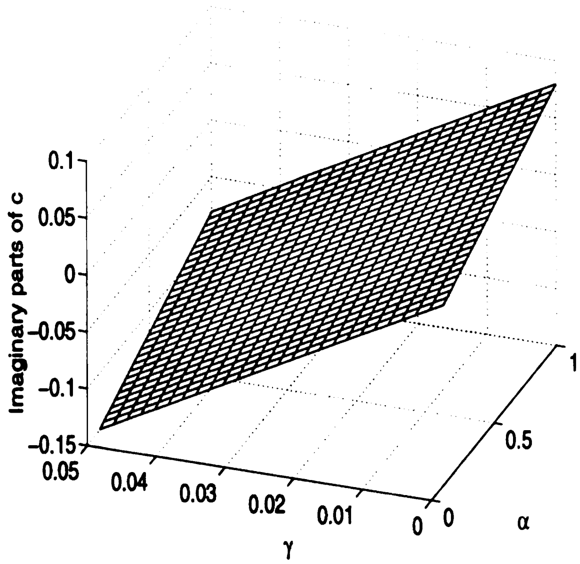

Figure 3.5. The imaginary parts of the characteristic solution including the internal damping coefficient γ. The maximum value of the imaginary parts is presented in the parameter domains α and γ. In this example $k = 1$.

the point $\gamma = 0.025$. Note that the high frequency terms, such as $k = 5$ in Figure 3.7, are easily influenced and stabilized as increasing internal damping γ.

Instabilities induced by internal damping have been reported for some specific systems such as rotation systems (Shaw and Shaw [39], Hendricks [38], Bolotin [16], Iwan and Stahl [76] and Iwan and Moeller [77]) and systems with follower forces (Higuchi and Dowell [9, 10]). In such systems, small internal damping can destabilize the system. For the instability by modal interactions, i.e., the instability accompanied by colliding of frequencies with changing parameters, it is reported that small internal damping can destabilize whole systems.

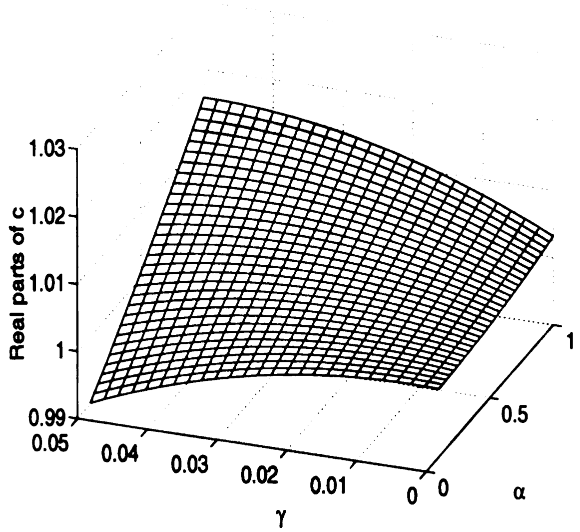

Figure 3.6. The real parts of the characteristic solution including the internal damping coefficient γ. The real parts of the characteristic solution corresponding to the maximum imaginary value is presented in the parameter domains α and γ. In this example $k = 1$.

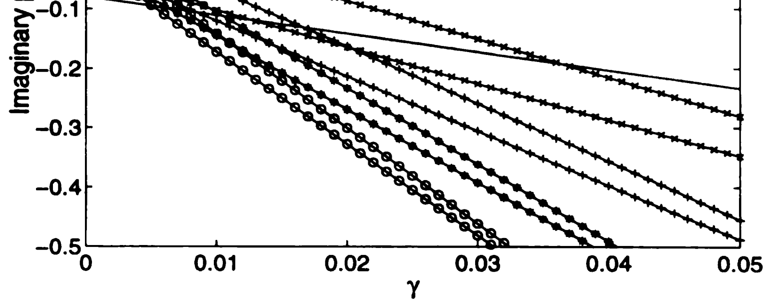

Figure 3.7. The imaginary parts of the characteristic solutions including the internal damping coefficient γ. In this example $\alpha = 1.0$.

3.3 Two-Dimensional Elastic System

A semi-infinite, linear elastic medium in contact with a moving semi-infinite rigid body is considered as a two-dimensional elastic system subjected to distributed friction (Martins *et al.* [25]).

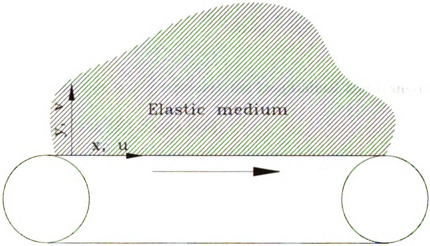

Figure 3.8. A schematic diagram for a semi-infinite, two-dimensional elastic medium in contact with a moving rigid body.

In this section, dynamic stability as affected by a constant coefficient of friction is investigated (Figure 3.8). The dynamic equation of the linear elastic material with respect to a static equilibrium state is represented by

$$\begin{aligned} G\nabla^2 u + (\lambda + G)\frac{\partial}{\partial x}\Delta &= \rho\ddot{u}, \\ G\nabla^2 v + (\lambda + G)\frac{\partial}{\partial y}\Delta &= \rho\ddot{v}, \end{aligned} \tag{3.12}$$

where $\nabla^2 = \frac{\partial^2}{\partial x^2} + \frac{\partial^2}{\partial y^2}, \Delta = \frac{\partial u}{\partial x} + \frac{\partial v}{\partial y}, G = \frac{E}{2(1+\nu)}$, and $\lambda = \frac{\nu E}{(1+\nu)(1-2\nu)}$. The variables u and v are displacements in the x and y directions with respect to the static equilibrium state, respectively. By rewriting equation (3.12) in terms of the speed of free vibration waves, the equations of motions are

$$\begin{aligned} c_T^2(\frac{\partial^2 u}{\partial x^2} + \frac{\partial^2 u}{\partial y^2}) + (c_L^2 - c_T^2)(\frac{\partial^2 u}{\partial x^2} + \frac{\partial^2 v}{\partial x \partial y}) &= \frac{\partial^2 u}{\partial t^2}, \\ c_T^2(\frac{\partial^2 v}{\partial x^2} + \frac{\partial^2 v}{\partial y^2}) + (c_L^2 - c_T^2)(\frac{\partial^2 u}{\partial x \partial y} + \frac{\partial^2 v}{\partial y^2}) &= \frac{\partial^2 v}{\partial t^2}, \end{aligned} \tag{3.13}$$

where $c_L = \sqrt{\frac{\lambda+2G}{\rho}}$ and $c_T = \sqrt{\frac{G}{\rho}}$ represent the longitudinal and transverse speed of waves, respectively (Fung [37], Saada [36]).

Boundary conditions on the contact surface at $y = 0$ are

$$\begin{aligned} v(x,0,t) &= 0, \\ \sigma_{yx}(x,0,t) &= \mu \sigma_{yy}(x,0,t), \end{aligned} \tag{3.14}$$

where μ is a coefficient of friction, assumed to be a constant. The stress-strain relations are $\sigma_{yx} = G(\frac{\partial v}{\partial x} + \frac{\partial u}{\partial y})$, and $\sigma_{yy} = \lambda \frac{\partial u}{\partial x} + (\lambda + 2G)\frac{\partial v}{\partial y}$. The boundary condition in equation (3.14) implies that there is no loss of contact between the medium and the moving rigid body.

The dynamic solutions subjected to periodic boundary conditions are assumed to have the form

$$u(x,y,t) = Ae^{-by}e^{ik(x-ct)}, \tag{3.15}$$

$$v(x,y,t) \;=\; Be^{-by}e^{ik(x-ct)},$$

where k is a positive real number, which represents an angular frequency along the x axis, and b is a complex number, which contains a positive real value that allows exponentially decreasing oscillations in the y direction. Such boundary conditions have been adopted in a development of the Rayleigh waves in elastic materials (Fung [37]). Here a complex value c determines the stabilities of traveling waves induced by friction. Note that a imaginary value of c implies a neutrally stable wave.

Applying equation (3.15) to equation (3.13), nontrivial solutions are

$$\mu(2-2\sqrt{1-L}\sqrt{1-T}-T) = iT\sqrt{1-L}, \tag{3.16}$$

where L and T are defined as $(c/c_L)^2$ and $(c/c_T)^2$, respectively. For a case of a compressible linear elastic material, i.e., the range $0 \le \nu < 1/2$, the equation (3.16) yields the following sixth order equation with respect to L (See Martins *et al.* [25] for details.)

$$L^2(L^4 + a_3L^3 + a_2L^2 + a_1L + a_0) = 0. \tag{3.17}$$

The coefficients a_0, a_1, a_2, and a_3 are given by

$$a_0 \;=\; 16\mu^2\tau^2(1+\mu^2\tau^2), \tag{3.18}$$

$$a_1 \;=\; -8\mu^2\tau(2+\tau(3+\mu^2(4\tau-1))),$$

$$a_2 = 4\mu^2(1 + 2\tau(2 + \tau) + (\mu^2(4\tau - 1) + 1)^2,$$

$$a_3 = -2(\mu^2(4\tau + 1)),$$

with $\tau = c_T/c_L$.

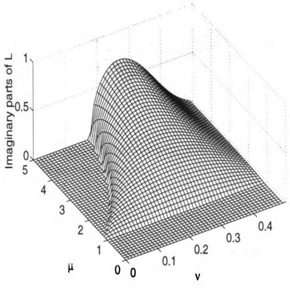

Figure 3.9. The imaginary parts of the characteristic solution L in the parameter plane of friction coefficient μ and Poisson's ratio ν.

A numerical analysis of equation (3.17) is performed in the domains μ and ν. Figure 3.9 and Figure 3.10 show the imaginary and real parts of L in equation (3.17). The zeros in the solutions over the parameter domains, which are located in regions of small μ and small ν, indicate that there are no nontrivial solutions which satisfy the boundary conditions in (3.14). Based on the relation of $c = \pm\sqrt{L}\, c_L$, the positive imaginary and real components of L, which are shown by the non-zero values in

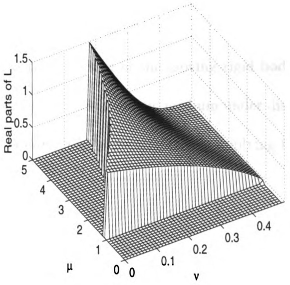

Figure 3.10. The real parts of the characteristic solution L in the parameter plane of friction coefficient μ and Poisson's ratio ν.

Figure 3.9 and Figure 3.10, correspond to the first and third quadrants of the complex plane c. Remember that the positive imaginary value of c implies an unstable wave and the sign of the real part of c determines the direction of the wave. Thus the solutions located in the first quadrant in the complex plane c (Real(c) > 0 and Imaginary(c) > 0) indicate unstable waves traveling toward the positive x axis. On the other hand, the solutions located in the third quadrant in the complex plane c (Real(c) < 0 and Imaginary(c) < 0) indicate stable waves traveling toward the negative x axis.

Therefore, according to these numerical solutions, the two-dimensional elastic medium has unstable traveling waves, even with a constant coefficient of friction, if Poisson's ratio and a friction coefficient are large enough. The numerical results from the two-dimensional elastic systems are consistent with the one-dimensional system developed in the previous sections. Both systems have unstable traveling waves, which propagate toward the direction of the moving rigid body, in any finite speed of the rigid body. (A two-dimensional elastic medium under distributed contact with fixed ends boundaries is numerically investigated by applying finite element analysis in Chapter 6.)

3.4 Conclusion

In this chapter, the dynamic stability of frictional steady sliding in one- and two-dimensional systems was investigated. Under the periodic boundary condition unstable traveling waves in a one-dimensional elastic system were found to be dependent upon a constant coefficient of friction and Poisson's ratio. It was demonstrated that high coupling in the coordinates due to Poisson's ratio destabilizes the two-dimensional elastic continuum.

It was concluded that a decreasing coefficient of friction is not a necessary condition for the occurrence of dynamic instability. In addition, the characteristic analysis showed that dynamic instability occurs in the form of self-excited, unstable, traveling waves. The stabilizing effects by adding external and internal damping were studied.

The system imposed by the fixed boundary conditions, presented in Chapter 2, has no instabilities under the condition of a constant friction coefficient. Thus the neutrally stable condition exists for the undamped one-dimensional system. However, according to the results of this chapter, the same system under the periodic boundary condition becomes unstable because of the unstable traveling waves.

It should be noted that these analyses were based on the steady state frictional sliding stability. Thus any noise and vibrations originated from the non-uniform motions should be analyzed by different approaches. Chapter 5 illustrates these phenomena.

CHAPTER 4

STABILITY ANALYSIS IN A LUMPED PARAMETER MODEL

4.1 Introduction

In order to investigate friction-induced vibrations and noise generated from large frictional contact surface, for example regarding bushing squeaking noise in a vehicle suspension system, noise generation from a band/drum brake system, and jerky motions of a clutch engagement, a construction of a mathematical model which can explain the dynamic behaviors including stick-slip oscillations is essential process in system analysis.

However, it could be a painstaking job in handling the continuous model to explain dynamic phenomena induced by friction. For a example, when the system undergoes stick-slip motions, the prediction of stick-slip motions are difficult through analytical approaches since they are dependent on the system states and occur anywhere over the domain of contact. In order to overcome such difficulties, it is necessary to build a descretized model based on space coordinates.

In Chapter 2, we saw that improper discretization of the PDE led to misleading results. If we are going to apply lumped parameter models to nonlinear stick-slip studies later, it is important to investigate the quality such a discretization. One way to gage the discretization is through a linear stability study, and its comparison with previous analytical results.

Most of the works in the previous chapters were investigated based on a assumption that the friction coefficient is a constant with respect to the relative speed. However, it has been reported that the frictional damping plays a crucial role in system stability and should be included in stability analysis. Theoretical and experimental studies by Brockley [66, 65], Tolstoi [48] have shown that a single degree-of-freedom model with negative slope in friction-speed relation is unstable and leads to self-excited vibrations.

In applied systems, for example automotive brake systems (Friesen [69], Abdelhamid[70]), aircraft brake systems (Black [71]) and water lubricated bearing systems (Simpson [74], Krauter [75], Bhushan [73]), the friction-speed relation strongly influences the overall system stability, and the cause of noise and vibrations. Such noise generation mechanism was broadly investigated by Nakai and Yokoi [72] and an importance of resultant structural damping has been recognized by Krauter [75] with linear analysis for generation of squealing noise caused by dry friction. By using two degree-of-freedom nonlinear models, Simson [74] and Krauter[75] have revealed that chattering and squealing noise are generated due to the resultant structural damping.

In this chapter, a lumped-parameter, multi degree-of-freedom model is constructed as a discretization of the previous continuous system. (This model is adopted for investigations of stick-slip oscillations in Chapter 5.) Non-symmetric properties in the eigenvalue problems, which are usually introduced by friction, are properly handled and analyzed. Stability analyses including damping, such as external, internal, and frictional damping, are evaluated.

4.2 Stability Criteria

The condition of stability, i.e., the boundary between stable and unstable domains, naturally depends on the parameters of the system such as boundary conditions, distribution of loads, system damping, and nonlinearities of materials. For most of the classical investigations related to the theory of elastic stability, the external forces are expressed through the potential energies and the problems usually have self-adjoint properties. Because the external forces have potentials, loss of stability can take place only in the form of static instability—divergence—which has zero frequency.

On the other hand, when a system contains nonconservative forces, for example panels or shells in air flow, follower forces in elastic materials, and systems including dry friction forces, the instability may occur either dynamically—flutter—or statically—divergence (Bolotin [16], Ziegler[17]).

For investigations of a stability of multi degree-of-freedom system the definition of linear stability with respect to eigenvalues is explained as follows. When the linear system has the form of a homogeneous matrix equation, then the eigenvalue problem is represented as

$$\mathbf{L\Phi} = \mathbf{0}, \tag{4.1}$$

where the system matrix $\mathbf{L}$ depends on the real load parameter and the complex eigenvalue, $\lambda = \alpha + i\omega$. We write the matrix $\mathbf{L}$ as a linear function of real matrices, specifying the dependence on λ explicitly by

$$\mathbf{L} = \lambda^2\mathbf{M} + \lambda\mathbf{C} + \mathbf{K}, \tag{4.2}$$

where the stiffness matrix $\mathbf{K}$, damping matrix $\mathbf{C}$, and the mass matrix $\mathbf{M}$ can be non-symmetric matrices in general.

The dynamic stability of the system is determined quantitatively by the eigenvalues, $\lambda_r = \alpha_r + i\omega_r$ for $r = 1, 2, \ldots, n$. The eigenvalue with the maximum real part is the important one and for this α_{max} since the stability of the whole system is dominated by this value. Let $\omega_{\alpha_{max}}$ be the imaginary eigenvalue corresponding to the α_{max}. Then motions and stability are categorized by

- Stable motion if $\alpha_{max} < 0$
- Critical motion (marginally stable) if $\alpha_{max} = 0$
- Flutter instability if $\alpha_{max} > 0$ and $\omega_{\alpha_{max}} \neq 0$
- Divergence instability if $\alpha_{max} > 0$ and $\omega_{\alpha_{max}} = 0$

Base on these stability criteria, the possible unstable motions are evaluated by eigenvalues of the system.

4.3 A Lumped-Parameter Model under Fixed Boundary Conditions

4.3.1 A Stability Analysis of an Undamped System

Investigations of the dynamic behaviors and stabilities of systems having considerably large rubbing surfaces may encounter some difficulties in the evaluation of the system eigenvalues since the classical approximate method which relies on the modal coordinates may no longer valid and their convergence of eigenvalues are not guaranteed as discussed in Chapter 2. There is no reason to expect other discretizations to converge, either. But we investigate the performance of other discretizations in hope that those difficulties are overcome, so that the discretization can be applied to nonlinear studies with some confidence.

In this section by using the lumped-parameter discretization method the continuous system is simplified to a multi degree-of-freedom model and the system stability is analyzed. (Analyses using the finite element method are shown in Chapter 6.)

Consider a system shown in Figure 4.1, which shows the lumped-parameter model from the continuous system in Figure 2.1. The mass blocks connected to linear springs are placed on the moving belt. There are frictional forces between the mass blocks and the moving belt. In this model, the each mass block plays a role not

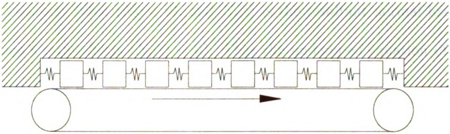

Figure 4.1. A schematic diagram for the undamped, lumped-parameter model subjected to distributed friction. Fixed end boundary conditions are applied.

only as a lumped-mass, but also as a discrete elastic mass which can contract and elongate based on the Poisson effect due to the forces exerted around the mass. Since the normal displacement is restricted as shown in Figure 4.1, the contraction and elongation influence the normal load, which causes the variation of the friction forces. The equation of motion for undamped i_{th} mass is written as

$$m\ddot{x}_i(t) + k\{-x_{i-1}(t) + 2x_i(t) - x_{i+1}(t)\} + f_i(t) = 0, \tag{4.3}$$

where m is a mass of each mass block, k is a spring stiffness, $x_i(t), \dot{x}_i(t)$, and $\ddot{x}_i(t)$ represent the displacement, velocity and acceleration of i_{th} mass, respectively and $f_i(t)$ is the friction forces on the i_{th} mass. Here the mass and stiffness are lumped from the evenly distributed system. Let us include the Poisson's ratio effect. Then the friction force is

$$f_i(t) = \mu N_i(t) = \mu[N_0 + \nu k\{x_i(t) - x_{i-1}(t)\}], \tag{4.4}$$

where μ is a friction coefficient and N_0 is the normal load on each block, which is a negative constant value ($N_0 < 0$), and $N_i(t)$ is the resultant normal load including the Poisson's ratio effects ($N_i(t) < 0$). Thus the undamped equation of motion for the i_{th} mass block is

$$\ddot{x}_i(\tau) - (1 + \mu\nu)x_{i-1}(\tau) + (2 + \nu\mu)x_i(\tau) - x_{i+1}(\tau) + \mu N_0/k = 0, \tag{4.5}$$

where $\tau = \omega_p t$, $\omega_p^2 = k/m$ and the time derivative $(\dot{\ })$ denotes $\frac{\partial}{\partial \tau}$. This is a difference equation of motion of the continuous system in equation (2.3).

It has been known that the system stability is closely dependent on its boundary conditions. Firstly, consider a fixed boundary condition of

$$\begin{aligned} x_0(t) &= x_{n+1}(t) = 0, \\ \frac{dx_0(t)}{dt} &= \frac{dx_{n+1}(t)}{dt} = 0. \end{aligned} \tag{4.6}$$

The equation of motion for the undamped system is expressed by

$$\mathbf{M}\ddot{\mathbf{X}} + \mathbf{K}\mathbf{X} = \mathbf{F_0}, \tag{4.7}$$

where

$$\mathbf{M} = \mathbf{I}, \tag{4.8}$$

$$\mathbf{K} = \begin{bmatrix} 2+\nu\mu & -1 & 0 & \dots & 0 & 0 \\ -(1+\nu\mu) & 2+\nu\mu & -1 & \dots & 0 & 0 \\ 0 & -(1+\nu\mu) & 2+\nu\mu & \dots & 0 & 0 \\ \dots & \dots & \dots & \dots & \dots & \dots \\ 0 & 0 & 0 & \dots & -(1+\nu\mu) & 2+\nu\mu \end{bmatrix},$$

and

$$\mathbf{F_0} = -\mu N_0/k\ [1, 1, \dots, 1]^T.$$

The matrix $\mathbf{I}$ denotes a unit matrix. The stiffness matrix $\mathbf{K}$ is non-symmetric due to the effect of friction and the Poisson's ratio. The eigenvalues for the dynamic systems are evaluated with respect to the static equilibria. Thus, the eigenvalue problem is represented by

$$\lambda \mathbf{M} \mathbf{\Phi} = \mathbf{K} \mathbf{\Phi}. \tag{4.9}$$

Since $\mathbf{K} \neq \mathbf{K^T}$, the orthogonal relations obtained from the symmetric properties are no longer valid. Furthermore, the expansion theorem derived from the symmetric relations can not be applied to decompose any arbitrary vectors in terms of a set of eigenvectors.

Let us briefly discuss the general eigenvalue problem, which covers the non-symmetric properties in equation (4.9), and then return to the problem of interest.

Consider the transposed eigenvalue problem associated with equation (4.9) and write it in the form

$$\lambda \mathbf{M} \mathbf{\Psi} = \mathbf{K}^{\mathbf{T}} \mathbf{\Psi}. \tag{4.10}$$

The eigenvalues of equation (4.10) are the same as those of equation (4.9). On the other hand, the eigenvectors of equation (4.10) are different from those of equation (4.9). Consider two distinct solutions of equation of (4.9) and (4.10). These solutions satisfy the equations

$$\lambda_i \mathbf{M} \phi_i = \mathbf{K} \phi_i, \quad i = 1, 2, \ldots, n, \tag{4.11}$$

and

$$\lambda_j \mathbf{M} \psi_j = \mathbf{K}^{\mathbf{T}} \psi_j, \quad j = 1, 2, \ldots, n. \tag{4.12}$$

The equation (4.12) can also be written in the left eigenvector form by

$$\lambda_j \psi_j^T \mathbf{M} = \psi_j^T \mathbf{K}, \quad j = 1, 2, \ldots, n. \tag{4.13}$$

Multiplying equation (4.11) on the left by ψ_i^T and equation (4.13) on the right by ϕ_i and subtracting one results from the other, then

$$(\lambda_i - \lambda_j) \;\; \psi_j^T \phi_i = 0, \tag{4.14}$$

so that for distinct eigenvalues

$$\psi_j^T \phi_i = 0, \quad \lambda_i \neq \lambda_j, \quad i, j = 1, 2, \ldots, n. \tag{4.15}$$

This means that the left eigenvectors and right eigenvectors of the system corresponding to distinct eigenvalues are orthogonal. It should be stressed that the eigenvectors are not mutually orthogonal in the same ordinary sense as those associated with the Hermitian matrix. Indeed, the two sets of eigenvectors ϕ_i and ψ_j are biorthogonal. The fact that the eigenvectors ϕ_i and ψ_j are biorthogonal permits to formulate an expansion theorem for general case. Assuming that any vector can be represented by infinite sum of eigenvectors there is a choice of expanding any arbitrary truncated n-vector $\mathbf{x}$ in terms of the eigenvector ϕ_i or ψ_j. Assuming that the truncated expansion in terms of ϕ_i closely approximates $\mathbf{x}$, then

$$\mathbf{x} = \mathbf{\Phi q}, \tag{4.16}$$

where $\mathbf{q} = [q_1, q_2, \ldots, q_n]^T$ is the vector of associated coefficients. Thus the coefficients are obtained by

$$\mathbf{q} = \mathbf{\Psi^T x}. \tag{4.17}$$

Similarly, an expansion in terms of the eigenvector ψ_j has the form

$$\mathbf{x} = \mathbf{\Psi r}, \qquad \mathbf{r} = \mathbf{\Phi^T x}, \tag{4.18}$$

where $\mathbf{r} = [r_1, r_2, \ldots, r_n]^T$ is the vector of associated coefficients associated with ψ_j. This procedure, which treats the non-symmetric eigenvalue problem in the lumped-parameter system, corresponds to the non-self adjoint eigenvalue problem in the continuous system discussed in Chapter 2.

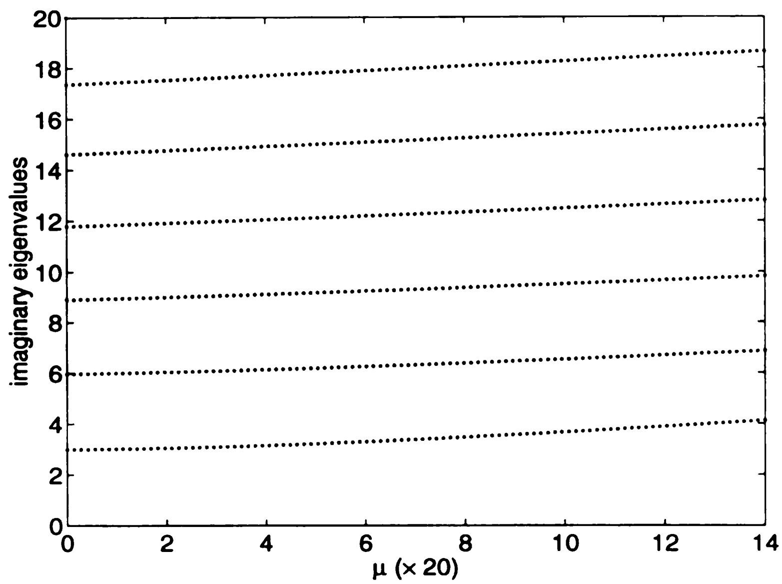

Figure 4.2. Trajectories of the eigenvalues versus friction coefficient μ in the undamped, lumped-parameter model.

Let us return to the problem of interest. Figure 4.2 shows the numerical results of the eigenvalues by changing the friction coefficient μ, which is assumed to be constant with respect to the relative speed. The calculated eigenvalues can also be compared to the exact eigenvalues of the continuous system, shown in Figure 2.10. As μ increases the frequencies simply increase and no destabilizations are found in Figure 4.2. This result shows a close approximation to the exact eigenvalues

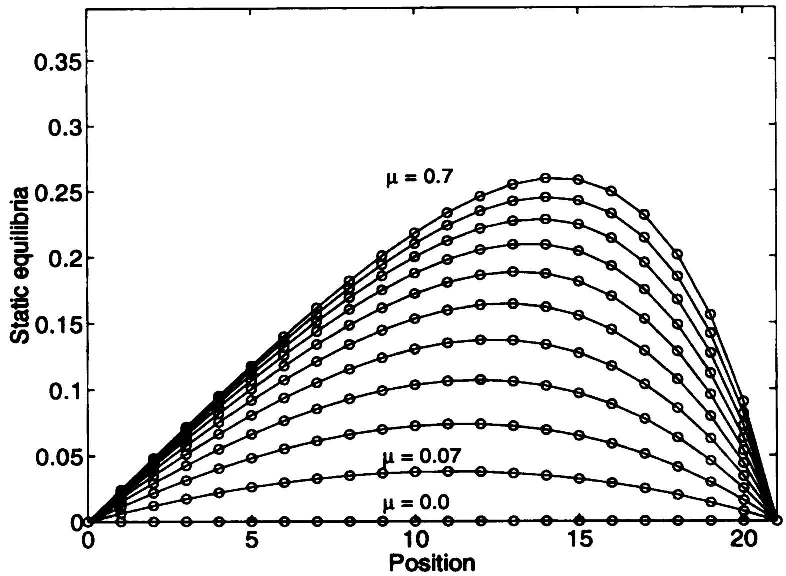

Figure 4.3. Static equilibria by increasing the friction coefficient μ. Here μ is increased from 0.0 to 0.7 by 0.07.

of the continuous system. Comparing with the exact eigenvalues the eigenvalues obtained from the lumped-parameter model are usually underestimated, which are explained in Chapter 6. In Chapter 2 the contradictory example in evaluation of eigenvalues was presented. In this section, fortunately, there are no contradictory results in evaluating the approximate eigenvalues in the lumped-parameter model since the numerical method used in this study (MATLAB) utilizes an adjoint property in evaluating the eigenvalues. We can expect that the numerical analysis using such an algorithm generate reliable results.

Figure 4.3 shows the dependence of the static equilibria on the coefficient of friction μ. Comparing this result to Figure 2.3, which shows the static equilibria obtained from the continuous model, indicates similar trends. Figure 4.4 shows eigenvectors

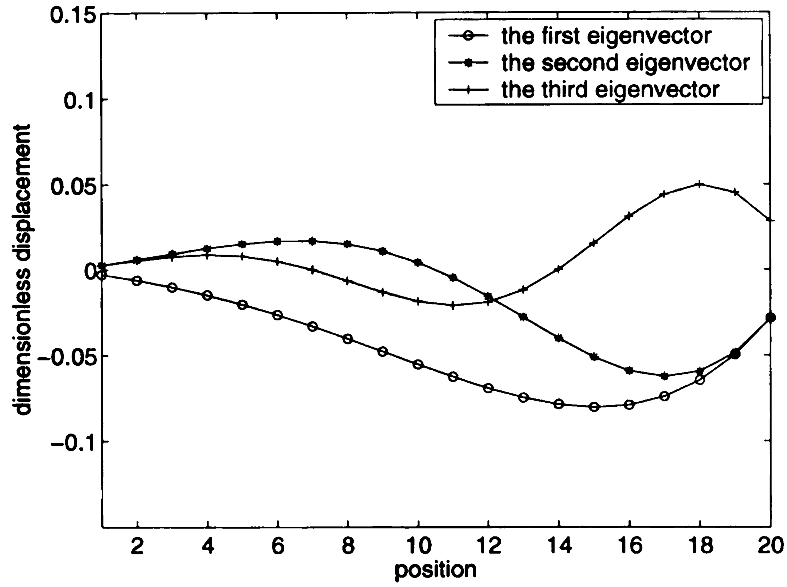

Figure 4.4. The non-symmetric eigenvectors corresponding to the three lowest eigenvalues.

corresponding to the three lowest frequencies. These results show a close approximation to the exact eigenfunctions obtained from the continuous model in Figure 2.6. It is verified that the non-symmetric system matrix produces the non-symmetric eigenvectors. It is concluded that the system does not have any unstable motions by the effects of parameter μ assuming that the coefficient of friction is constant with respect to relative speed.

4.3.2 Addition of Damping

In this section by including damping we evaluate the dynamic stabilities and show the effect of damping on the system stability. Three typical damping are included: external, internal, and general friction damping. In the previous chapters we investigated the system stability by the effects of damping. Because it is difficult to find analytical solutions by including a negative-slope friction damping we did not adopt the negative-slope friction damping in the previous model. In this section we evaluate the system stability by including a negative-slope friction damping.

The equation of motion including the damping is

$$\begin{aligned} m\ddot{x}_i(t) &+ d\dot{x}_i(t) + \gamma\{-\dot{x}_{i-1}(t) + 2\dot{x}_i(t) - \dot{x}_{i+1}(t)\} \\ &+ k\{-x_{i-1}(t) + 2x_i(t) - x_{i+1}(t)\} + f_i(t) = 0, \end{aligned} \tag{4.19}$$

where the parameter d, γ, and $f_i(t)$ represent the external, internal and frictional damping, respectively. The frictional force including the effect of Poisson's ratio is

$$\begin{aligned} f_i(t) &= \mu N_i(t) \\ &= \mu[N_0 + \nu\{k(x_i - x_{i-1}) + \gamma(\dot{x}_i - \dot{x}_{i-1})\}]. \end{aligned} \tag{4.20}$$

Let us assume the friction characteristics in friction-speed relations is

$$\begin{aligned} \mu = \mu(\dot{x}_i) &= \text{sign}(V - \dot{x}_i)\{\mu_s + (\mu_s - \mu_k)e^{-c_3|V-\dot{x}_i|}\}, \\ &= \text{sign}(V - \dot{x}_i)\{c_1 + c_2\, e^{-c_3|V-\dot{x}_i|}\}, \end{aligned} \tag{4.21}$$

where the μ_s and μ_k represent static and dynamic coefficient of friction, respectively ($\mu_s > \mu_k$) and the c_3 has a positive value. The typical friction force $f_i(t)$, which is dependent on the relative slipping speed between the i_{th} mass and driving speed V,

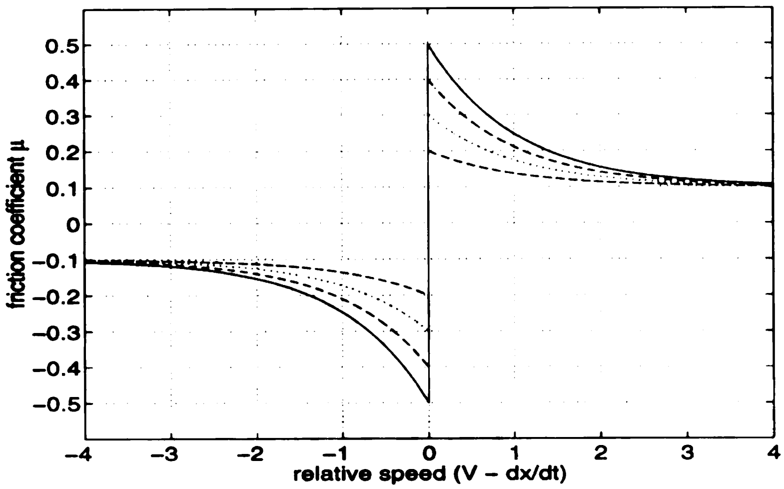

Figure 4.5. The discontinuous coefficient of friction μ versus relative velocity $|V - \dot{x}_i|$. The coefficients of friction are represented by $\mu = \text{sign }(V - \dot{x}_i)\ \{c_1 + c_2 e^{-c_3|V-\dot{x}_i|}\}$, where $c_1 = 0.1, c_3 = 1.0$, and $c_2 = 0.1$ for the dashed line, $c_2 = 0.2$ for the dotted line, $c_2 = 0.3$ for the dash dot line, and $c_2 = 0.4$ for the solid line.

is shown in Figure 4.5.

Substituting equation (4.20) to equation (4.19), the non-linear coupled equation of motion is obtained as

$$\begin{aligned} \ddot{x}_i &+ \gamma\{-(1+\mu\nu)\dot{x}_{i-1} + (d/\gamma + 2 + \nu\mu)\dot{x}_i - \dot{x}_{i+1}\} \\ &+ \{-(1+\mu\nu)x_{i-1} + (2+\mu\nu)x_i - x_{i+1}\} + \mu N_0/k = 0, \end{aligned} \tag{4.22}$$

where the time derivative ($\dot{}$) implies $\frac{\partial}{\partial\tau}$ with $\tau = \omega_p t,\ \omega_p^2 = k/m = 1$.

Examining the system's dynamic stability can be facilitated by change coordinates with respect to the static equilibrium state. The total displacements $x_i(t)$ are represented by $\bar{x}_i + y_i(t)$, where the $\bar{x}_i$ denotes the static equilibria satisfying the equilibria status, i.e., $\dot{x}_i = \ddot{x}_i = 0$, and the $y_i(t)$ indicates small displacement around

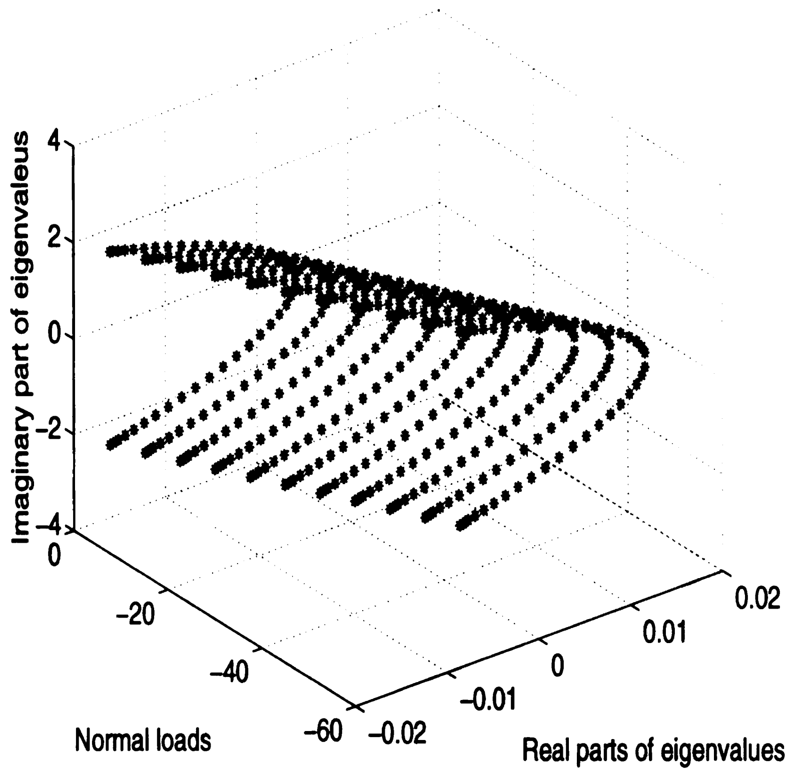

Figure 4.6. The locus of eigenvalues with varying normal loads for the damped model under a fixed boundary condition. The normal load is increased by 5.0 N. Here $\gamma = 0.01, d = 0, c_1 = 0.1, c_2 = 0.2$, and $c_3 = 5.0$ are selected.

the static equilibria. By taking the Taylor series expansion for the friction forces the linearized equations of motion with respect to equilibria are obtained. The static equilibria satisfies the following equation.

$$\mathbf{K\bar{X}} = \mathbf{F_0}, \tag{4.23}$$

where the $\mathbf{\bar{X}}$ is composed of $[\bar{x}_1, \bar{x}_2, \ldots, \bar{x}_n]^T$ and $\mathbf{F_0} = -\mu(0)N_0/k[1, 1, \ldots, 1]^T$. And

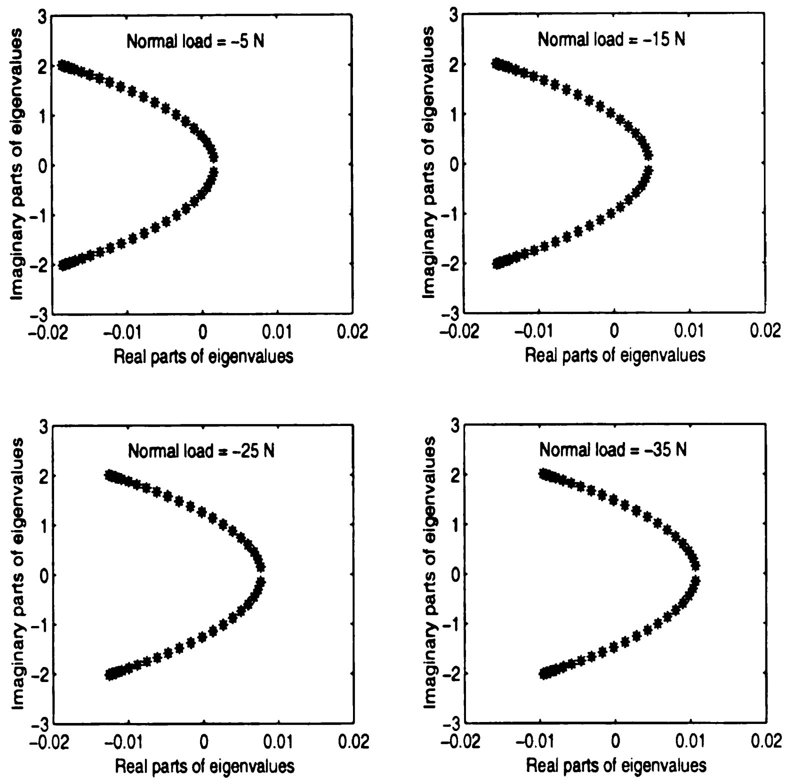

Figure 4.7. The detailed presentations of the eigenvalues by increasing the normal loads.

the linearized equation of motion with respect to the equilibria is

$$\mathbf{M}\ddot{\mathbf{Y}} + \mathbf{C}\dot{\mathbf{Y}} + \mathbf{K}\mathbf{Y} = \mathbf{0}, \tag{4.24}$$

where $\mathbf{M}$ is the identity matrix, $\mathbf{K}$ is the same stiffness matrix to the undamped model in (4.8), and the $\mathbf{Y}$ represents $[y_1, y_2, \ldots, y_n]^T$. The resultant damping matrix

$\mathbf{C}$ is

$$\mathbf{C} = \begin{bmatrix} c_{11} & -\gamma & 0 & \dots & 0 & 0 \\ -\gamma(1+\nu\mu(0)) & c_{22} & -\gamma & \dots & 0 & 0 \\ 0 & -\gamma(1+\nu\mu(0)) & c_{33} & \dots & 0 & 0 \\ \dots & \dots & \dots & \dots & \dots & \dots \\ 0 & 0 & 0 & \dots & -\gamma(1+\nu\mu(0)) & c_{nn} \end{bmatrix}, \quad (4.25)$$

where

$$c_{ii} = d + \gamma\{2 + \nu(c_1 + c_2 e^{-c_3 V})\} + (c_2 c_3 e^{-c_3 V})[\nu\{\bar{x}_i - \bar{x}_{i-1}\} + N_0/k].$$

The elements in $\mathbf{C}$ are evaluated with respect to the static equilibria and they are affected by the normal loads and friction forces. Consequently, the friction forces and the Poisson's ratio are responsible for the non-symmetric properties of $\mathbf{K}$ and $\mathbf{C}$. The system matrix in the form of state space is

$$\mathbf{M}^*\dot{\mathbf{Z}} + \mathbf{K}^*\mathbf{Z} = \mathbf{0}, \quad (4.26)$$

where the $\mathbf{Z}$ is defined as $[\dot{\mathbf{Y}} \vdots \mathbf{Y}]$. Here the $\mathbf{M}^*, \mathbf{K}^*$ are defined by

$$\mathbf{M}^* = \begin{bmatrix} \mathbf{M} & \mathbf{0} \\ \mathbf{0} & -\mathbf{K} \end{bmatrix}, \quad \mathbf{K}^* = \begin{bmatrix} \mathbf{C} & \mathbf{K} \\ \mathbf{K} & \mathbf{0} \end{bmatrix}. \quad (4.27)$$

This eigenvalue problem should be solved by following the general eigenvalue problems, which are discussed in the previous section, since it has non-symmetric properties. When there is a negative slope in friction characteristic ($c_3 > 0$) the whole system is destabilized by the resultant negative damping as the normal load increases. In the compressive region, ($\bar{x}_i - \bar{x}_{i-1} < 0$), destabilizing effects are amplified. Obviously, external and internal damping have stabilizing effects as presented in (4.25).

Figure 4.6 shows the locus of the eigenvalues with varying normal loads when the coefficient of friction is expressed by equation (4.21). For small normal loads with sufficient external and internal damping, the system is stable because the maximum real parts of the eigenvalues is negative. When the normal load increases and produces large compressive stress some eigenvalues placed in the left half plane approach and cross over the imaginary axis. Then the system contains at least one positive real eigenvalue, which indicates dynamic instability. The detailed transition steps of the eigenvalues are shown in Figure 4.7 with varying the normal loads.

4.4 A Lumped-Parameter Model under a Periodic Boundary Condition

4.4.1 A Stability Analysis of an Undamped System

The onset of self-excited oscillations in a continuous medium by linear instability has been investigated by several researchers (Adams[24, 23], Martins *et al.*[25]). According to these studies a system with a periodic boundary condition becomes unstable in the form of self-excited motions for any finite driving speeds even under a constant friction coefficient.

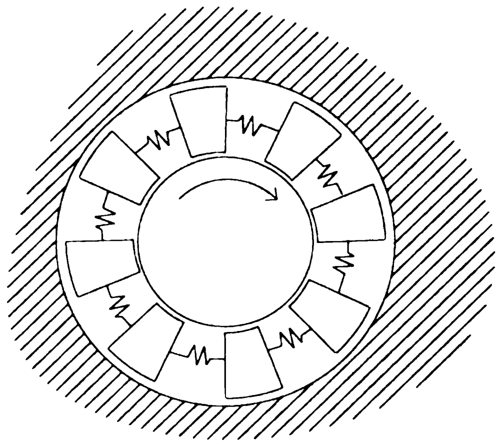

Figure 4.8. A schematic diagram for the lumped-parameter model with a periodic boundary condition.

Figure 4.8 shows a schematic diagram of the bushing system represented by lumped elements. Assuming that any motions are expressed by circular coordinates and any centrifugal effects are neglected (large radius), an equation of motion for the undamped mass is

$$m\ddot{x}_i(t) + k\{-(1+\mu\nu)x_{i-1}(t) + (2+\nu\mu)x_i(t) - x_{i+1}(t)\} + \mu N_0 = 0, \tag{4.28}$$

where the friction coefficient μ is a constant. The periodic boundary conditions are

$$\begin{aligned} x_1(t) &= x_{n+1}(t), \\ \frac{dx_1(t)}{dt} &= \frac{dx_{n+1}(t)}{dt}, \end{aligned} \tag{4.29}$$

which represent the ring-shaped configuration in Figure 4.8.

The system matrices consist of an identity mass matrix $\mathbf{M}$ and the stiffness matrix

$$\mathbf{K} = \begin{bmatrix} 2+\nu\mu & -1 & 0 & \dots & 0 & -(1+\nu\mu) \\ -(1+\nu\mu) & 2+\nu\mu & -1 & \dots & 0 & 0 \\ 0 & -(1+\nu\mu) & 2+\nu\mu & \dots & 0 & 0 \\ \dots & \dots & \dots & \dots & \dots & \dots \\ -1 & 0 & 0 & \dots & -(1+\nu\mu) & 2+\nu\mu \end{bmatrix}. \quad (4.30)$$

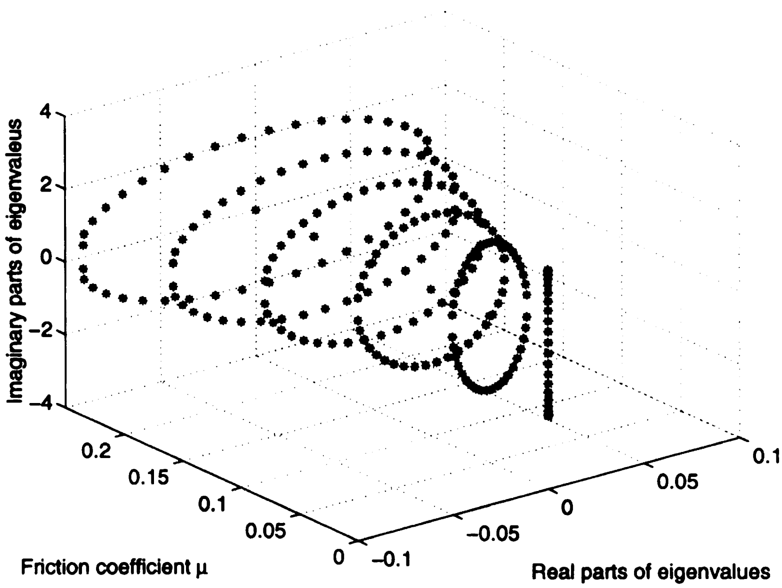

Figure 4.9. The locus of eigenvalues with varying μ for the undamped lumped-parameter model under a periodic boundary condition. Here μ is increased by 0.05.

Figure 4.9 shows the locus of eigenvalues with various values of μ, where μ is assumed a constant with respect to relative speed. When μ equals to zero, all eigen-

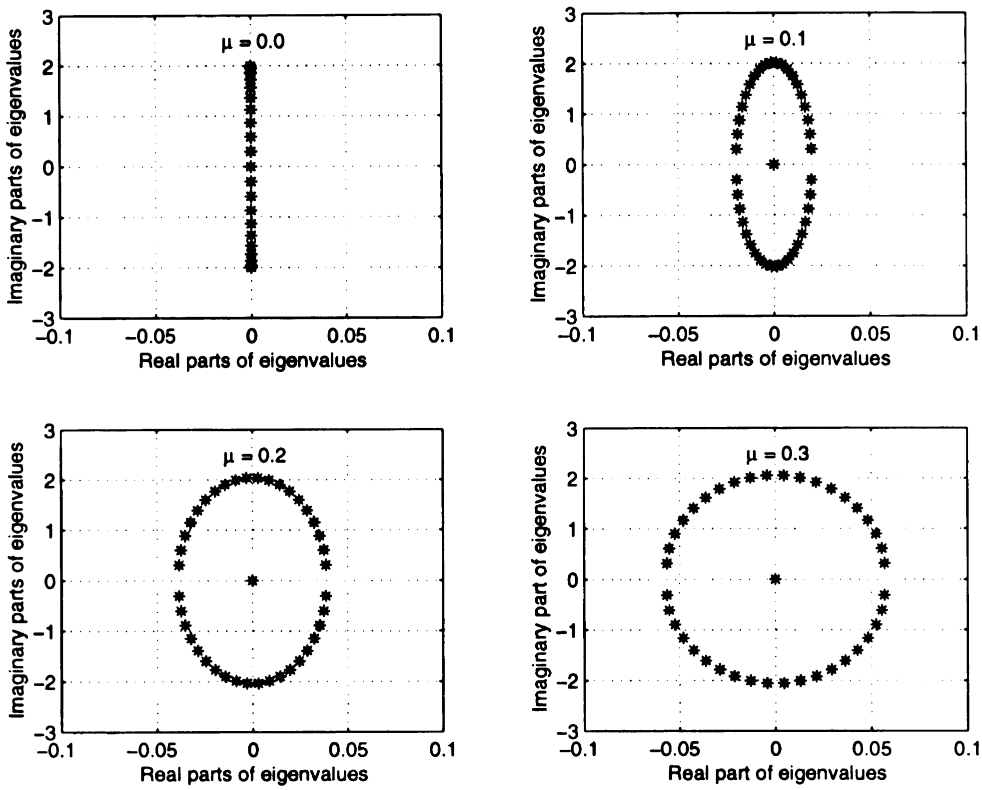

Figure 4.10. The detailed presentation of the trajectories of the eigenvalues by increasing the friction coefficient.

values are located on the imaginary axis, which represents marginally stable pure oscillations without increasing and decreasing motions. As the friction coefficient μ increases, complex conjugate eigenvalues, which have positive and negative real components, come into existence (Figure 4.10). Any non-zero value in the friction coefficient destabilizes the system. Comparing this result to those in Chapter 3, similar trends are found. According to equation (3.6) in Chapter 3, the low frequency terms (for small k) have a crucial role in destabilization since they have large imaginary components in the characteristic equation. (Remember that in the analysis in Chapter 3, the imaginary part of the characteristic solution determines overall system stabilities.

Refer to Figure 3.1 for the unstable solutions.) Figure 4.10 verifies this trend by showing the large positive real eigenvalue corresponding to the low frequencies. Here the zero eigenvalue indicates the rigid body motion with no oscillations.

4.4.2 Addition of Damping

Consider the system again by including internal, external and general frictional damping. The equation of motion has the same form as equation (4.22). In order to find the linear stability, take the coordinate change with respect to the static equilibrium, and followed the same procedures of the previous section. Then linearized equation of motion with respect to the equilibria is

$$\mathbf{M}\ddot{\mathbf{Y}} + \mathbf{C}\dot{\mathbf{Y}} + \mathbf{K}\mathbf{Y} = \mathbf{0}, \tag{4.31}$$

where $\mathbf{M}$ and $\mathbf{K}$ are identical to that of the undamped system. The damping matrix is

$$\mathbf{C} = \begin{bmatrix} c_{11} & -\gamma & 0 & \dots & 0 & -\gamma(1+\nu\mu(0)) \\ -\gamma(1+\nu\mu(0)) & c_{22} & -\gamma & \dots & 0 & 0 \\ 0 & -\gamma(1+\nu\mu(0)) & c_{33} & \dots & 0 & 0 \\ \dots & \dots & \dots & \dots & \dots & \dots \\ -\gamma & 0 & 0 & \dots & -\gamma(1+\nu\mu(0)) & c_{nn} \end{bmatrix} \tag{4.32}$$

.

where

$$c_{ii} = d + \gamma\{2 + \nu(c_1 + c_2 e^{-c_3 V})\} + (c_2 c_3 e^{-c_3 V})[\nu\{\bar{x}_i - \bar{x}_{i-1}\} + N_0/k].$$

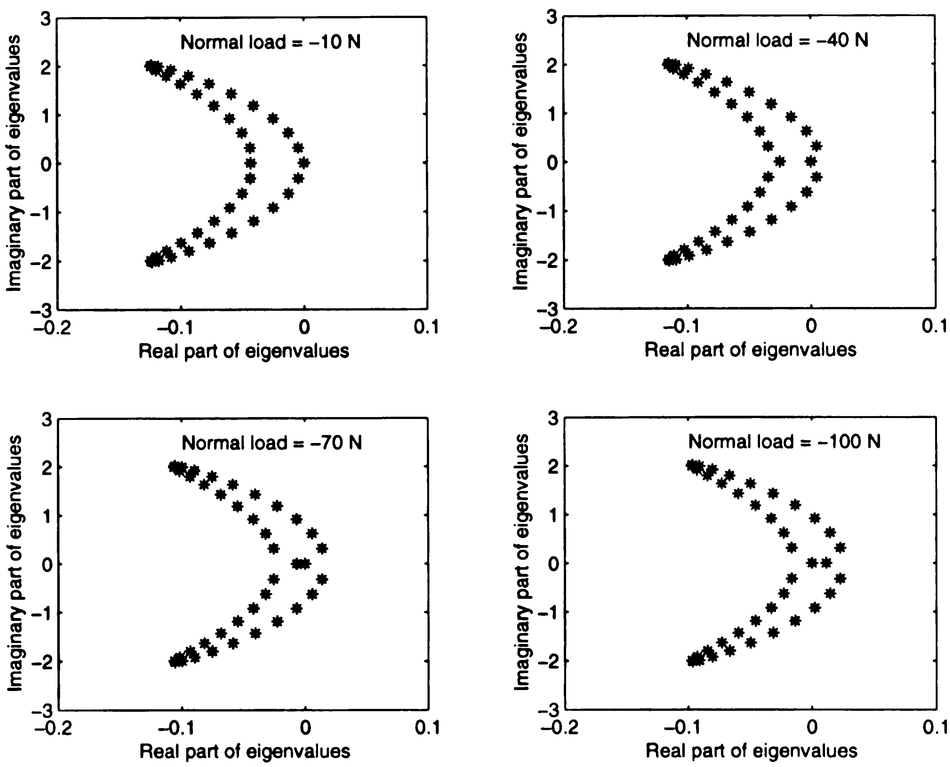

Figure 4.11. Trajectories of the eigenvalues for the damped lumped-parameter model under a periodic boundary condition. Here $\gamma = 0.05, d = 0.05, c_1 = 0.1, c_2 = 0.2$, and $c_3 = 5.0$ are selected.

Figure 4.11 shows locus of eigenvalues with varying normal loads. When the normal load is relatively small, the eigenvalues are placed on the left side of complex plane, which indicates that the system is stable due to sufficient damping. However, as the normal load increases the eigenvalues move toward the imaginary axis from the left-half plane and cross over the imaginary axis at critical value of normal load. This produces positive real eigenvalues and makes the system unstable.

4.5 Conclusion

In this chapter the discretized lumped-parameter model has been established. In the lumped-parameter model, the stiffness matrix is non-symmetric due to the friction force. The general eigenvalue problem, which dealt with the non-symmetric eigenvalue problem, was reviewed and the linear stability was evaluated.

Under the fixed boundary condition, the system is marginally stable when the friction is a constant. This result is consistent with the exact results obtained in Chapter 2. External and internal damping stabilize the system. On the other hand, friction damping which has a negative slope in friction-speed relation destabilizes the overall system. Under the periodic boundary condition the system becomes unstable one even with a constant coefficient of friction. This is also consistent with the results obtained in Chapter 3.

The consistency of results from the lumped-parameter system suggest that such a discretization of the non-symmetric problem converges to true solutions without having contradictory results. Thus we can use this lumped-parameter model for further non-linear studies. We will use this lumped-parameter model in Chapter 5 in order to investigate non-linear phenomena.

CHAPTER 5

STICK–SLIP OSCILLATIONS

5.1 Introduction

Investigation and characterization of dynamic responses of systems subjected to friction are made difficult by the presence of stick-slip oscillations. Such stick-slip oscillations have been believed to be responsible for mechanisms of generating the noise and vibrations. In explanations of such noise generating mechanisms most of the previous researchers have devoted their efforts on system stabilities and characterizations by using low-dimensional models.

Dynamic behaviors of multi-degree-of-freedom models including the stick-slip oscillations were investigated by Awrejcewicz and Delfs [89, 90]. They showed the qualitative changes of equilibria by changing system parameters and explained numerical integration techniques applicable to problems involving stick-slip oscillations. Later, Pfeiffer [91] studied the turbine blades as a multi-dimensional stick-slip system. Popp has explained and reviewed the previous stick-slip systems with various examples [78, 79].

In addition, some works have focused on the characterization of stick-slip oscillations induced by friction. Stelter and Sextro [85] investigated the characterization of one- and two-degree-of-freedom frictional systems and provided the bifurcation behaviors due to friction. Later, Galvalnetto *et al.* [86, 87] investigated the stick-slip vibrations of two-degree-of-freedom mechanical model. They showed that the global dynamics of the system can be characterized by the periodic, quasi-periodic, and chaotic oscillations in presence of friction.

Most of the previous research, however, has dealt with the models having low degrees of freedom, and with simplified friction models, such as the point-contact model. A distributed friction system has been eluded in most of the previous studies since it is hard to implement and analyze through numerical or experimental approaches.

In spite of these difficulties, several approaches using distributed contact systems have been found in areas of the geophysics. The model consisting of blocks of masses has been used to describe the earthquake fault phenomena and have explained the dynamics of the multi-dimensional systems with stick-slip oscillations [95, 96, 97, 98]. Carlson and Langer [96, 97, 98] have incorporated stick-slip phenomena and provided mechanisms responsible for noise and the sequences of earthquake-like events. Extended ideas to chaotic behaviors of earthquake events are found by Huang and Turcotte [88].

Through experiment, the generation mechanisms for noise and vibrations in a distributed contact friction system have been investigated. Vallette and Gollub [101] studied the stick-slip oscillations of a spatiotemporal system by means of stretched latex membranes in contact with a translating glass rod and measured the internal displacement field, $u(x,t)$, with imaging techniques. They showed the experimental behaviors of the stick-slip motions as propagating waves. Some other works related to elastomeric friction systems are found in the works by De Togni *et al.* [99] and Rorrer [100]. However, the analytical and numerical approaches for investigating the mechanism responsible for noise and vibrations induced by friction need further development.

Here are issues to be addressed through this study. The mechanisms responsible for the generation of the stick and slip oscillations in elastic media subjected to a distributed friction contacts are to be identified. In addition, the system parameter effects on the generation of such noise need to be investigated through this study.

In this chapter, a discretized multi-degree-of-freedom model is adopted to analyze the dynamic behaviors of the elastic media subjected to distributed friction. We choose the lumped-parameter model established in Chapter 4, because its linear stability is convergent and it is straight forward to simulate and analyze stick-slip motions. The numerical techniques in handling the stick-slip oscillations are presented and the detailed explanations associated with the stick-slip oscillations are provided. The contributions of parameters, such as a normal load, a driving speed, the Poisson's ratio, and friction characteristics, are studied and their influences on the stick-slip noise generation are explained. In this numerical study we also choose a particular set of initial conditions, which have to do with motivational topic of a squeaky bushing. The initial conditions are chosen as stuck since that might be representative of bushing at beginning of some maneuver. We also seek the possibility of sustained stick-slip motions regardless of linearized stability in this chapter.

5.2 Numerical Aspects of Stick-Slip Phenomena

When a system is modeled as a discretized multi-degree-of-freedom and expected to undergo alternating stick-slip oscillations during a time of interest, a numerical algorithm to simulate the system behavior needs a special attention in handling the problem. Since the alternating stick-slip oscillations produce a time-varying degree of freedom and a time-varying boundary condition, an analytical approach looking for the system behaviors is not an easy job and is limited only for a low-degree-of-freedom system.

Theoretical backgrounds for handling such problems have been presented by several researchers, who have formulated the switching contact status in terms of constraint indicator functions (Pfeiffer [111], Glocker and Pfeiffer [113], and Wösle and Pfeiffer [114]). For example, impulsive and stick-slip phenomena for percussion drilling machines (Glocker and Pfeiffer [113]), assembling and mating processes (Pfeiffer and Glocker [112]), and frictional damping in turbine blade (Pfeiffer and Hajeck [91]) have been analyzed with the constraint indicator functions. The described phenomena, such as the stick-slip motions, the sliding-stop motion device, and the impulsive impact process, have a common fact that the beginning and end of any of the changing status are always represented by certain constraint indicator functions, which are controlled by the dynamical process itself.

Let us consider the system of interest which includes distributed friction force.

Though the switching status, i.e., the changes from stick to slip, or vice versa, influences the system's degree of freedom and results in the variable multi-degree-of-freedom systems, their motions are simply categorized by "stick" or "slip" state dependent on their state variables. The undamped, n degree-of-freedom, lumped-parameter model constructed in Chapter 4 is represented by

$$m\ddot{x}_i(t) + k\{-x_{i-1}(t) + 2x_i(t) - x_{i+1}(t)\} + f_i(t) = 0, \qquad i = 1, 2, \ldots, n. \tag{5.1}$$

This can be rewritten as

$$m\ddot{x}_i(t) + g_i(x_{i-1}, x_i, x_{i+1}) + f_i(t) = 0, \qquad i = 1, 2, \ldots, n, \tag{5.2}$$

where $f_i(t)$ and $g_i(t)$ are implicitly time dependent variables. The $f_i(t)$ is the friction force and $g_i(t)$ is the elastic force exerted to the i_{th} mass at specific time t. (See the system configuration in Figure 4.1.)

By setting kinetic and kinematic constraint indicator functions, which signal the beginning and end of each switching status, the status of the i_{th} lumped mass is determined as stick or slip. The kinetic constraint indicator function $h_i(t)$ is defined by

$$h_i(t) \stackrel{\text{def}}{=} |f_i(t)| - |g_i(t)|, \tag{5.3}$$

which indicates a magnitude difference of elastic spring and friction forces. Similarly, the kinematic constraint indicator function $s_i(t)$ is defined by

$$s_i(t) \stackrel{\text{def}}{=} v_{rel,i} = \dot{x}_i - V, \tag{5.4}$$

where the $s_i(t)$ indicates the relative velocity between the i_{th} mass and the driving speed V.

The condition $h_i(t) \geq 0$ with zero relative velocity ($s_i(t) = 0$) implies the "stick state", which means that the i_{th} mass remains without relative motion with respect to the moving rigid body. In this state friction force is sufficient to counteract against elastic force, so a mass can remain without having relative motion. The condition of non-zero relative velocity ($s_i(t) \neq 0$) represents the "slip state", which means the i_{th} mass has relative motion with respect to the moving rigid body at specific time t. In between the two states, there always is an instant in which the signs of the constraint indicator functions changes. At this moment, called an event, the kinetic and kinematic constraint functions are always complementary. Thus their scalar product is always zero (Pfeiffer [111]).

Detection of events during each integration time step in digital computation needs highly accurate numerical techniques. Calculation of the accurate switching moments, which determine the beginning and end of the friction events causing the time-variant or unsteady topological behaviors, influences the quality of the solutions.

The concepts of adapted integration algorithms are presented as follows. Firstly, an ϵ-limit should be chosen for computational tolerance. Then integration take place over a predetermined time interval $[t_0, t_1]$, during which indicator functions are checked in order to detect the switching time if any events occur in that time interval. Let us check the kinematic indicator function for the i_{th} mass. If the relation

$$s_i(t_0) \cdot s_i(t_1) \ < \ 0 \tag{5.5}$$

holds during the time interval $[t_0, t_1]$, this indicates that the kinematics events happened during the interval. Then an adapted integrated time t_{s_i} is evaluated from the equation

$$\mid s_i(t_{s_i}) \mid < \ \epsilon_i^s, \tag{5.6}$$

where the t_{s_i} should be detected by several backstepping iterations to satisfy the equation (5.5) within the kinematic accuracy limit ϵ_i^s.

Similarly, the kinetic constraint indicator function is checked. If the relation

$$h_i(t_0) \cdot h_i(t_1) \ < \ 0 \tag{5.7}$$

holds during the time interval $[t_0, t_1]$, an adapted integrated time t_{h_i} is evaluated based on the equation

$$\mid h_i(t_{h_i}) \mid < \ \epsilon_i^h \tag{5.8}$$

in order to satisfy the kinetic accuracy limit ϵ_i^h.

Considering a n degree-of-freedom model with n possible constraints, the time instant for which a change of status first occurs should be determined. The smallest time step in kinematic event $t_{s_{min}}$ is defined by

$$t_{s_{min}} = \min_{i=1,2,\ldots,n} \{t_{s_i} \mid s_i(t_{s_i}) = 0\}, \tag{5.9}$$

and the smallest time step in kinetic event $t_{h_{min}}$ is also defined by

$$t_{h_{min}} = \min_{i=1,2,\ldots,n} \{t_{h_i} \mid h_i(t_{h_i}) = 0\}. \tag{5.10}$$

Therefore, the final smallest adapted time integration step t_f is selected by

$$t_f = \min\{t_{s_{min}}, t_{h_{min}}\}. \tag{5.11}$$

After finding the final adapted time integration step t_f, the ending time is set to t_f instead of t_1 in integration time interval on $[t_0, t_f]$.

5.3 Stick-Slip Oscillations with Fixed Boundary Conditions

Numerical investigations for stick-slip oscillations using the lumped-parameter model subjected to a distributed frictional contact are conducted to seek mechanisms related to generating noise and vibrations. In this section descriptions of system configurations and investigations related to stick-slip oscillations are presented.

5.3.1 Conditions of Numerical Simulations

In this study the adaptive step size Runge-Kutta-Fehlberg integration methods using a fourth and fifth pair, which have been proved to have high accuracies with small time steps, are used in numerical integrations. In order to acquire the high quality simulation results small predetermined integrations time steps are selected. Regarding

Normal Load	Friction			Mass	Stiffness	Poisson's ratio	Driving Speed
$N_0[N]$	c_1	c_2	c_3	m [kg]	k [N/m]	ν	V [m/s]
-1.0	0.1	0.2	0.1	1.0	1.0	0.4	+1

Table 5.1. The typical system parameters selected for numerical simulations in Chapter 5.

to the system configuration, twenty blocks of lumped-masses connected with linear springs are placed under evenly distributed normal loads. (Mass positions are assigned from left to right direction in Figure 4.1.) In addition, fixed boundary conditions are imposed at both ends. Neither external or internal damping is included in this development. The friction-speed relations, which have primary effects on the stability and dynamic behaviors, are expressed by equation (4.21), i.e.,

$$\mu = \mu(\dot{x}_i) = \text{sign}(V - \dot{x}_i)\{c_1 + c_2\, e^{-c_3|V-\dot{x}_i|}\}. \tag{5.12}$$

Since we have already investigated Coulomb friction effects on system stability we choose the speed-related friction model in this chapter. The typical parameter values selected in numerical simulations are summarized in Table 5.1. Throughout this chapter, the same initial conditions are imposed for all numerical studies: zero relative velocities and zero initial displacements to all masses. The set of initial conditions might be a representative of bushing at beginning of some maneuver.

5.3.2 Investigations of Stick-Slip Oscillations

In this section stick-slip oscillations of the one dimensional multi-degree-of-freedom system are presented and their dynamic characteristics are explained based on their numerical results. Investigations based on displacements and velocity responses with typical initial conditions in Table 5.1 are performed.

Analyses based on the Velocity Response

Figure 5.1 shows the time evolution of the mass velocities. At the beginning of the time evolution, all masses move together with the moving rigid body. For better presentation the velocities are placed on the negative velocity axis, so -1 [m/s] indicates the driving velocity. The potential energies in the left and right ended springs gradually increase as the rigid body moves. There are particular moments, such that the increased spring forces are no longer resisted by the counting frictional forces. At this moment the masses begin to slide on the driving rigid body, which implies the stick to slip event.

The sudden changes in motions from the stick to slip state give the momentum to the neighbor masses and sometimes can trigger series of events in a short time like falling "domino blocks". The slip motions are shown as the peaks in Figure 5.1.

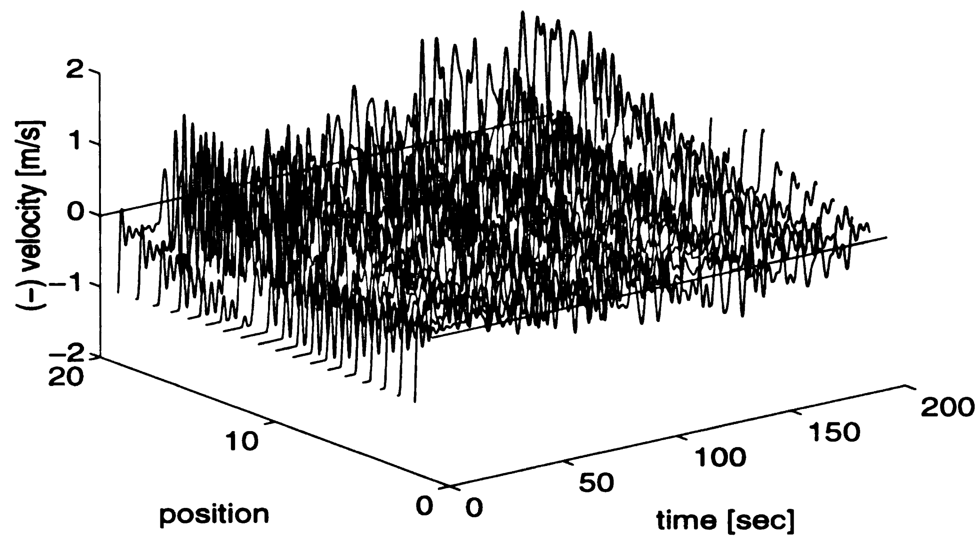

Figure 5.1. Velocity responses of stick-slip oscillations for the lumped-parameter model. (The selected parameters are in Table 5.1.)

Phenomena which are similar to that events are also found in nature, for examples, avalanches in a pile of sand and an earthquake fault phenomena. When small amounts of sand are added on a pile of sand very slowly, it is expected to exhibit avalanches once a sandpile achieves steady state.

The earthquake fault phenomena have similar structures. Series of the events of stick-slip motions, sometimes happened only in localized regions or over whole domains of contact, are generated and amplified, which result in the earthquake fault phenomena (Huang and Turcotte[88]). Carlson and Langer [97, 98] and Carlson *et al.* [96] investigated that possible sizes of events and slip wave instabilities for explanation of catastropical events of earthquake faults by using the Burridge and Knoppoff model, which consists of infinite masses connected with springs. They showed that

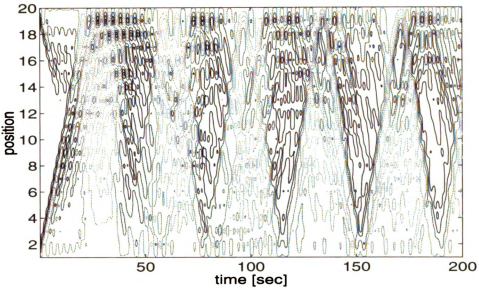

Figure 5.2. A contour plot of the stick-slip response in velocity. (The selected parameters are in Table 5.1.)

such events from stick to slip are responsible for generations of the noise, which are based on the nature of frictional characteristics (Carlson *et al.* [96]). Generally, the difference between static and dynamic friction coefficient (i.e., a condition of $\mu_s > \mu_k$) produces sudden changes in accelerations. The changing forces can influence the neighboring masses. When the systems have large discontinuities in the static and kinetic friction characteristics, their effects on the neighbor masses are generally increased. Detailed explanations about the stick-slip motions related to the friction parameters are shown in the next section.

With the presence of the Poisson's ratio in elastic materials, the stick-to-slip events are more apt to occur in axial tensioned regions then compressive regions. Since in the tensioned region the potentially countable static friction forces are reduced by

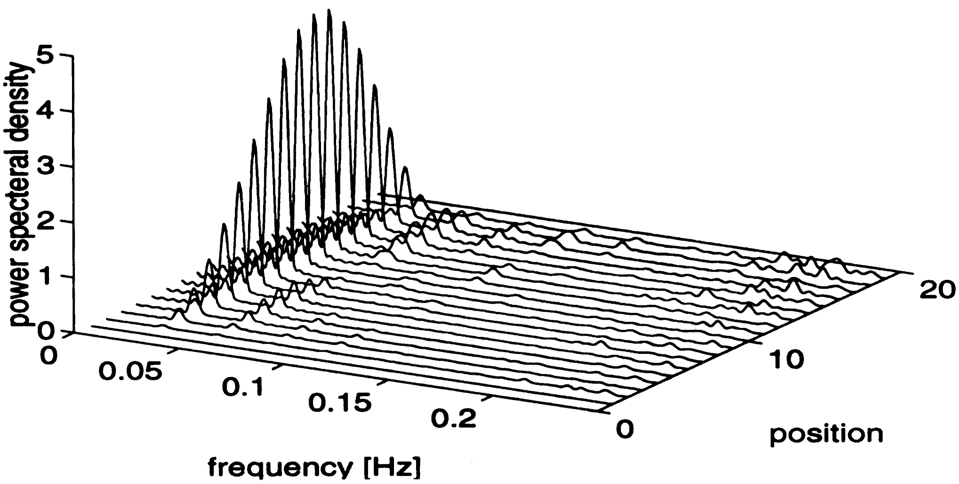

Figure 5.3. A power spectral density of the velocity responses. (The selected parameters are in Table 5.1.)

effects of the Poisson ratio, the stick-to-slip events are more likely initiated from the axially tensioned regions. The stick-to-slip motions, called detachments [26], are first triggered in the axially tensioned regions, and propagate toward the compressive regions. Thus the series of the detachment motions, which are like propagating waves of detachments, travel over the contact domain. They may collide each other and bounced back from the boundary conditions. Shallamach [26] has observed these detachment waves in his experimental works by rubbing a rubber on a hard track.

The series of stick-to-slip events are amplified from the local motions to the whole scale motions. Such stick-to-slip phenomena over whole regions are believed to be responsible for frequencies of the noise. The frequency dependency on the stick-slip motions are investigated in the next section.

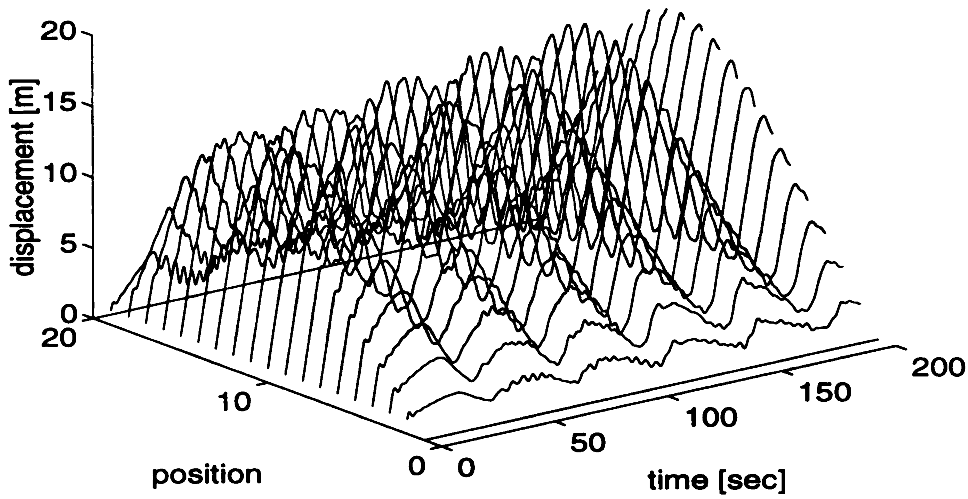

Figure 5.4. Displacement responses of stick-slip oscillations for the lumped-parameter model. (The selected parameters are in Table 5.1.)

Figure 5.2 shows the contour presentation of the velocity responses. The series of stick-slip events, which are shown as the crossing lines from the one boundary to the other boundary, are observed distinctly. The high slipping velocities are observed around the rear masses since the presence of the Poisson's ratio increase the friction forces for the rear masses. (Refer to a configuration of the mass position in Figure 4.1. The rear masses are defined the masses positioned at the end of driving direction. Thus in Figure 4.1 the masses positioned at right hand side are the rear masses.) The power spectral density diagrams (FFT) of the velocity responses are shown in Figure 5.3.

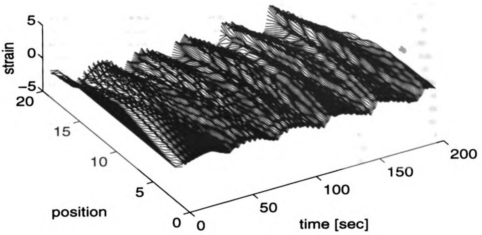

Figure 5.5. Strain presentations from the displacement responses. (The selected parameters are in Table 5.1.)

Analyses based on the Displacement Response

Figure 5.4 shows the displacement responses of the stick-slip oscillations. All the masses oscillate with respect to their static equilibria. Each mass experienced low frequency stick-slip oscillations accompanied by high frequency oscillations. The stick-slip oscillations are not distinguishable in Figure 5.4. By considering the strains, defined by $\Delta x_i(t) = x_i(t) - x_{i+1}(t)$, the releasing strain energies are observed in Figure 5.5.

The strains, which represent the potential energies stored in the connected springs, are released abruptly under the stick-to-slip events in a short time interval. These are seen as the propagating sharp waves of relieved strains. The waves sweeping over the domains represent the series of relieved energy over the stick-to-slip events. The

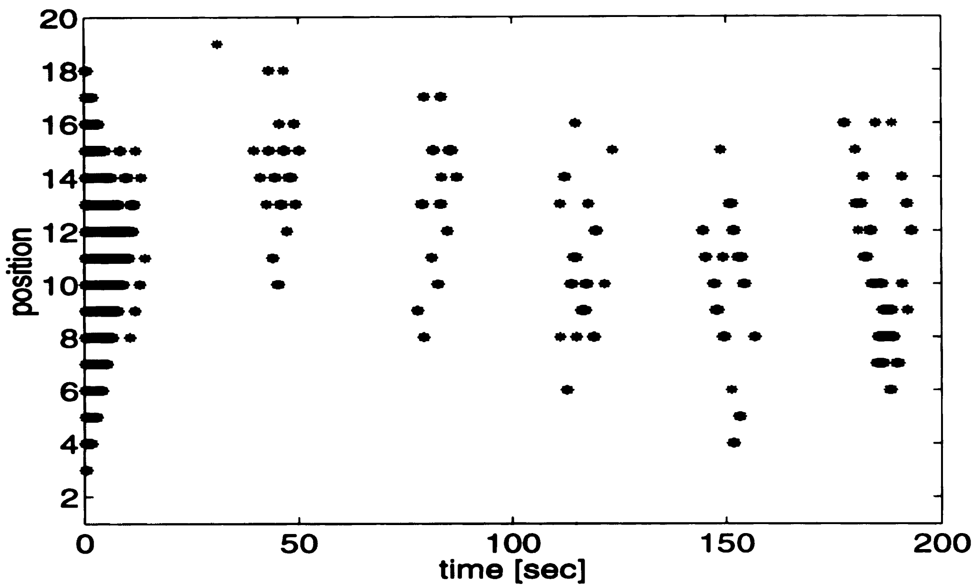

Figure 5.6. Sticking events versus time. The mark '$*$' indicates "the stick state" and the others (the blanks) indicate "the slip state" for each mass. (The selected parameters are in Table 5.1.)

propagating wave speeds are influenced by system parameters and are investigated in the next section. According to the works by Carlson and Langer [97, 98], the small spatial inhomogeneities in displacement are amplified during the large scale stick-to-slip event.

Figure 5.6 shows the time evolution of the sticking regions. The '$*$' marks positions with sticking status in a specific time. The state-space (displacement-velocity) presentations for 5th, 9th, 13th, and 17th positioned masses are shown in Figure 5.7. The each mass experienced stick-slip oscillations with respect to its static equilibrium position.

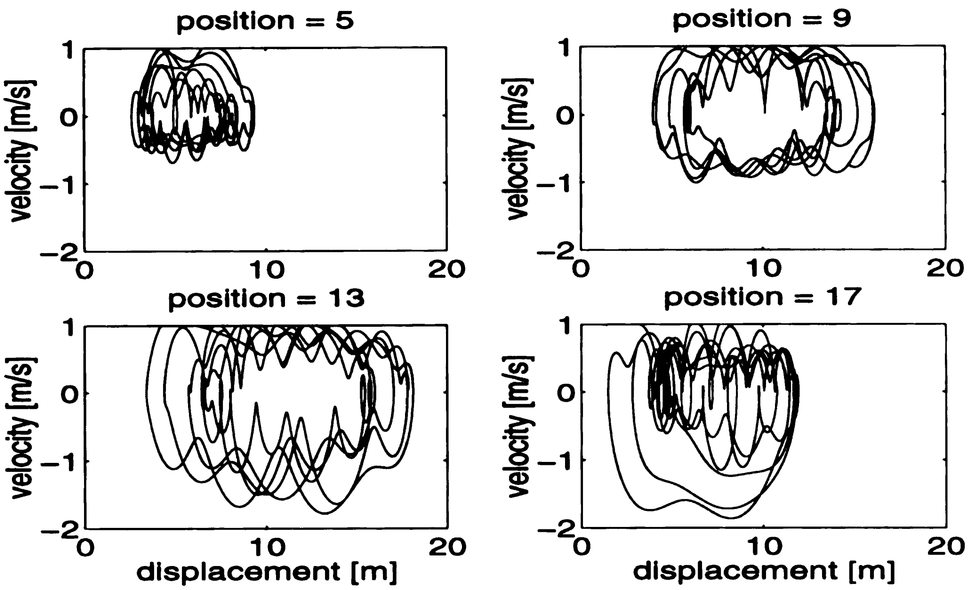

Figure 5.7. State-space (displacement versus velocity) presentations for several positioned masses. (The 5th, 9th, 13th, and 17th positioned masses are shown.) The selected parameters are in Table 5.1.

5.4 Parameter Effects on Stick-Slip Oscillations

Limited studies have been conducted to predict, analysis, and control the stick-slip oscillations resulting the chattering and squealing noise and vibrations. Moreover, experimental investigations of the previous studies have not clearly explained the general mechanisms generating the stick-slip noise and vibrations induced by friction since the experimental results and analyses have been closely related to the experimental apparatuses and operating environmental conditions, such as contact surface conditions and small geometrical misalignment of contacting materials. These may generate non-repeatable responses even in the same operating conditions and may cause difficulty in doing system analyses via systematic approaches. Explanations of the stick-slip mechanisms using mathematical models have not been fully achieved so far, especially for the parameter effects on distributed friction contacts, and systematic approaches for the analyses of the noise generation mechanisms have not been conducted as well.

In this section, analyses and interpretations of numerical results and discussions associated with system parameter effects, such as the normal load, driving speed, Poisson's ratio, and the friction characteristics, are provided.

5.4.1 Effects of Normal Loads

The experimental and analytical approaches in the previous studies have shown that the normal load has a primary influence on the ability to generate noise, and the frequency and intensity of the noise. Generally, the friction-induced noise are distinguished by the chattering and squealing noise according to their frequencies and intensities of noise signals.

The squealing noise is characterized by the high frequency with small amplitudes of oscillations, while the chatter is usually generated at low frequency with relatively large amplitudes and much higher intensity than the squealing noise. For example, in the experiment associated with a rubber-bearing noise investigation by Bhushan [73], the noise which had low frequency characteristics, namely chatter, typically had frequencies around 30 to 310 Hz with the maximum amplitude of 15 μm. On the other hand, the high frequency squealing noise, which had 770 to 830 Hz, had the maximum amplitude of 1.5 μm. Though these frequency values were not typical frequencies representing the chattering and squealing noise, but they were totally dependent on system parameters, especially the normal load. It should be noted that the chattering noise had large amplitude with low frequencies, while the squealing noise had relatively high frequencies and small amplitude from the real experimental results. In the following discussions, the low frequency noise is termed "chatter" and the high frequency noise is termed "squeal" for explanations of the noise signal characteristics.

Figure 5.8 shows responses of displacements of each mass by increasing the normal load with $-1, -5$, and -10 N. The static equilibria for the masses are changed by the normal load. The static equilibria have unsymmetric shapes along the spatial axis and their unsymmetries are amplified as the normal load increases, as can be recalled from the static equilibria for the continuous system in equation (2.6) and for the lumped-model in equation (4.7).

Normal Load	Mass position			
$N_0[N]$	5th mass	9th mass	13th mass	17th mass
-1	7	12	14	10
-5	12	17	17	15
-10	25	40	45	25

Table 5.2. The approximate peak-to-peak amplitudes in displacement responses by changing the normal load.

In Figure 5.9 trends in the velocity response with increasing normal load are shown. The maximum velocity magnitudes are increased as the normal load increases. For

Normal Load	Mass position			
$N_0[N]$	5th mass	9th mass	13th mass	17th mass
-1	1.5	2	1.7	1.8
-5	2.5	3	3	3.5
-10	3.5	5.5	9	7

Table 5.3. The approximate peak-to-peak amplitudes in velocity responses by changing the normal load.

an example, comparing the maximum velocity the velocities in the slipping state reach about 2, 3, and 8 m/sec magnitude when the normal loads are -1 N, -5 N, and -10 N, respectively. (Recall that (-) velocity responses are plotted in Figure 5.9.) Moreover, the amplitude of the stick-slip oscillations (measured by peak-to-peak amplitudes during the stick-slip oscillations) of the displacements and velocities are increased by the normal load increases. As shown in Figure 5.10 of the displacement-velocity presentations of several masses (the 5th, 9th, 13th and 17th positioned mass), the approximate stick-slip oscillating amplitudes are increased in high normal load. Table 5.2 and 5.3 show the summarized approximate peak-to-peak amplitudes in displacement and velocity responses, respectively.

With a closer look in Figure 5.9 and 5.10, small amplitude high frequency oscillations, which are usually superposed on the low frequency responses, are observed. Especially, under the high normal load condition, these small amplitude stick-slip oscillations, called as "creep motions" by Carson and Langer [97, 98], dominate in responses along with the low frequency responses. They attribute the high frequency of stick-slip oscillations, which implies the partial relaxation of strain energy in the form of "small-grouped motions". In this numerical response the localized small-grouped motions are observed under the high normal load condition. Such oscillations are responsible for the high frequency noise (the squeaking noise) under the high normal load. These phenomena can be analyzed by using frequency analysis.

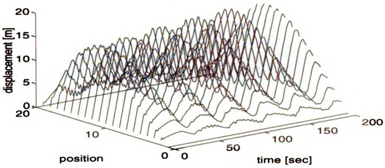

(a)

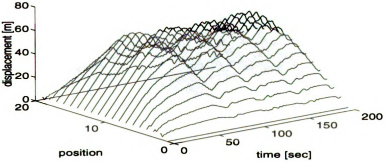

(b)

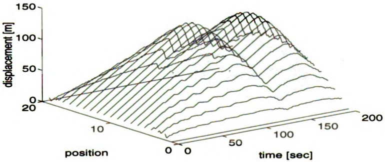

(c)

Figure 5.8. The stick-slip displacement responses for normal loads of (a) $N_0 = -1$ N, (b) $N_0 = -5$ N, (c) $N_0 = -10$ N. The other parameters are in Table 5.1.

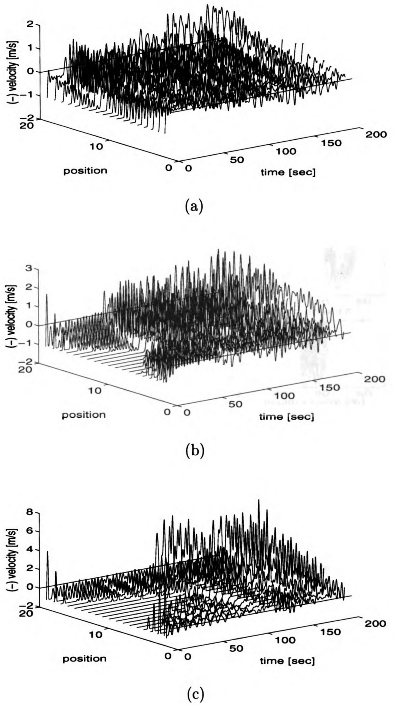

Figure 5.9. The stick-slip velocity responses for normal loads of (a) $N_0 = -1$ N, (b) $N_0 = -5$ N, (c) $N_0 = -10$ N. The other parameters are in Table 5.1.

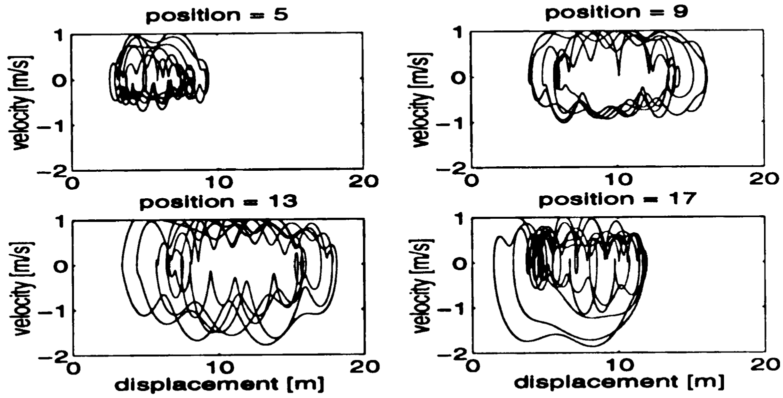

(a)

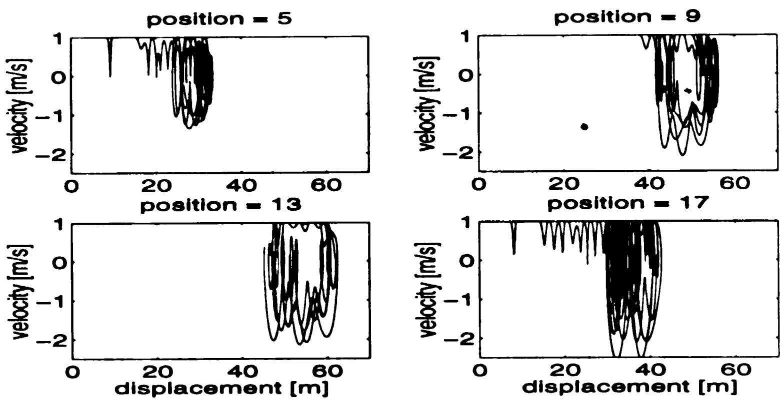

(b)

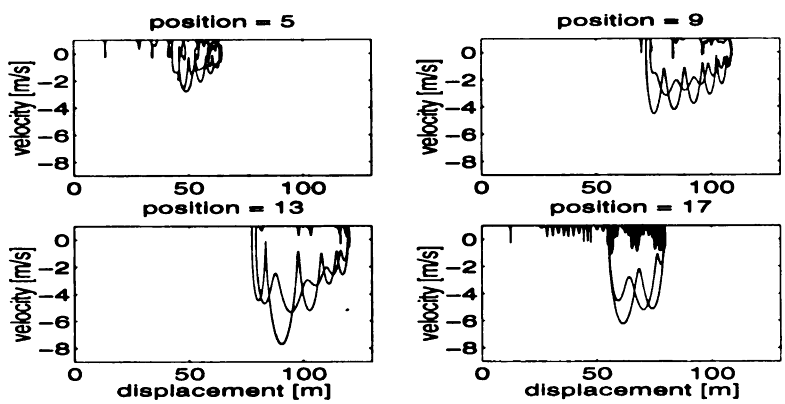

(c)

Figure 5.10. Projections of state-space trajectories (displacement versus velocity) for several positioned masses (the 5th, 9th, 13th, and 17th positioned masses) for normal loads of (a) $N_0 = -1$ N, (b) $N_0 = -5$ N, (c) $N_0 = -10$ N. The other parameters are in Table 5.1.

As shown in Figure 5.11 the intensity of the low frequency spectra, which are lower than 0.05 Hz, increases as the normal load increases. This is a reason for the chattering noise has low frequencies under the high normal load condition. In addition, the high frequency terms are also affected by the normal load. The intensity of high frequency spectra increases as the normal load increases because of the prevailing small-grouped motions in stick-slip oscillations. (The lowest natural frequency of the linear model is 0.0328 Hz.)

As the normal loads increases, the mass positioned in the middle domain (around the middle positioned mass over the twenty masses in this response) experiences low frequency stick-slip oscillations. On the other hand, the masses positioned around the boundary ends show the high frequency oscillations even under the high normal load condition. Note that this stick-slip phenomenon totally depends on the applied boundary conditions. Thereby, if the boundary conditions are changed different stick-slip oscillations are expected.

Consequently, as the normal load increases from -1 N to -10 N, the high normal load contributes to both low and high frequency terms in the noise generated from the stick-slip oscillations. In other words, as the normal load increases the low frequencies of the signals, which are originated from the propagating waves of detachments, are lowered (Dweib and D'Souza [55, 56], Nakai and Yokoi [72, 57], and Bhushan [73]). On the other hand, the high normal load increase the high frequencies of signals, which generally come from the stick-slip oscillations with the localized small-grouped motions.

Strain distributions over the domain can give clear explanations about the strain recoveries. Figure 5.12 shows that the speed of the sweeping strain relief waves are lowered as the normal load increases. On the other hand, the creeping motions in part (c), which are characterized by high frequency small-grouped motions, usually can not give enough strain relief compared to the effects of propagating wave of detachment represented by the crossing lines in Figure 5.12. The propagating waves of detachments have been also observed in the work by Carlson and Langer [97]. They claimed that such motions give large irregularities in strain of the elastic materials after experiencing the stick-slip oscillations. The irregularities are amplified after each event, so the system may experience catastrophic events or chaotic behaviors under the stick-slip oscillations.

By presentations in contour plots, shown in Figure 5.13, the high and low velocity regions are clearly distinguished on the two-dimensional plots. The sweeping waves of detachments are shown as the deflected lines reflecting off the boundary ends. Under the high normal load conditions in Figure 5.13 (c), the transient motions from the initial condition to the formation of the propagating waves of detachments are shown in detail. At the beginning stage in Figure 5.13 (c), from 0 to about 100 seconds of the simulation time, the small-grouped stick-slip motions are initiated and gradually propagate toward the stick regions by repeating the stick and slip oscillations. Because that repetition of the stick-slip oscillations can not release enough strain energies the localized stick-slip motions around the both boundary ends are observed. Such repetitive stick-slip oscillations, which has begun from both boundary ends, proceed until both detachment waves meet each other. At around 110 seconds in Figure 5.13 (c), both proceeding waves of detachments collide and produce large strain reliefs over the entire domain. After such transitions of strain reliefs, finally the large strain relief motions are observed in the form of the waves of detachments over the entire domain. Such phenomena can explain the generating mechanisms of the low frequency chattering noise.

Effects of the normal load on the sticking area, i.e., the contact area, are shown in Figure 5.14. The high normal loads make possible to produce the large sticking areas, which are shown as the extend areas in Figure 5.14 (c). Under the light normal load condition, shown in Figure 5.14 (a), the relatively small sticking areas localized in the middle-positioned masses are observed. However, as the normal load increases (-5 N, -10 N), the sticking areas are enlarged and almost extended to the boundary ends (Figure 5.14 (b) and (c)). These phenomena can be explained by the fact that high static friction force capacity which can hold the masses with no relative motions, $f_i(t)$ in equation (5.2), is increased under the high normal load condition.

On the other hand, under the light normal load condition, stick-slip oscillations are rarely observed since the kinetic constraint indicator functions in equation (5.3) can not easily satisfy the sticking condition. Thus in this condition the oscillations can not experience the stick-slip oscillations and the motions are observed under the pure slipping motions with relatively high frequencies than the stick-slip oscillations. These phenomena are confirmed in Chapter 6 by finite element analysis.

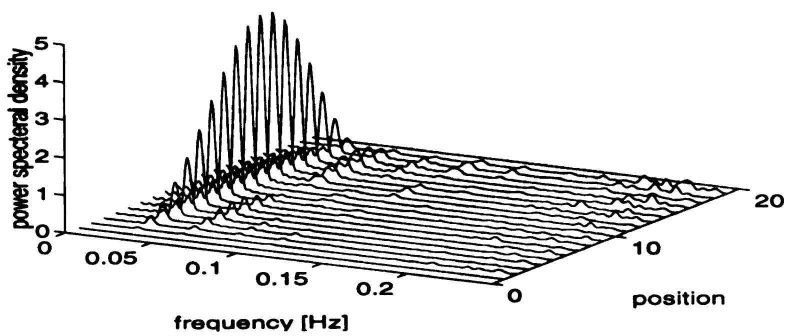

(a)

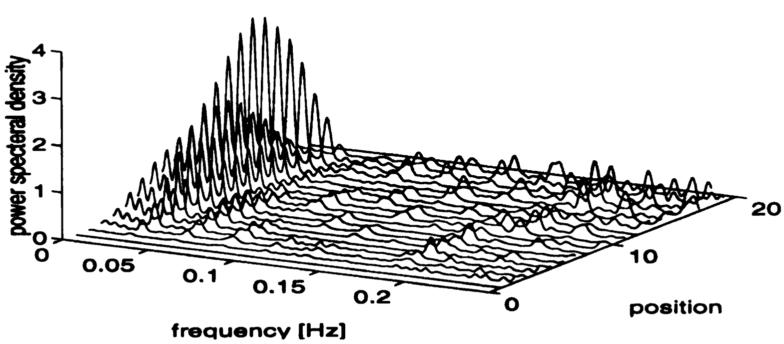

(b)

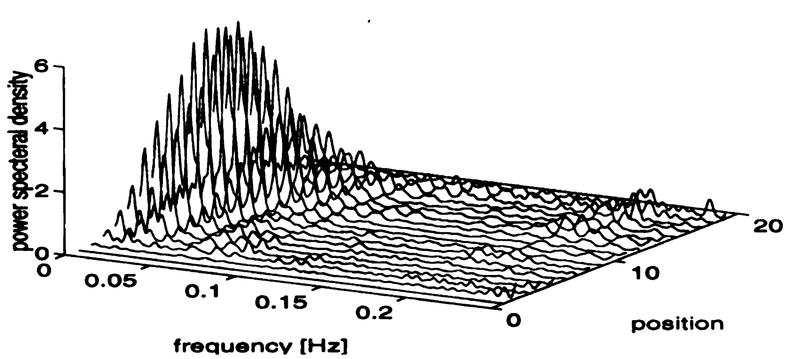

(c)

Figure 5.11. Power spectral density of the stick-slip velocity responses for normal loads of (a) $N_0 = -1$ N, (b) $N_0 = -5$ N, (c) $N_0 = -10$ N. The other parameters are in Table 5.1.

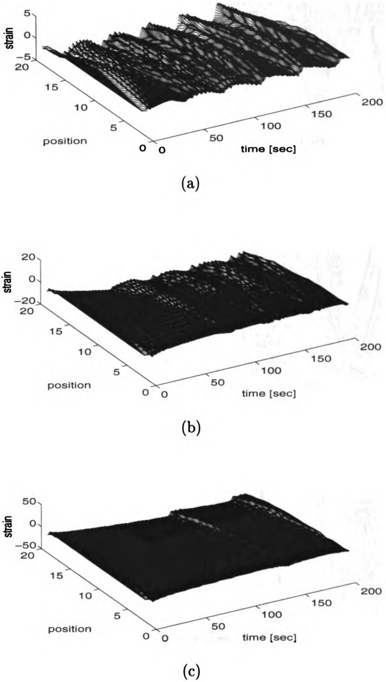

Figure 5.12. Stick-slip strain responses for normal load of (a) $N_0 = -1$ N, (b) $N_0 = -5$ N, (c) $N_0 = -10$ N. The other parameters are in Table 5.1.

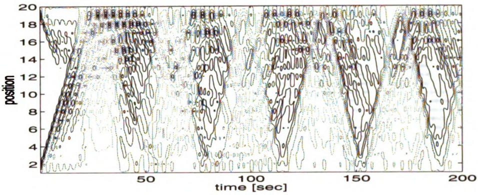

(a)

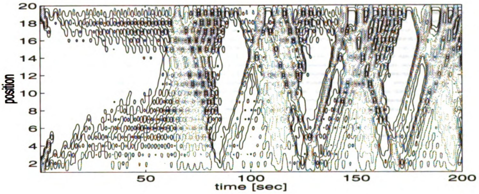

(b)

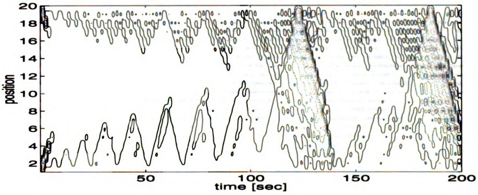

(c)

Figure 5.13. Stick-slip responses in contour plot of velocity for normal load of (a) $N_0 = -1$ N, (b) $N_0 = -5$ N, (c) $N_0 = -10$ N. The other parameters are in Table 5.1.

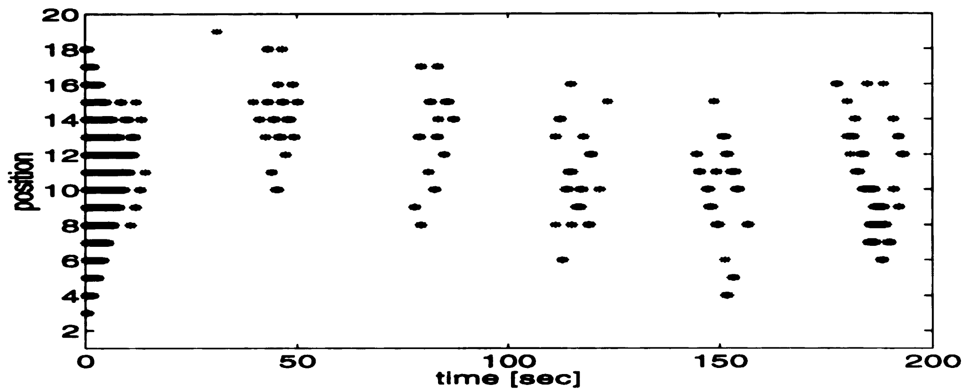

(a)

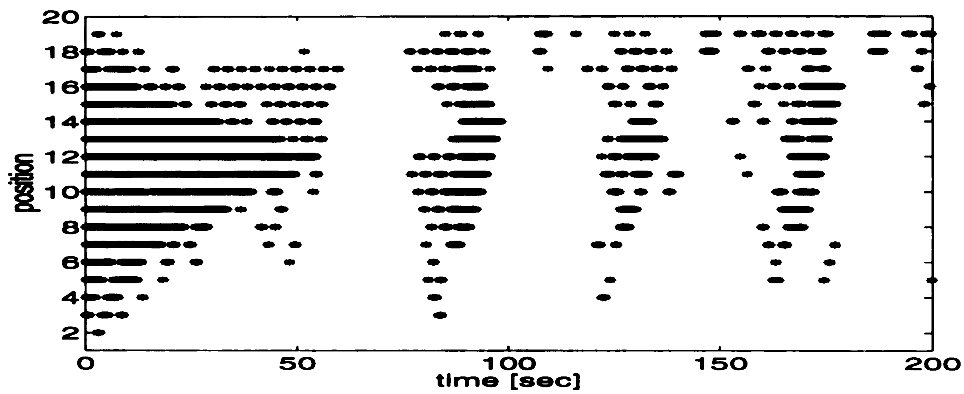

(b)

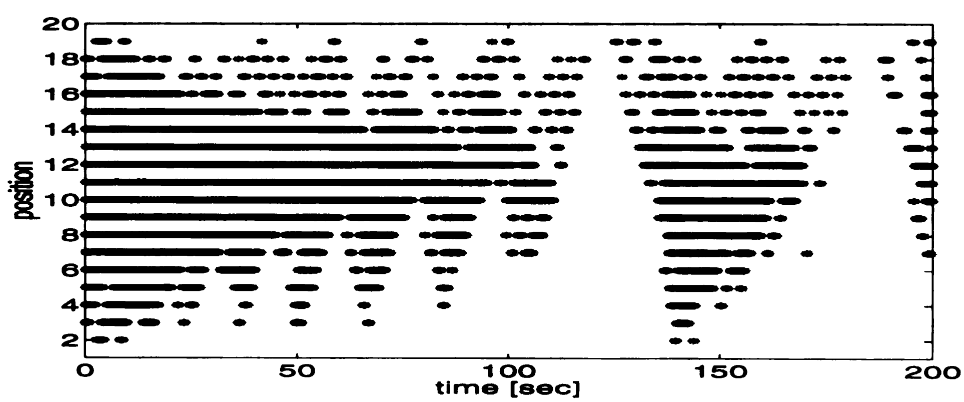

(c)

Figure 5.14. Sticking events versus times for normal loads of (a) $N_0 = -1$ N, (b) $N_0 = -5$ N, (c) $N_0 = -10$ N. The other parameters are in Table 5.1.

5.4.2 Effects of Driving Speed

Figure 5.15 shows numerical results in the velocity of each mass as the driving speed V increases. Parameter values are based on Table 5.1. In this numerical analysis a negative slope friction model is adopted. As the driving speed increases the maximum velocities are increases. For $V = 0.1$, 0.5, and 1.0 m/sec, the magnitude of maximum velocities of 0.2, 1.2, and 2.0 m/sec are obtained, respectively.

In the low driving speed ($V = 0.1$ m/sec), the small-grouped stick-slip motions are dominated as shown in Figure 5.16 (a). This means when the masses are driven by the low driving speed, the slipping velocities are usually low since the kinetic energies stored during the stick state are relatively low compared to the high speed driving condition.

When kinetic energy is not enough to provoke the series of triggering events from stick to slip motions to neighboring masses, this appears as intermittent stick-slip oscillations in the form of small-grouped motions. They are shown as the creeping motions in the beginning of simulation time in Figure 5.16 (a). Thus under the low driving speed, the intermittent small-grouped stick-slip motions are expected to be observed. Under very low driving speeds it is expected that the distinct low frequency stick-slip motions expressed in the form of waves of detachments may not be obtained since the small-grouped, high frequency, creeping motions are generated. In real situations, having large material damping, this high frequency can easily be damped out by the system internal damping, so the noise may not be a serious problem.

On the other hand, under a very high driving speed, the system can not experience steady-state stick-slip motions, but it can only undergo pure slipping motions. In this case the system experiences high frequency slipping motions generating high frequency noise. The frequency spectra of the velocity responses and projections of the state-space trajectories for selected masses are shown in Figure 5.17 and Figure 5.18, respectively.

Driving Speed	Mass position			
V [m/sec]	5th mass	9th mass	13th mass	17th mass
0.1	1.0	1.1	2.0	2.0
0.5	3.7	7.0	8.0	6.0
1.0	7.0	14.0	17.0	11.0

Table 5.4. The maximum peak-to-peak amplitudes in displacement response by changing the driving speed.

Driving Speed	Mass position			
V [m/sec]	5th mass	9th mass	13th mass	17th mass
0.1	0.15	0.2	0.25	0.3
0.5	0.8	1.0	1.3	1.5
1.0	1.7	2.1	2.7	3.1

Table 5.5. The maximum peak-to-peak amplitudes in velocity responses by changing the driving speed.

According to this investigation, the high driving speed increases the amplitudes of oscillations in stick-slip motions. In Table 5.4 and 5.5 the approximate peak-to-peak displacement and velocity amplitudes in stick-slip motions are presented, respectively.

As the driving speed increases the amplitude of stick-slip oscillations are increases. It should be noted that such responses are affected by the frictional properties. The dependency on frictional properties are shown in the work by Martins *et al.* [118]. According to his work, as the driving speed increases the stick-slip amplitudes are decreased when they adopted the positive slope friction model.

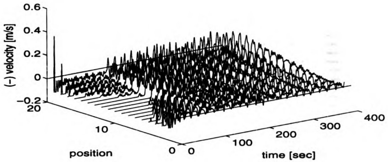

(a)

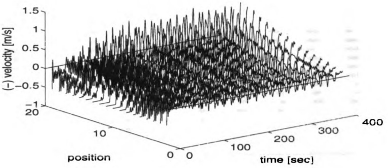

(b)

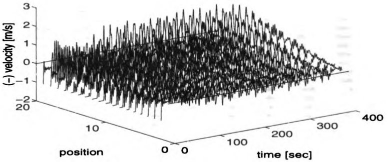

(c)

Figure 5.15. The stick-slip responses for driving speeds of (a) $V = 0.1$m/s, (b) $V = 0.5$m/s, (c) $V = 1.0$m/s. The other parameters are in Table 5.1.

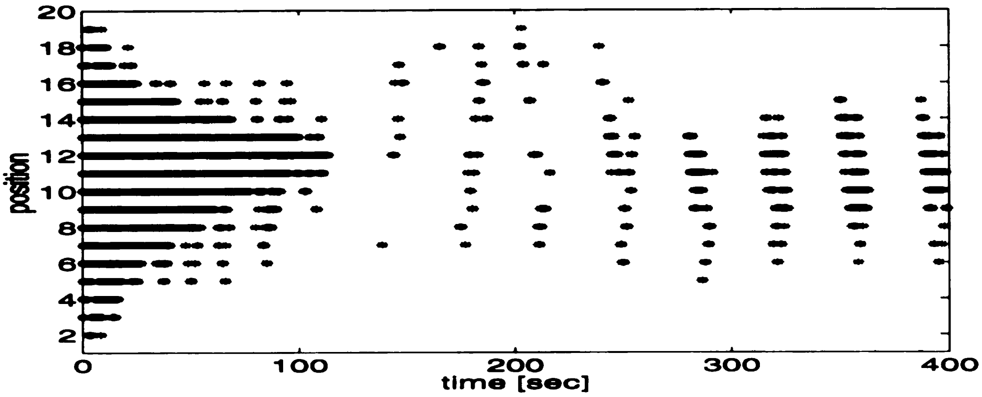

(a)

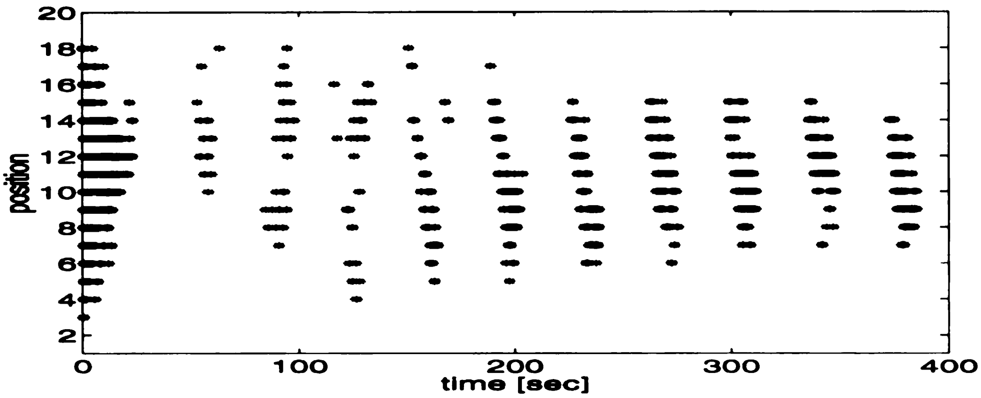

(b)

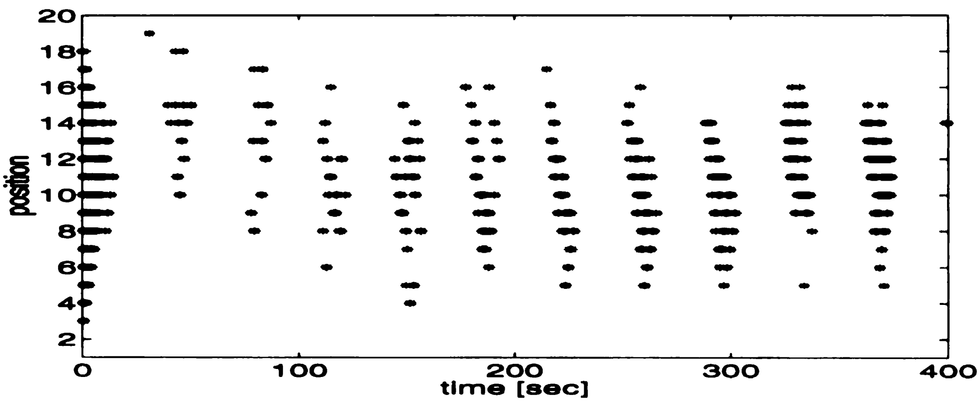

(c)

Figure 5.16. Sticking events for driving speeds of (a) $V = 0.1\text{m/s}$, (b) $V = 0.5\text{m/s}$, (c) $V = 1.0\text{m/s}$. The other parameters are in Table 5.1.

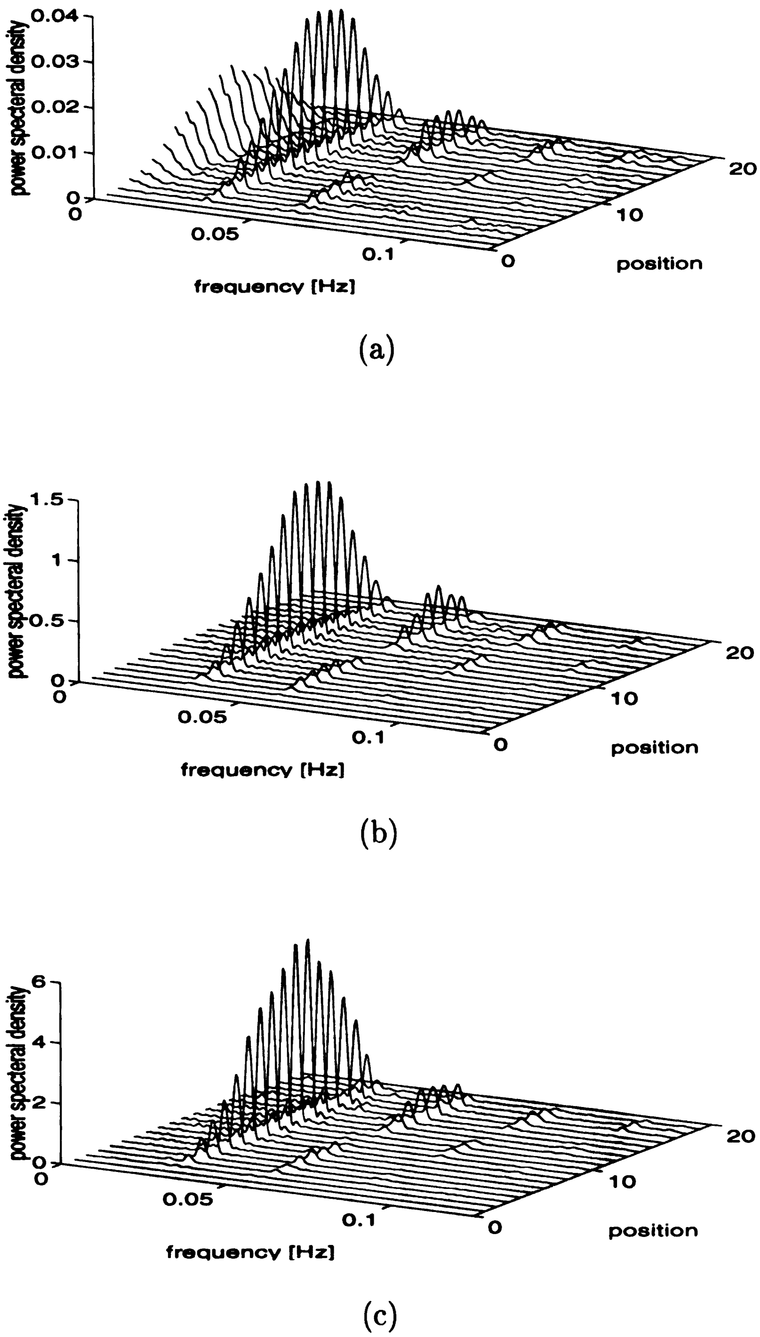

Figure 5.17. Power spectral density of the stick-slip velocity responses for driving speeds of (a) V = 0.1m/s, (b) V = 0.5m/s, (c) V = 1.0m/s. The other parameters are in Table 5.1.

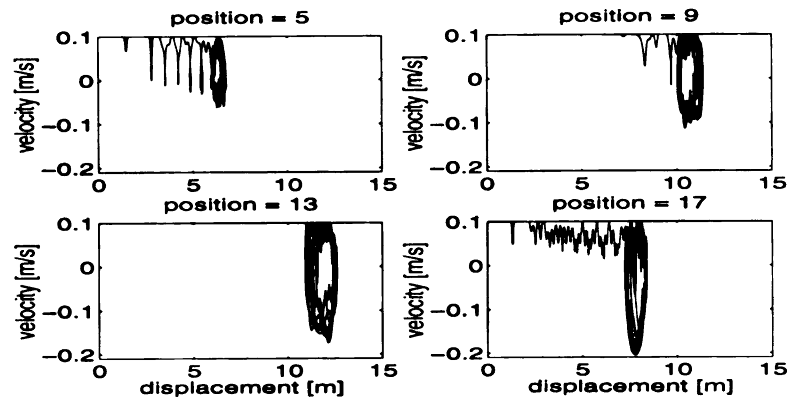

(a)

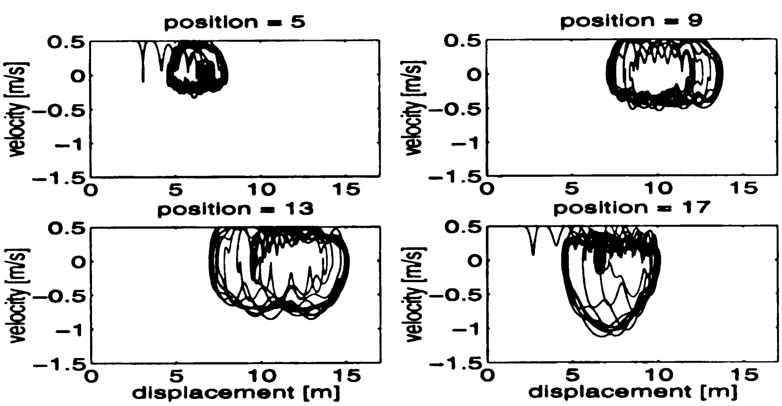

(b)

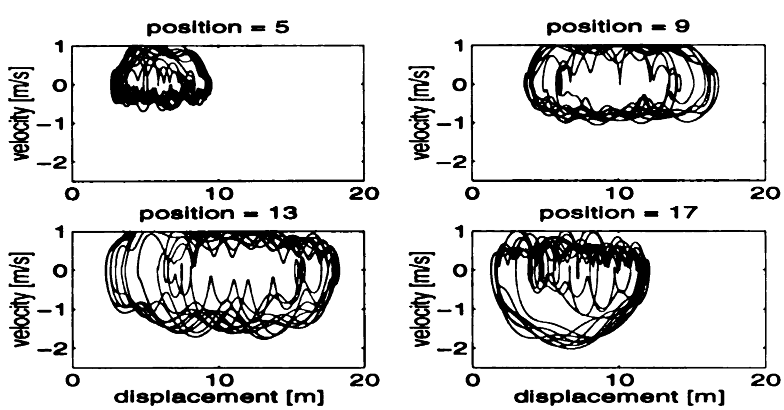

(c)

Figure 5.18. Projections of state-space trajectories of the stick-slip response by changing the driving speeds of (a) V = 0.1m/s, (b) V = 0.5m/s, (c) V = 1.0m/s. The other parameters are in Table 5.1.

5.4.3 Effects of the Poisson's ratio

The Poisson's ratio effects on the linearized system stability have been investigated in the previous chapters. Here let us check Poisson effects on stick-slip oscillations using the lumped-parameter model. The stick-slip regions for the several different Poisson's ratio are shown in Figure 5.19. For a case $\nu = 0.0$ in Figure 5.19 (a), the system is symmetric in the stick-slip oscillations. These phenomena can also be confirmed by checking the strains, as shown in Figure 5.20 (a). The shapes of stick regions and their strains are symmetric, and this symmetry is preserved in time.

However, when there is a non-zero Poisson's ratio, the system can not preserve its symmetry in the stick-slip behaviors. It is reasonable to expect such unsymmetric stick-slip behaviors because the eigenvectors have non-symmetric shapes along the spatial axis in the lumped-parameter model. Strain profiles in Figure 5.20 show that the strain evolutions are distorted as the Poisson's ratio increases. The asymmetric and propagating profiles are also found in Figure 5.21 presenting with contour plots.

Moreover, the Poisson's ratio can contribute to the frequencies of stick-slip oscillations. The frequencies of stick-slip oscillations are increased as shown in Figure 5.19 and Figure 5.22. Since the system's modal frequencies are increased as the Poisson's ratio increases (refer to the result in section 2.3 of this study), it is obvious that the stick-slip oscillation with non-zero Poisson's ratio have relatively high frequencies than the case of zero Poisson's ratio.

State-space presentations for the masses positioned at the 5th, 9th, 13th, and 17th are shown in Figure 5.23 and their approximate peak-to-peak amplitudes in displace-

Poisson's ratio	Mass position			
ν	5th mass	9th mass	13th mass	17th mass
0.0	9.0	16.0	16.0	7.0
0.1	8.5	16.0	16.0	7.5
0.4	6.5	12.0	15.0	10.0

Table 5.6. The maximum peak-to-peak amplitude in displacement responses by changing the Poisson's ratio.

Poisson's ratio	Mass position			
ν	5th mass	9th mass	13th mass	17th mass
0.0	2.1	2.5	2.4	2.0
0.1	2.0	2.4	2.4	2.2
0.4	1.5	2.0	2.7	2.8

Table 5.7. The maximum peak-to-peak amplitudes in velocity responses by changing the Poisson's ratio.

ment and velocity are summarized in Table 5.6 and Table 5.7 versus the Poisson's ratio. For the front positioned masses (in this example the 5th and 9th positioned masses) the peak-to-peak amplitude of displacement and velocity are decreased by increasing the Poisson's ratio. However, for the rear positioned masses (17th positioned masses) the peak-to-peak amplitudes of displacement and velocity are increased by increasing the Poisson ratio. The asymmetry due the Poisson's ratio changes the resultant friction force and apparently increases the friction force at the rear positioned masses.

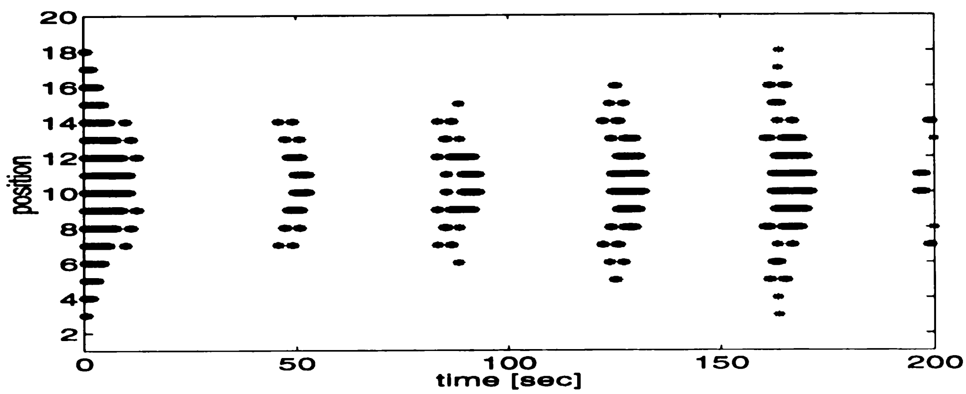

(a)

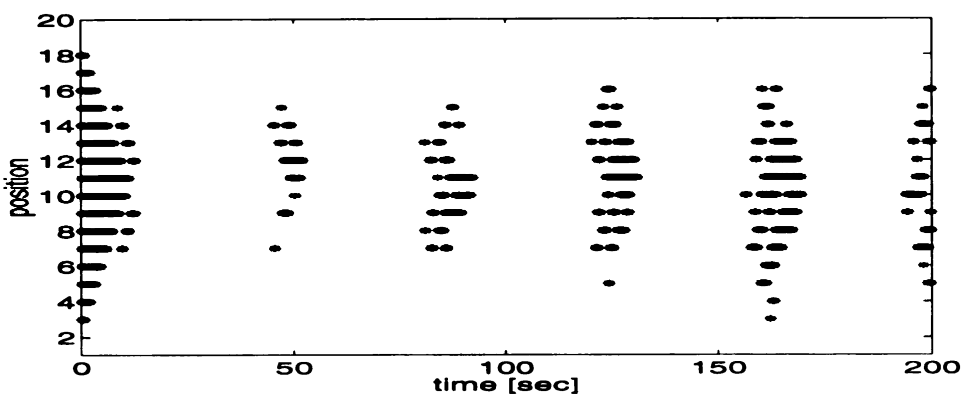

(b)

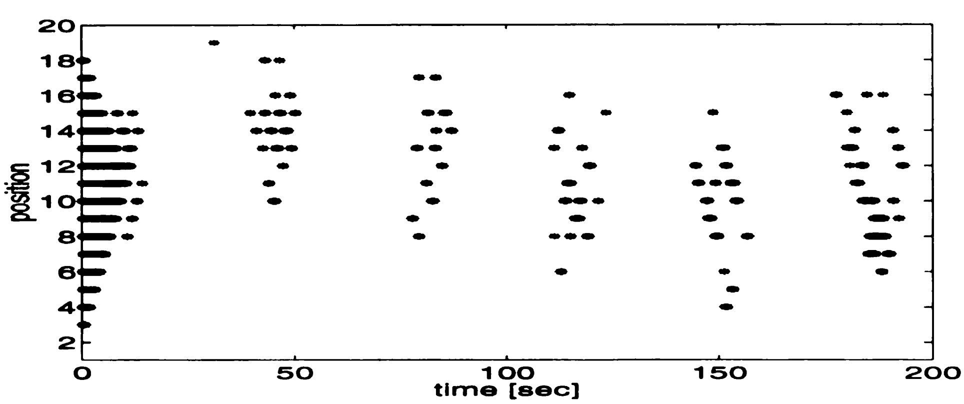

(c)

Figure 5.19. Sticking events versus time for Poisson's ratios of (a) $\nu = 0.0$, (b) $\nu = 0.1$, (c) $\nu = 0.4$. The other parameters are shown in Table 5.1.

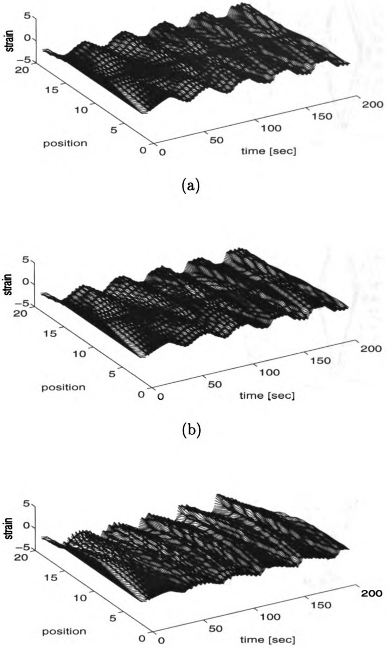

(a)

(b)

(c)

Figure 5.20. The stick-slip response in strains for Poisson's ratios of (a) $\nu = 0.0$, (b) $\nu = 0.1$, (c) $\nu = 0.4$. The other parameters are shown in Table 5.1.

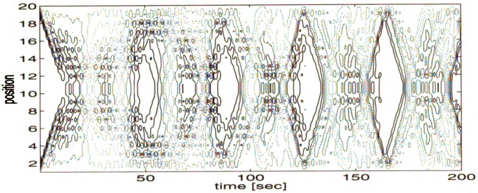

(a)

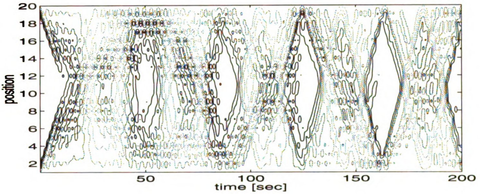

(b)

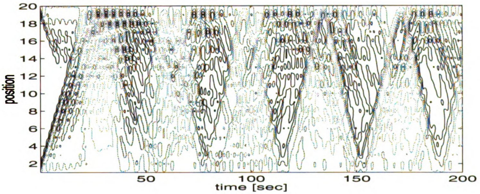

(c)

Figure 5.21. The stick-slip responses in contour plot of velocity for Poisson's ratios of (a) $\nu = 0.0$, (b) $\nu = 0.1$, (c) $\nu = 0.4$. The other parameters are shown in Table 5.1.

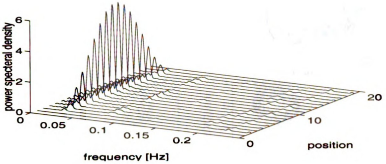

(a)

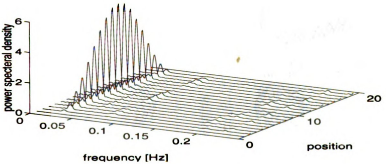

(b)

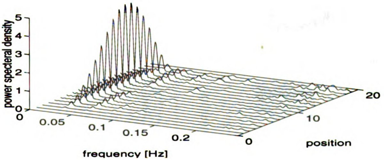

(c)

Figure 5.22. Power spectral density presentations of the stick-slip responses of velocity for Poisson's ratios of (a) $\nu = 0.0$, (b) $\nu = 0.1$, (c) $\nu = 0.4$. The other parameters are shown in Table 5.1.

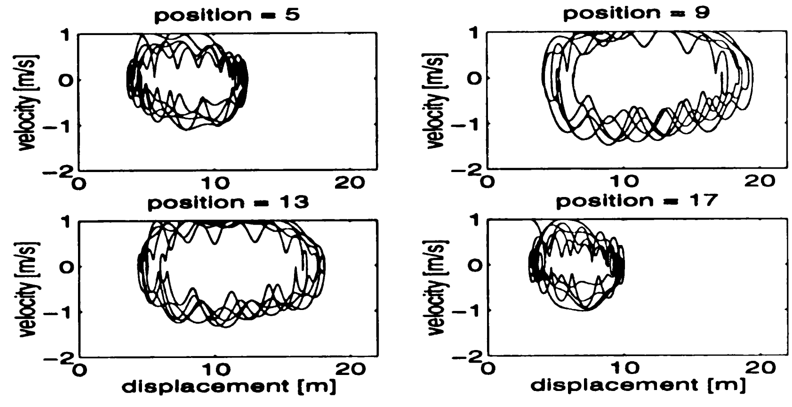

(a)

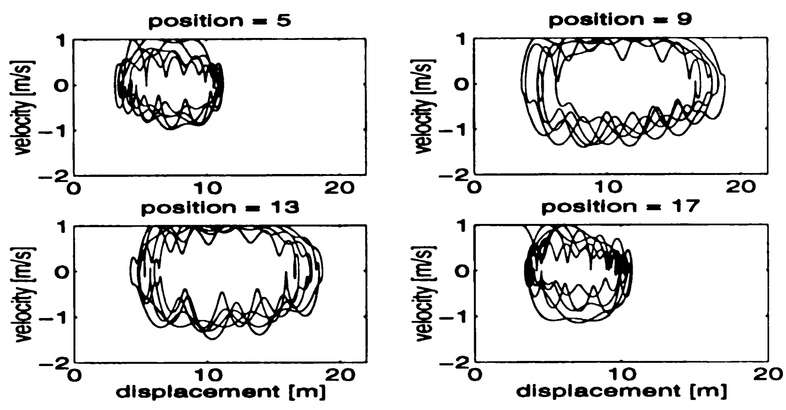

(b)

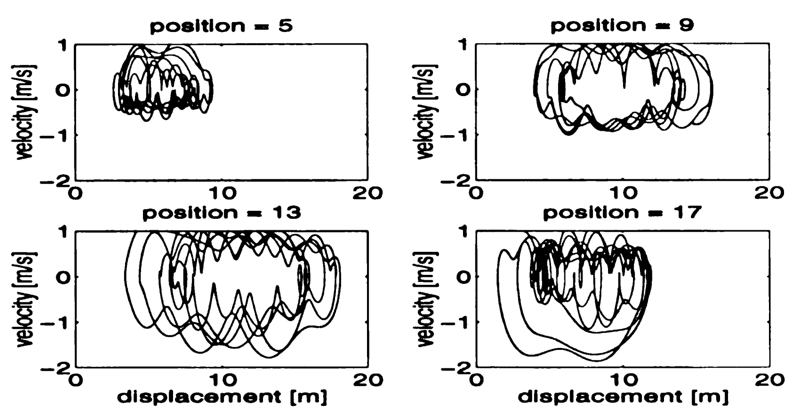

(c)

Figure 5.23. Projections of state-space trajectories for Poisson's ratios of (a) $\nu = 0.0$, (b) $\nu = 0.1$, (c) $\nu = 0.4$. The other parameters are shown in Table 5.1.

5.4.4 Effects of Friction Characteristics

From the analysis of the single degree-of-freedom model a negative slope in the friction-speed relations destabilizes the system as a result of apparent negative damping effects. This results also can be applied to the lumped parameter model having negative frictional characteristics. As shown in the previous chapter, the negative slope in lumped multi degree-of-freedom model make the whole system unstable based on the linear stability criteria. In this section the dependence of stick-slip oscillations on the friction characteristics are investigated.

If the static and dynamic friction coefficients are constants and equivalent to each other, i.e., $\mu_s = \mu_k$ condition, the steady state oscillations do not experience the stick-slip oscillations under the fixed boundary conditions. Figure 5.24 (a) shows the transient stick-slip oscillations subjected to the specific initial condition. After the transient oscillations are damped out the steady-state oscillations have no stick-slip oscillations in their responses (which is not shown).

A case of discontinuous coefficient of friction characteristics, for example $\mu_s = 0.3$ and $\mu_k = 0.1$, the stick-slip oscillations are observed after transient responses are damped out, as shown in Figure 5.24 (b). When the system has a negative slope in the friction-speed relation the system can experience the stick-slip motions, as shown in Figure 5.24 (c). Since that condition indicates the unstable motions in slipping state, the motions generate more stick-slip oscillations. The state-space presentations are shown in Figure 5.25 for the specific masses.

As mentioned earlier, since the system stability is closely related to friction-speed characteristics, the peak-to-peak amplitudes during stick-slip oscillations (Figure 5.25) and the dynamic behaviors during the stick-slip oscillations are influenced by the operating driving speed (V) as well.

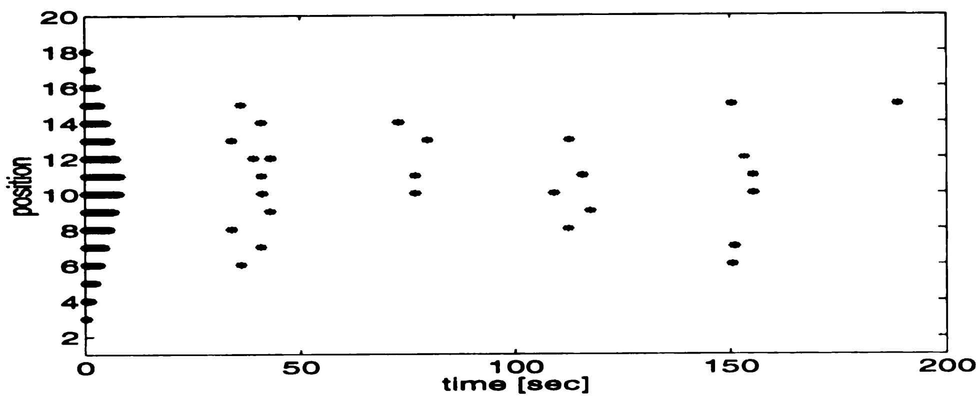

(a)

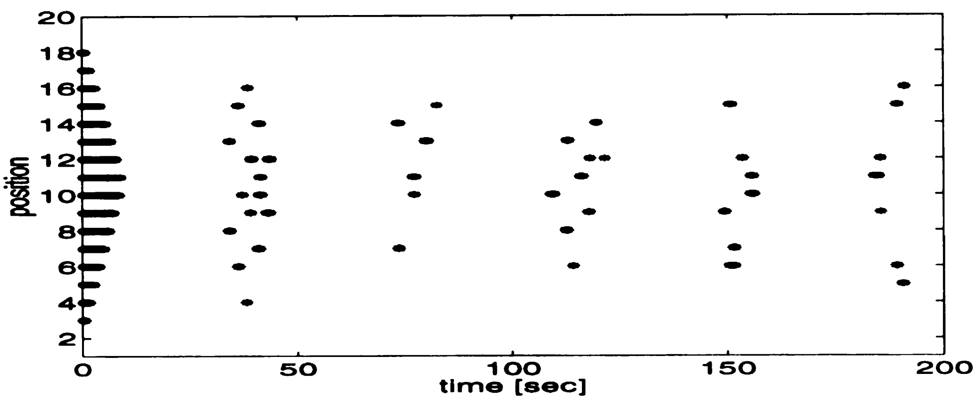

(b)

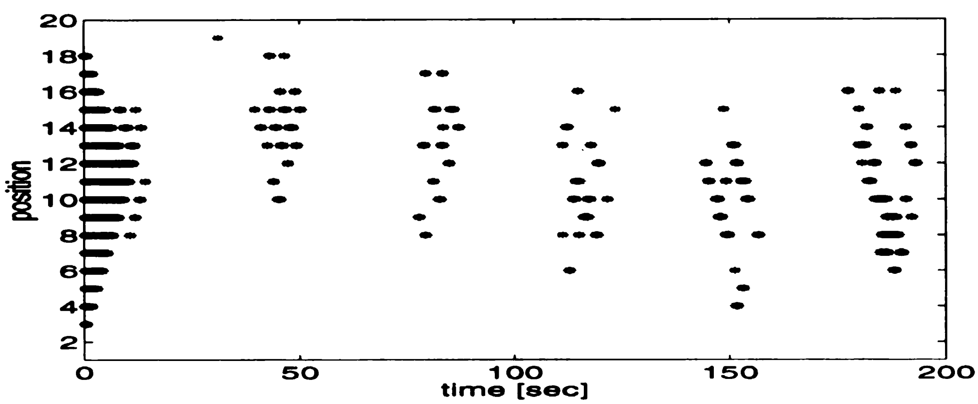

(c)

Figure 5.24. Sticking events versus time for the following friction-speed relations: (a) a discontinuous function, $\mu_s = \mu_k = 0.1$, (b) a discontinuous function, $\mu_s = 0.3$, $\mu_k = 0.1$, (c) $\mu = c_1 + c_2 e^{-c_3|\dot{x}_i - V|}$, where $c_1 = 0.3$, $c_2 = 0.2$, and $c_3 = 0.1$. The other conditions are in Table 5.1.

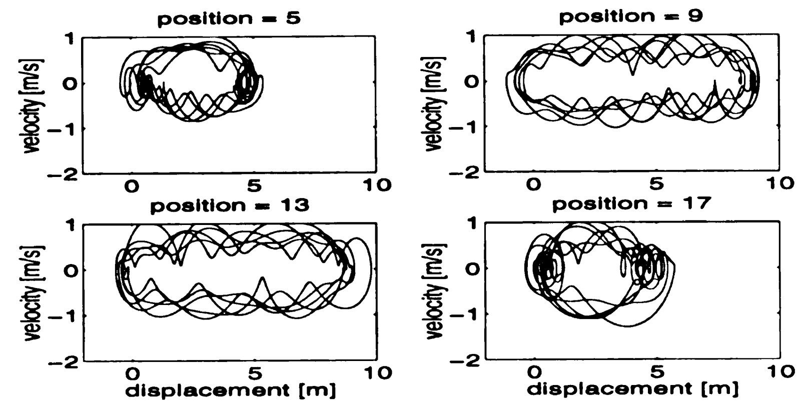

(a)

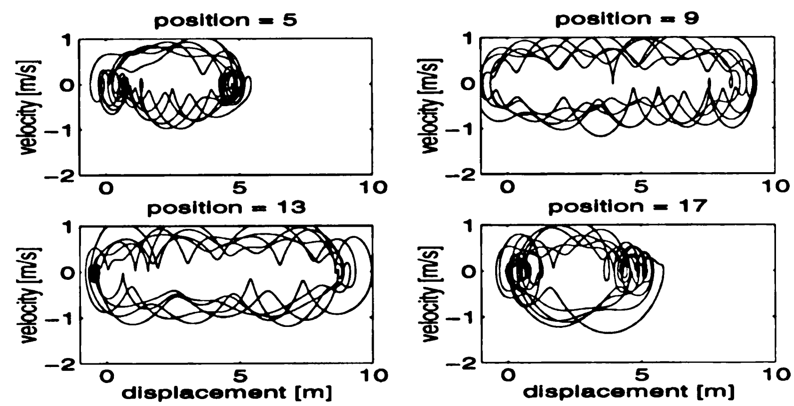

(b)

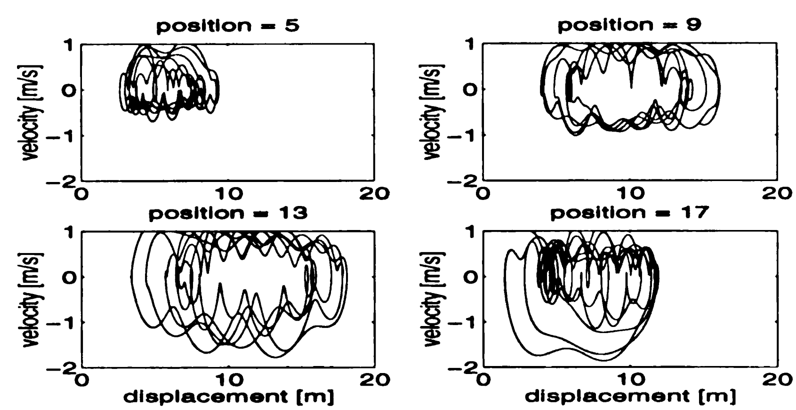

(c)

Figure 5.25. Projected state-space trajectories for the following friction-speed relations: (a) a discontinuous function, $\mu_s = \mu_k = 0.1$, (b) a discontinuous function, $\mu_s = 0.3$, $\mu_k = 0.1$, (c) $\mu = c_1 + c_2 e^{-c_3|\dot{x}_i - V|}$, where $c_1 = 0.3$, $c_2 = 0.2$, and $c_3 = 0.1$. The other conditions are in Table 5.1.

5.4.5 Effects of Other Parameters

Numerical results for different values system stiffness k are shown in Figure 5.26. As the stiffness k increases the stick-slip oscillation frequencies increases. When the stiffness is high, the system can not satisfy the kinematic constraint function for the sticking condition. Figure 5.27 shows the state-space presentation for several specific masses.

As investigated in Chapter 3, the boundary condition plays an important role in system stability. In this section the investigations are thoroughly devoted to the fixed boundary conditioned model, which is on the neutrally stable state in the stability under a constant coefficient of friction. If periodic boundary conditions are used, the system is linearly unstable from the result of Chapter 3 and is able to experience more nonlinear stick-slip oscillations, as will be seen in section 5.6.

It has been reported that the surface roughness is able to increase a apparent coefficient of friction and may contribute to stick-slip oscillations in real situations (Nakai and Yokoi [72]). Thus the final treatment for contacting surface affects the stick-slip conditions and the generation of noise induced by friction.

Small geometric misalignment in system may generate stick-slip motions. According to the experimental work in compliant rubber bearings in ships (Bhushan [73]) the shape of elastic materials between the channels was an important factor for generating stick-slip oscillations. The divergent shape of elastic materials along the sliding direction can more easily generate the stick-slip oscillations than the convergent shaped materials. Dweib and D'Souza [55, 56] and Tworzydlo *et al.*[52] investigated the influence of the angle of attack of the contact on the stability. In the experimental work, the small misalignment of the angle of attack in the sliding contact caused the coupling of the normal and rotational mode. This result confirmed a well known sensitivity of stability to the angle of attack, which is one of the reasons for the poor reproductivity of the results of various frictional experiments.

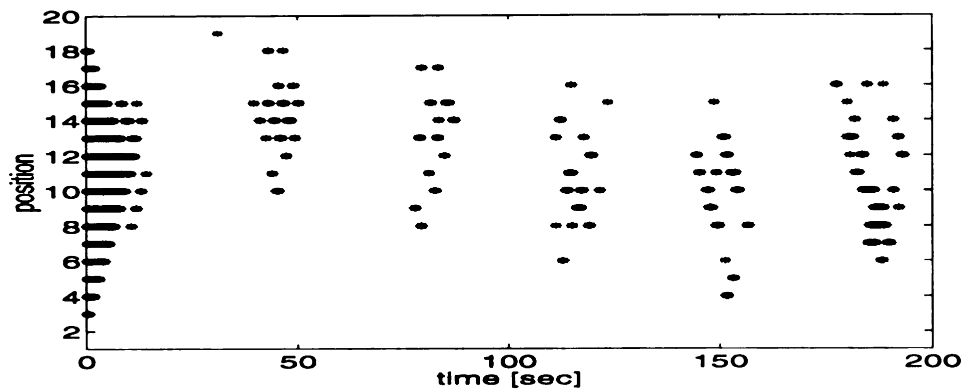

(a)

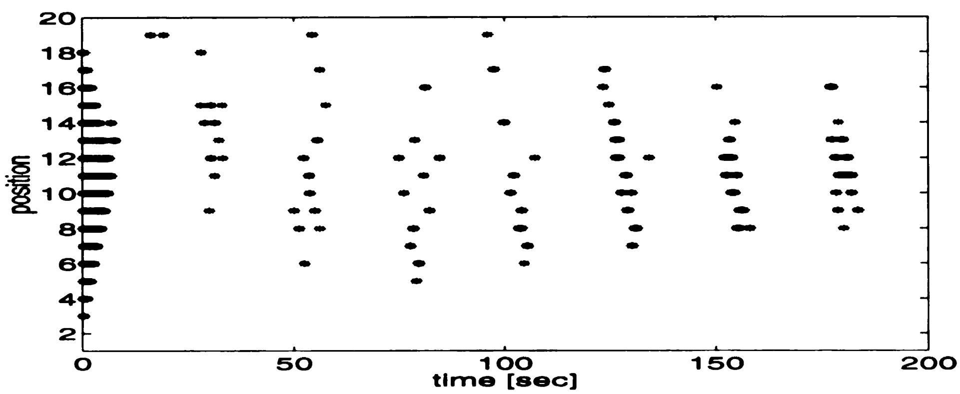

(b)

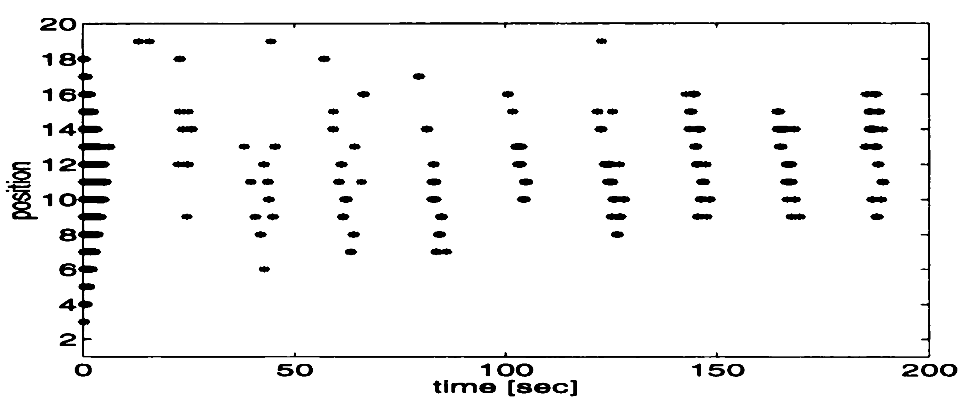

(c)

Figure 5.26. Stick events versus time for stiffnesses of (a) $k = 1$, (b) $k = 2$, (c) $k = 3$. The other conditions are in Table 5.1.

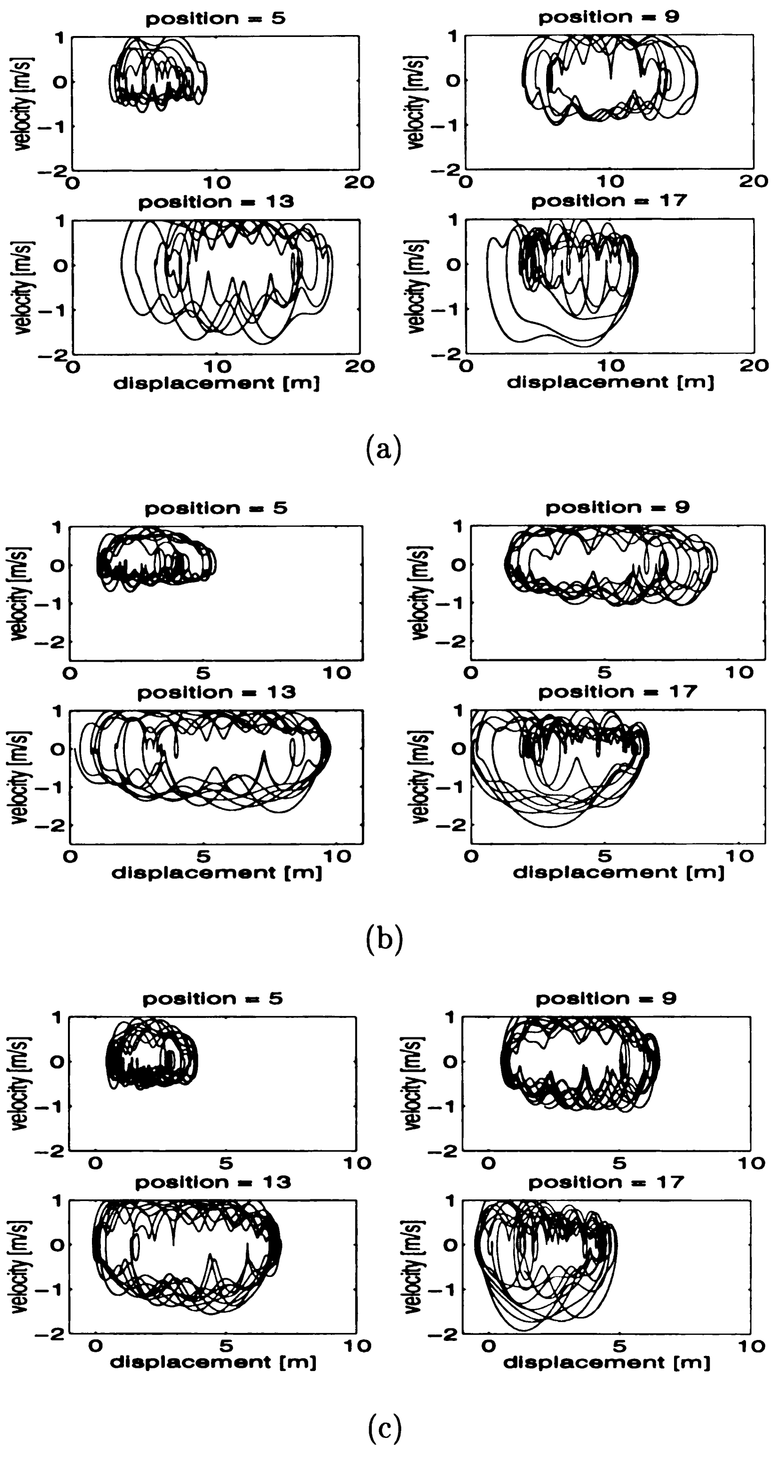

Figure 5.27. Projected state-space trajectories for stiffness values of (a) $k = 1$, (b) $k = 2$, (c) $k = 3$. The other conditions are in Table 5.1.

5.5 Stick-Slip Oscillations: Modal Projection Method

In the previous sections we have used the lumped-parameter model to show multi-dimensional behaviors of stick-slip oscillations. In this section, by applying the modal projection method to the continuous system a possible alternative method in handling the low-dimensional stick-slip oscillations is proposed.

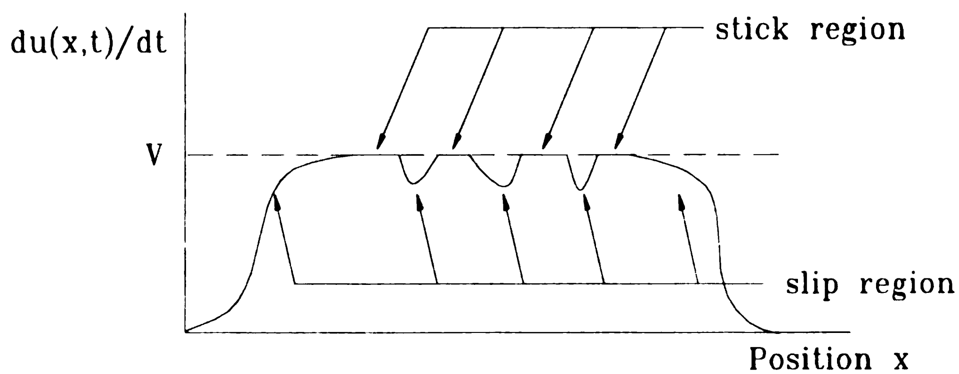

Figure 5.28. A possible velocity profile showing the stick-slip motions in a continuous one-dimensional system: High dimensional model.

We may encounter some difficulties in analyzing the continuous system experiencing stick-slip phenomena since a system may have high frequency oscillations and discontinuous properties within their domains. For an example, as shown in the Figure 5.28, a possible stick-slip configuration at specific instant in time has numerous stick and slip regions within the domain. There are infinitely many possible stick-slip

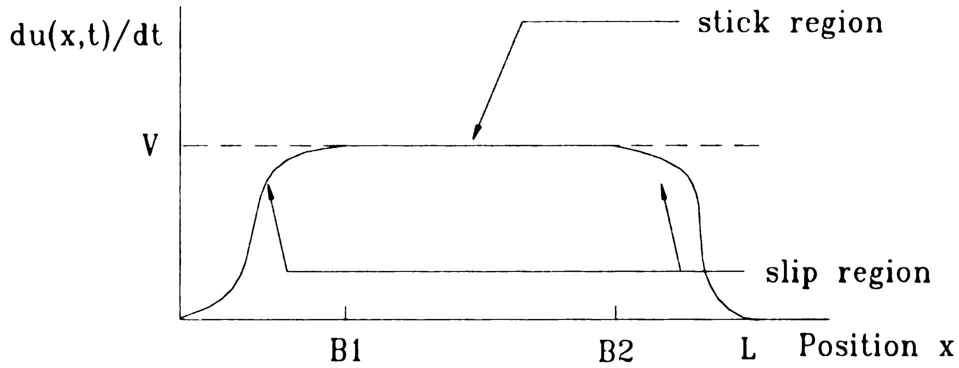

Figure 5.29. A possible velocity profile showing the stick-slip motion in a continuous one-dimensional system with bounded boundary condition model: Low dimensional model.

configurations, making it difficult to formulate analytical or numerical solutions.

On the other hand, when we consider low frequencies in stick-slip motions only, we can simplify the stick-slip system and are able to overcome the difficulty. Possible typical subregions are shown in Figure 5.29. We divide the whole system ($x \in [0, L]$) into three subregions of low dimensional systems—a slipping region in the front ($x \in [0, B_1]$), a sticking region in the middle ($x \in [B_1, B_2]$), and a slipping region in the rear ($x \in [B_2, L]$). The low dimensional characteristics of each region are assembled to approximate the whole system behaviors.

Assuming that the system has a configuration shown in Figure 5.29, the indicator function for the kinetic constraint equations at the stick-slip boundaries ($x = B_1$, or B_2) are

$$H(x,t) \stackrel{\text{def}}{=} |F(x,t)| - |G(x,t)|, \tag{5.13}$$

	A slipping region, $x \in [0, B_1]$	A slipping region, $x \in [B_2, L]$
Equation	$\frac{\partial}{\partial x}\{e^{-\bar{\alpha}x}\frac{\partial u}{\partial x}\} = e^{-\bar{\alpha}x}\frac{\partial^2 u}{\partial t^{*2}}$	$\frac{\partial}{\partial x}\{e^{-\bar{\alpha}x}\frac{\partial u}{\partial x}\} = e^{-\bar{\alpha}x}\frac{\partial^2 u}{\partial t^{*2}}$
Boundary condition	$u(0,t) = \frac{\partial u}{\partial t}(0,t) = 0,$ $\frac{\partial u}{\partial t}(B_1,t) = V$	$u(L,t) = \frac{\partial u}{\partial t}(L,t) = 0,$ $\frac{\partial u}{\partial t}(B_2,t) = V$
Solution	$u(x,t) = v(x,t) + \frac{x}{B_1}Vt$ $= \sum_{j=1}^{\infty}\phi_j^{0B_1}(x)r_j(t) + \frac{x}{B_1}Vt$	$u(x,t) = w(x,t) + \frac{L-x}{L-B_2}Vt$ $= \sum_{j=1}^{\infty}\phi_j^{B_2L}(x)s_j(t) + \frac{L-x}{L-B_2}Vt$
Projected motion	$\ddot{r}_j + \omega_{r,j}^2 r_j = 0,$ $r_j(0) = \frac{2}{B_1}\int_0^{B_1}\psi_j^{0B_1}(x)v(x,0)dx,$ $\dot{r}_j(0) = \frac{2}{B_1}\int_0^{B_1}\psi_j^{0B_1}(x)\dot{v}(x,0)dx$	$\ddot{s}_j + \omega_{s,j}^2 s_j = 0,$ $s_j(0) = \frac{2}{L-B_2}\int_{B_2}^{L}\psi_j^{B_2L}(x)w(x,0)dx,$ $\dot{s}_j(0) = \frac{2}{L-B_2}\int_{B_2}^{L}\psi_j^{B_2L}(x)\dot{w}(x,0)dx$

Table 5.8. Equations of motion, boundary conditions, and projected motions on modal coordinates for the stick-slip oscillations with fixed boundary conditions. Here $\bar{\alpha} = \frac{\mu\nu}{A}$, $t^* = t/\sqrt{\frac{\rho}{AE}}$, $\phi_j^{mn}(x) = e^{\frac{\bar{\alpha}}{2}}\sin(\frac{j\pi(x-m)}{n-m})$, $\psi_i^{mn}(x) = e^{-\frac{\bar{\alpha}}{2}}\sin(\frac{i\pi(x-m)}{n-m})$.

where

$$F(x,t) = \frac{\partial^2 u(x,t)}{\partial x^2}, \tag{5.14}$$
$$G(x,t) = \mu_s\{-\frac{\sigma_0}{AE} - \frac{\nu}{A}\frac{\partial u(x,t)}{\partial x}\}.$$

And the indicator function for kinematic constraint equation is

$$S(x,t) \stackrel{\text{def}}{=} |\frac{\partial u}{\partial t}(x,t) - V|. \tag{5.15}$$

The $F(x,t)$ represents the stiffness forces at stick-slip boundary x and time t. The function $G(x,t)$ express the frictional forces including the Poisson effect of the materials at the boundary. The condition of $H(x,t) \geq 0$ with zero relative velocity ($S(x,t) = 0$) is necessary for the stick status. On the other hand, non-zero relative velocity ($S(x,t) \neq 0$) yields a slipping status. These constraint formulations are similar to those of the lumped-parameter models in the previous study.

Considering the system which can be divided into the slip and stick regions (Figure 5.29), characteristics for each slipping region ($x \in [0, B_1]$, and $x \in [B_2, L]$) are summarized on Table 5.8. Table 5.8 presents the equations of motion, boundary conditions, the modal projected motions and solution for each slipping region.

Within the sticking region, which is placed on between those two slipping regions, all motions are constrained. Thus it is represented as

$$\frac{\partial u}{\partial t}(x,t) = V, \tag{5.16}$$

where $x \in [B_1, B_2]$.

By taking its adjoint function $\psi_i(x)$, the motion in both slipping regions are obtained by casting to the modal coordinates $r_j(t)$ and $s_j(t)$, respectively. (Refer to Table 5.8.) Note that the obtained equations of motion are only valid until the kinetics and kinematic conditions do not change their sign at their boundaries.

	A slipping region, $x \in [0, L]$
Equation of motion	$\frac{\partial}{\partial x}\{e^{-\bar{\alpha}x}\frac{\partial u}{\partial x}\} = e^{-\bar{\alpha}x}\frac{\partial^2 u}{\partial t^{*2}}$
Boundary condition	$u(0,t) = \frac{\partial u}{\partial t}(0,t) = u(L,t) = \frac{\partial u}{\partial t}(L,t) = 0$
Solution	$u(x,t) = \sum_{j=1}^{\infty} \phi_j^{0L}(x) q_j(t)$
Projected motion	$\ddot{q}_j + \omega_{q,j}^2 q_j = 0,$ $q_j(0) = \frac{2}{L}\int_0^L \psi_j^{0L}(x) u(x,0)dx,$ $\dot{q}_j(0) = \frac{2}{L}\int_0^L \psi_j^{0L}(x) \dot{u}(x,0)dx$

Table 5.9. The equation of motion, boundary condition, and projection to modal coordinates for pure sliding oscillations under the fixed boundary condition.

When the system is in a pure sliding state, i.e., the state that does not have any stick regions inside of the domain $x \in [0, L]$, the whole system is represented in Table 5.9. The integration should continue as long as the constraint equations (5.13) and (5.15) do not change their sign during its integration period. In each iteration the boundary conditions must be updated from the system state. In doing so its

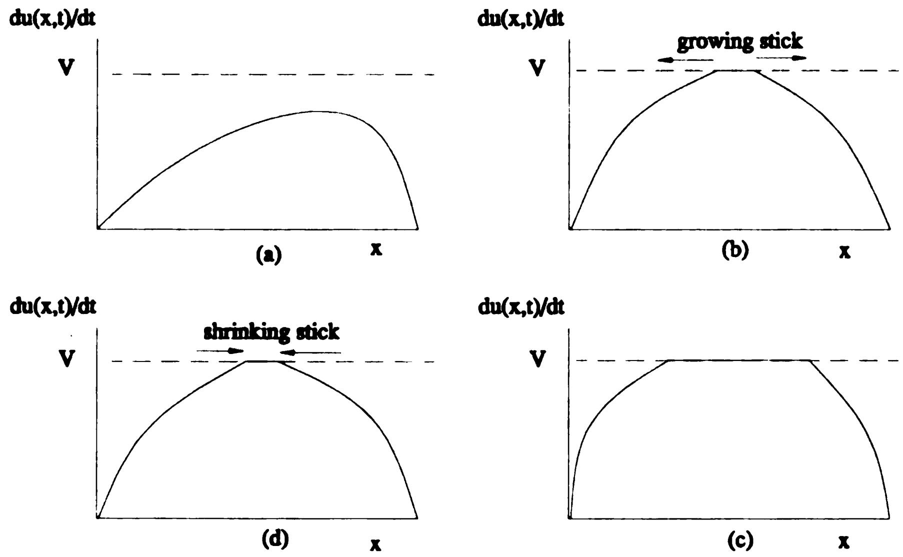

Figure 5.30. Schematic diagrams showing stick-slip oscillations. (a) a pure sliding stage, (b) a growing sticking stage, (c) an enlarged sticking stage, and (d) a shrinking sticking stage.

motion is de-projected to have real configuration and projected again to integrate its states in time. The growing and shrinking of the sticking regions are determined by checking the constraint boundary equations (5.13) and (5.14). In this simulation we discretized the domain $x \in [0, L]$ with 20 divisions and applied a difference method to equation (5.13) in order to determine and update the sticking boundaries B_1 and B_2. Schematic diagrams of stick-slip oscillations are shown in Figure 5.30. Figure 5.30 (a) represents a schematic diagram showing a pure sliding stage. In Figure 5.30 (b) and (c) a sticking region is grown and extended. A shrinking sticking stage is shown in Figure 5.30 (d).

Figure 5.31 shows a displacement profile of a numerical simulation and Figure 5.32 shows the stick events on the contact surface. (All stuck initial conditions are

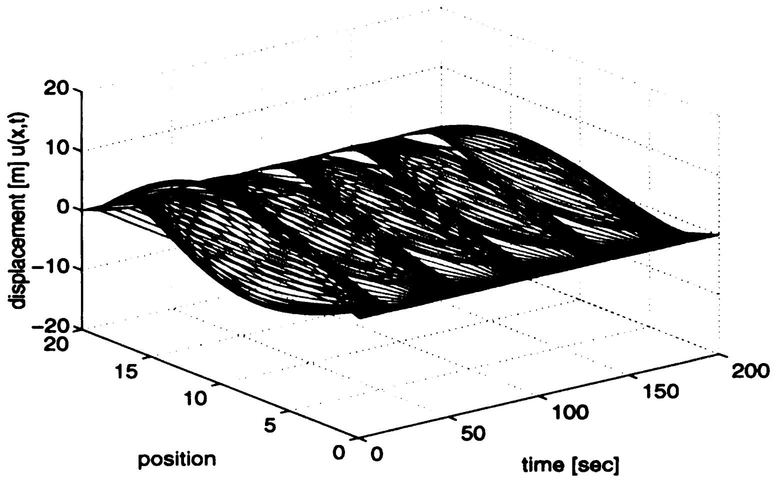

Figure 5.31. Stick-slip responses in displacement by applying the modal projection method. Here $\mu_s = 0.3$, and $\mu_k = 0.1$. (Displacement variations with respect to static equilibria are shown.)

selected.) Comparing the results obtained in Figure 5.8 (a) and Figure 5.14 (a) these results reveal qualitative agreement in the analysis of low dimensional stick-slip motions.

Note this approach still has some limitations in its application to all parameter conditions. If actual frequencies of bushing squeak noise are too high and the frequency of the low-dimensional model suggested in this study is too low then we may need to use high-frequency models. However many other applications can be analyzed with low-frequency models. This algorithm only valid as long as the system can keep the configuration in Figure 5.29. Alternatively the high dimensional dynamic motions can be obtained by finite element analysis, presented in Chapter 6.

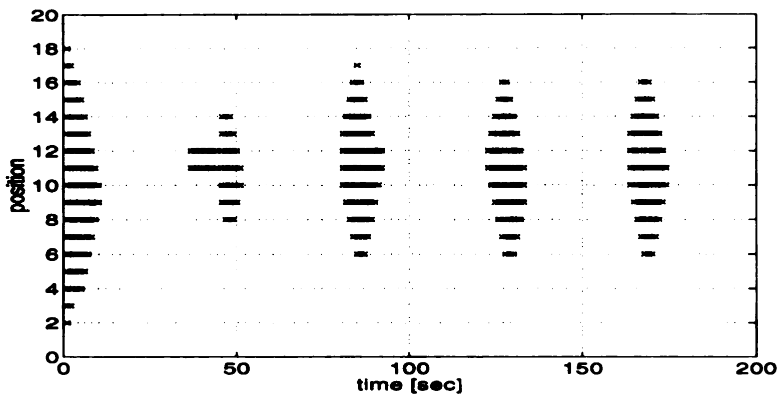

Figure 5.32. Sticking region versus time by applying the modal projection method.

5.6 Stick-Slip Oscillations under Periodic Boundary Conditions

Let us return to the motivation of this study—the bushing model. The simplified model and its stability have been investigated in the previous chapters. In this section stick-slip oscillations with periodic boundary conditions are investigated. The model in Figure 4.8 and boundary condition (4.29) in Chapter 4 are adopted for numerical studies. The equation of motion is shown in (4.22), and small damping which can suppress several unstable modes are added.

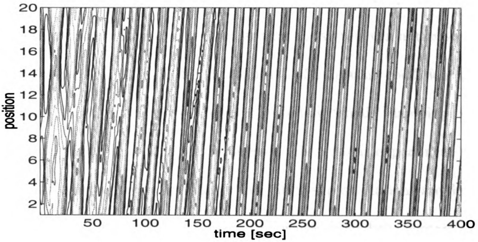

Figure 5.33. A contour presentation of the velocity response for the model with periodic boundary conditions. Here $d = 0.01, \gamma = 0.01, \mu_s = 0.3$, and $\mu_k = 0.1$. The other parameters are in Table 5.1.

Figure 5.33 shows a contour plot of stick-slip responses in velocity with small external ($d = 0.01$) and internal ($\gamma = 0.01$) damping terms. With sufficient damping,

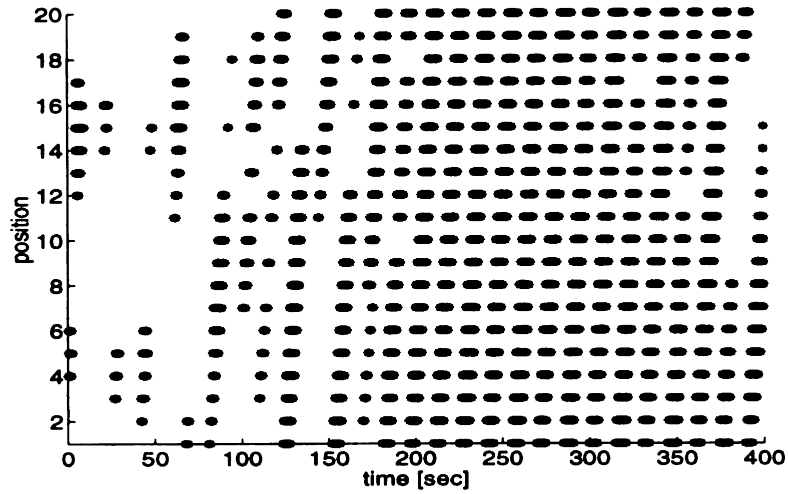

Figure 5.34. Stick events versus time for the periodic boundary condition model.

such that the overall system is stable based on the linear stability criteria, it is observed that the oscillations are damped out, so that the system can not experience any sustained stick-slip oscillations under the condition of a constant coefficient of friction (which are not shown in a figure). However including "small" damping, such that suppress several unstable modes are suppressed, the system experiences sustained stick-slip oscillations, as shown in Figure 5.33. Stick-slip oscillations are detected as series of detachments and shown as propagating waves around the contact surface.

Figure 5.34 shows the stick events versus time. The series of detachments, like as falling dominos, are observed distinctly. The state-space presentations for selected masses are shown in Figure 5.35. Under this condition with small damping, the responses seem to have steady state sustained stick-slip oscillations. In this numerical simulation the system is slightly modified by adding small spring stiffness (1/10 of the connected spring stiffness k) between each mass and the ground. Random velocities

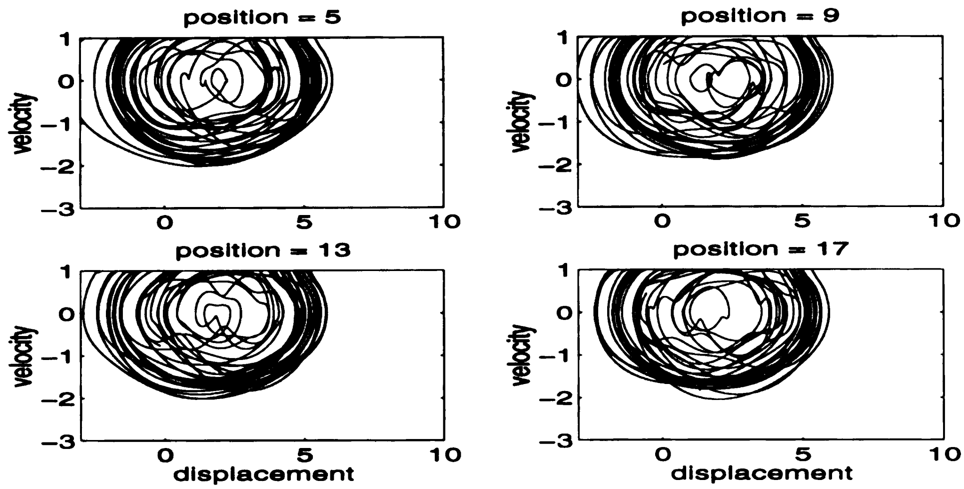

Figure 5.35. A state space diagram for several positioned masses under a periodic boundary condition model.

are selected as the initial conditions.

Note that since the model used in this section is a simplified one-dimensional model the responses obtained from numerical analysis may not express the whole dynamic behaviors for the actual bushing squeaking phenomena. Detailed mathematical modeling, which includes coordinate couplings such as the interactions between the radial and circumferential motions and radial and coriolis acceleration effects, is needed for future study. (The influence of the interactions of two coordinates on stick-slip oscillations are shown in Chapter 6 for the two-dimensional system through finite element analysis.)

5.7 Conclusion

In order to explain the stick-slip oscillations in the distributed contact system,. the discretized, lumped-parameter model was established and the numerical techniques for handling such systems—the variable degree of freedom and the variable boundary conditions—were presented. Since it was confirmed that linear stability of the lumped-parameter model is convergent in the previous chapter, we adopted that model for simulations and analyses of stick-slip oscillations.

Detailed dynamic behaviors in presence of distributed friction are presented and the parameter effects on system responses were investigated. According to the numerical responses of the stick-slip oscillations, the generation of noise and vibrations originated from the mechanisms of series of detachments on the contact surface [26]. The characteristics of series of detachments slips were influenced by various system parameters. The high normal loads had two effects: decrease the frequencies of detachements slips and increase the frequencies of small-grouped stick-slip oscillations. Moreover, the sticking regions were enlarged by increasing the normal loads. The driving speed and the characteristics of friction were closely related in responses of stick-slip oscillations. The Poisson's ratio increased the stick-slip frequencies and broke the symmetry of system responses. The friction characteristics had effects on the stick-slip oscillations and the discontinuous friction model ($\mu_s > \mu_k$) produced the steady state stick-slip motions in the multi-degree-of-freedom model.

By applying the modal projection method to the continuous system a possible alternative method in handling the low-dimensional stick-slip oscillations was proposed. Numerical algorithms in handling such a system were presented. The qualitative agreement in the analysis of low-dimensional stick-slip oscillations was obtained. By using the modal projection method we simulated the low-dimensional system in less computational time.

Under periodic boundary conditions—the same boundary condition of the bushing model—the system with small damping underwent sustained stick-slip oscillations even with a constant friction coefficient. Stick-slip oscillations were detected as series of detachments. With sufficient damping, such that the overall system was stable, oscillations were damped out and sustained oscillations were not observed.

CHAPTER 6

FINITE ELEMENT ANALYSIS

6.1 Introduction

Finite element analysis has became the dominant system analysis method as a result of the continual developments in computer technologies. In recent years, a rapid development of the digital computer has made the finite element approach to nonlinear contact problems possible, and its applications have become numerous in engineering practice. Some applied examples include a shrink-fitted shaft in a gear (Okamoto and Nakazawa [116]), rail-wheel contact problems (Schneider and Popp [115]), and cutting systems (Marusich and Ortiz [119]).

However, there have been limited studies for investigation of friction-induced vibrations of elastic media with distributed contact. Oden and Pires [44] have formulated contact problems in elasticity and investigated the dynamic behaviors due to the distributed contact. Later, Oden and Martins [117] established an elastodynamic model and developed the computational methods for dynamic friction phenomena.

In this chapter a formulation of frictional elastodynamics in the form of finite element analysis is performed in order to verify and confirm the results obtained in the previous chapters. The comparisons between the computational results obtained from the lumped-parameter method and finite element analysis are shown. By adopting a smooth approximation to the nonsmooth friction characteristic, responses of the continuous system under the distributed contact are analyzed. One- and two-dimensional elastic systems are numerically investigated by using finite element analysis.

6.2 One-Dimensional System

6.2.1 Formulation and Algorithm for Nonlinear Finite Element Analysis

This section is devoted to a finite element formulation of the one-dimensional time dependent problem and its numerical technique for solving a nonlinear problem. An equation of motion for the model of interest is written as

$$\frac{\partial^2 u}{\partial x^2} - \alpha \frac{\partial u}{\partial x} + \alpha\beta = \frac{\partial^2 u}{\partial t^2}, \tag{6.1}$$

where the α is a velocity dependent parameter, $\alpha = \alpha(\mu(\dot{u}))$, and the β depends on the normal load and friction coefficient, $\beta = \beta(N_0, \mu(\dot{u}))$. Here the fixed boundary conditions, which are expressed as $u(0,t) = u(L,t) = 0$, are applied.

The algorithm for solving the discrete dynamical system is based on the schemes in nonlinear structural dynamics calculations. Let us begin with the presentation of a Newmark-type algorithm that has been proved to be effective for many problems in computational studies. Assuming that the velocities and accelerations at time t_k are expressed as functions of the displacement, velocities and accelerations at time t_{k-1} and displacement at time t_k, the following relations are obtained.

$$\dot{u}_k = \frac{\theta_0}{\theta_1 \Delta t}(u_k - u_{k-1}) + (1 - \frac{\theta_0}{\theta_1})\dot{u}_{k-1} + \Delta t(1 - \frac{\theta_0}{2\theta_1})\ddot{u}_{k-1}, \tag{6.2}$$

$$\ddot{u}_k = \frac{1}{\theta_1 \Delta t^2}(u_k - u_{k-1}) - \frac{1}{\theta_1 t}\dot{u}_{k-1} - (\frac{1}{2\theta_1} - 1)\ddot{u}_{k-1}, \tag{6.3}$$

where θ_0 and θ_1 are called as Newmark parameters (usually those parameters are used as β and γ in finite element analysis, respectively), and $\Delta t (= t_k - t_{k-1})$ denotes the interval of time length for integration time in the whole time domain of $[0,\ T]$ with $t_0(=0), t_1, \ldots, t_k, \ldots, t_M(=T)$. The parameter θ_0 and θ_1 are selected based on the stability schemes in numerical convergence, thus $\theta_0 = \frac{1}{2}$ and $\theta_1 = \frac{1}{4}$ are selected since the Newmark-type algorithm has been proved to be an unconditionally stable algorithm, which corresponds to the constant-average-acceleration method.

The equation of motion (6.1) is put in the operator form of defined residual $R_k(u_k)$, then

$$R_k(u_k) = \ddot{u}_k - u_k'' + \alpha u_k' - \alpha\beta. \tag{6.4}$$

From the weighted residual method, the solution u_k is approximated by setting the integral of the weight residual of the approximations over the domain to zero, that is

$$< R_k(u_k), v > = < \ddot{u}_k - u_k^{''} + \alpha u_k^{'} - \alpha\beta, v > = 0. \tag{6.5}$$

Let $K_k(u_k) = DR_k(u_k)$ be the derivative of the R_k at u_k. Then the Newton-Rapson iteration technique for solving the weighted residual becomes an iteration process seeking for the solution.

Using the standard finite element procedure, the system can be constructed in finite-dimensional subspaces. For each of a certain mesh h, the nodal values the displacements v^h, velocity $\dot{v}^h$, and accelerations, $\ddot{v}^h$ are expressed in the form of

$$\begin{aligned} v^h(x,t) &= \sum_{i=1}^{N_e} N_i(x) v_i(t), \\ \dot{v}^h(x,t) &= \sum_{i=1}^{N_e} N_i(x) \dot{v}_i(t), \\ \ddot{v}^h(x,t) &= \sum_{i=1}^{N_e} N_i(x) \ddot{v}_i(t), \end{aligned} \tag{6.6}$$

where N_e denotes the number of nodes of the elements, $N_i(x)$ is the element shape test function associated with the node i.

Given the starting value of $\mathrm{u}_k^{(0)}$, successive approximations of the solution u_k are obtained by using the recurrence formula

$$u_k^{(i+1)} = u_k^{(i)} - \frac{R_k(u_k^{(i)})}{K_k(u_k^{(i)})}, \tag{6.7}$$

where (i) is the iteration counter. The termination of iterative procedure at each time k can be checked by a convergence ratio in relative displacement conditions. The convergence ratio is defined as

$$\text{convergence ratio} = \frac{|\delta u|_{max}}{|du|_{max}} = \frac{|\Delta u^{(i+1)} - \Delta u^{(i)}|_{max}}{|\Delta u^{(i)}|_{max}}, \tag{6.8}$$

where $|\delta u|_{max}$ and $|du|_{max}$ denote the maximum displacement change and maximum displacement increment in each iteration, respectively. In this numerical analysis (MARC/MENTAT [120]) the relative displacement tolerance is set as 0.1 and the maximum iteration number is set as 30.

6.2.2 Eigenvalue Comparison

In this section the system eigenvalues calculated from both models—the finite element model and the lumped-parameter model—are compared under the same parameter conditions. The system domain selected in the finite element analysis is an elastic medium of 10 inches $\times$ 1 inch with the unit thickness (1 inch). The continuum is assumed to be in plane strain. It has fixed boundary conditions at both ends and under goes a compressive stress by means of a preload on top of the elastic medium. The elastic material selected in this simulation is polyethelen, which has a properties of $E = 2.0 \times 10^4$ lb/in^2, Poisson's ratio $\nu = 0.45$, and the mass density $\rho = 0.033$ lb/in^3 (=8.55 $\times 10^{-5}$ lb-sec^2/in^4). Refer to the system description in Figure 6.1. Here front and rear nodes are defined the nodes positioned in the left- and right-hand sides, respectively.

The equivalent discrete system is obtained by dividing the material into n equal

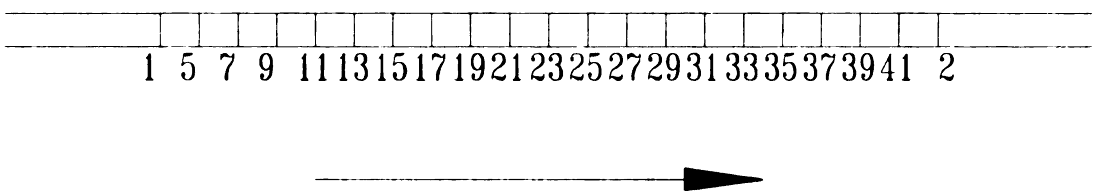

Figure 6.1. A schematic diagram of the system used in finite element analysis. The model is composed of twenty elements. The top rigid body is stationary without friction. The lower rigid body moves at 1 inch/sec to the positive x direction. There is friction between the elastic material and the lower moving body. Selected nodes are shown.

segments, lumping the mass of the segment in the center and regarding the each lumped mass M as being connected by springs of equivalent stiffness k, where k is selected such that the springs undergo the same elongation as the corresponding material segment would under identical loading. Thus the each lumped mass has the value of $m = \rho AL/n$ and the spring constant is $k = nEA/L$, where L, A is the length and the area of cross section of the material, respectively. The normal load on each mass in the distributed loading condition can also be discretized by $N_i = \sigma_0 AL/n$, where the σ_0 denotes the normal stress.

Table 6.1 presents the approximated eigenvalues with $\alpha = 0$, which is a condition without friction forces. The left column in Table 6.1 shows the exact eigenvalues

	Exact Freq.	10 elements		20 elements		40 elements	
	$\times 10^3[Hz]$	$\times 10^3[Hz]$	Error[%]	$\times 10^3[Hz]$	Error[%]	$\times 10^3[Hz]$	Error[%]
1	0.7647	0.767	0.41	0.765	0.10	0.764	0.02
2	1.5294	1.555	1.67	1.536	0.43	1.531	0.10
3	2.2941	2.380	3.74	2.315	0.91	2.299	0.03
4	3.0588	3.262	6.67	3.109	1.67	3.071	0.42
5	3.8236	4.216	10.26	3.922	2.57	3.848	0.63
6	4.5883	5.246	14.33	4.759	3.72	4.631	0.93
7	5.3530	6.322	18.10	5.625	5.08	5.421	1.26
8	6.1177	7.348	20.11	6.523	6.62	6.219	1.65
9	6.8824	8.132	18.15	7.458	8.36	7.026	2.08

Table 6.1. The approximate modal frequencies by applying finite element analysis. The numerical results including 10, 20, and 40 elements are presented with the exact frequencies.

	Exact Freq.	10 masses		20 masses		40 masses	
	$\times 10^3[Hz]$	$\times 10^3[Hz]$	Error[%]	$\times 10^3[Hz]$	Error[%]	$\times 10^3[Hz]$	Error[%]
1	0.7647	0.5718	25.2	0.6546	14.0	0.7099	7.17
2	1.5294	1.1339	25.8	1.3164	13.9	1.4188	7.23
3	2.2941	1.6766	26.9	1.9662	14.2	2.1258	7.33
4	3.0588	2.1907	31.0	2.6060	14.8	2.8297	7.49
5	3.8236	2.6673	30.3	3.2324	15.4	3.5298	7.68
6	4.5883	3.0983	32.4	3.8424	16.2	4.2249	7.92
7	5.3530	3.4761	35.0	4.4329	17.1	4.9141	8.19
8	6.1177	3.7965	37.9	5.0008	18.2	5.5963	8.52
9	6.8824	4.0479	41.1	5.5432	19.4	6.2708	8.88

Table 6.2. The approximate modal frequencies from the lumped-parameter model. The numerical results including 10, 20, and 40 masses are presented with the exact frequencies.

of one-dimensional axial motions with natural frequencies of $\omega_r = r\pi\sqrt{\frac{EA}{\rho L^2}}$, where $r = 1, 2, \ldots .9$. From this table it is obvious that with high numbers of nodes, i.e., with fine meshes in the finite element model, the more accurate approximate solutions which approach the exact solutions are guaranteed. Table 6.2 shows the numerical solution for the lumped-parameter model in evaluating the approximate frequencies.

The system eigenvalues of the lumped-parameter model are lower than the exact solutions calculated from the continuous model. The reason is that, although the total mass is the same in both systems, in the discrete model the mass is shifted toward the center of the system instead of being uniformly distributed (Meirovitch [19]). This tends to increase the effect of the system inertia relative to its stiffness, resulting in lower natural frequencies. Of course, accuracy can be improved by increasing the number of degrees of freedom of the lumped-discrete system.

It should be noted that when the friction forces are large, i.e., large value α in the equation of motion in (6.1) it is expected that the finite element method may be poor in accuracy. The argument is quite general. The Galerkin's approximate method may be unsatisfactory when the odd-derivative term is of significant size (Strang and Fix [121]). Since α strongly influences the eigenvalues and eigenfunctions in the PDE solution as $|\alpha|$ increases to ∞, the first order term dominates the second derivative, and the system model is a boundary-layer problem. Thus at the far end there should be a rapid variation in x in order to satisfy the boundary condition, and an extremely fine mesh is required to satisfy good approximations in such case. In this study extremely large values α of are excluded for good convergence.

6.2.3 Numerical Results

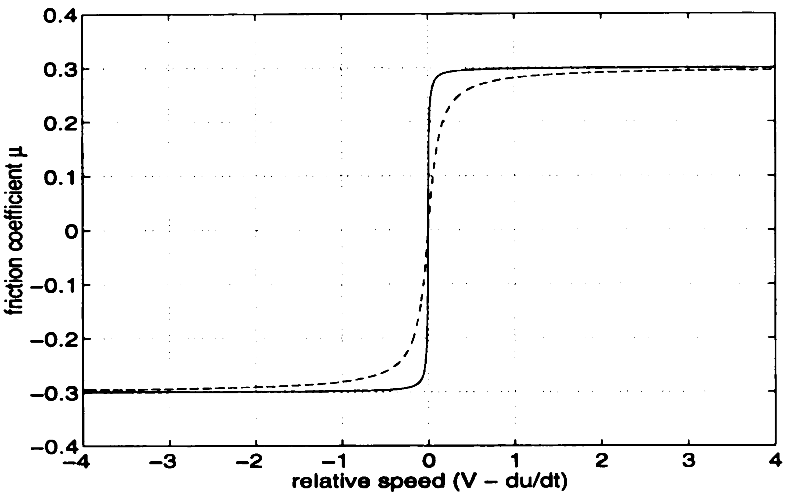

Figure 6.2. The friction coefficient versus relative velocity. $\mu = \text{sign}\,(V - \dot{u})\mu_k \frac{2}{\pi}\arctan(\frac{|V-\dot{u}|}{C})$, where $C = 0.1$ for dotted line and $C = 0.01$ for solid line.

In order to formulate and analyze the friction system we need to model the friction characteristics in a mathematical form. The friction function used in the previous chapter, which is a discontinuous function, may be inappropriate for finite element analysis. Instead of using the discontinuous friction function a smooth function having a steep variation of friction coefficient is usually adopted in finite element analysis. When we choose a steep slope and a small integration time step we can expect this smooth function can represent the discontinuous properties well. Strictly, stick-slip motion no longer exits, but approximate or near stick-slip behavior takes place (Feeny and Moon [107]). The analytical model for the friction coefficient used in this study is expressed as

$$\mu = \text{sign}(V - \dot{u}) \; \mu_k \frac{2}{\pi} \arctan(\frac{|V - \dot{u}|}{C}), \tag{6.9}$$

where the parameter C determines the slope of the dynamic friction coefficient at zero relative velocity. Figure 6.2 shows typical continuous friction model used in finite analysis. For a small value C a steep slope is generated around the relative velocity of zero. Thus a small integration time step is needed to satisfy the dynamics around near sticking conditions. For a large value C an gentle slope is generated, but near stick-slip dynamics may not be seen. In this study $C = 0.01$ and $\mu_k = 0.3$ are chosen.

The finite element meshes used in this analysis consist of twenty-four-node isoparametric quadratic elements, illustrated in Figure 6.1. The total simulation time is set as T = 0.005 sec, and iteration steps during the time are 5,000, which make the time step for the integration is set as $\Delta t = 1 \times 10^{-6}$ sec. The initial conditions applied to this numerical analysis are $u^i(t) = 0$, and $\dot{u}^i(t) = +1$ inch/sec for all nodes i.

In the presence of Poisson's ratio, in this study $\nu = 0.45$, the distributions of the friction forces, which are not symmetric along the nodes on contact, are shown in Figure 6.3. Since the near sticking motions are associated with the steep slope with respect to relative velocity, the friction forces around the sticking regions can have a value between $-|\mu_k \sigma_{22}|$ to $+|\mu_k \sigma_{22}|$, where the normal stress σ_{22} is not a constant, but a variable value. Higher friction forces are observed around the rear nodes than the front nodes. The friction forces traveling on the contact surface are observed like the sliding rubber mechanisms performed by Schallamach [26].

The axial strain ϵ_{11} changes the normal stress and also influences the friction forces since the system is under a constraint in y direction. The variations in axial stress σ_{11} are shown in Figure 6.4. The front and rear nodes are under tensile ($\sigma_{11} > 0$) and compressive ($\sigma_{11} < 0$) stress conditions, respectively. After the stick to slip transition the traveling stress waves propagate back and forth within the medium.

Figure 6.5 shows a velocity response of nodes 19. Since the friction model used in this simulation has identical static and dynamic friction coefficients ($\mu_s = \mu_k$), "pure sliding oscillations" are observed, which agrees with results obtained in the previous chapters. (See Figure 5.24 (a) for details.) Quasi-harmonic oscillations which carry high frequencies are observed. From the investigation by De Togni *et al.* [99] in the bushing-squeak system, similar oscillations, which have sawtooth waveforms, are detected in their experimental studies. Usually they have higher frequencies and smaller amplitudes in pure sliding oscillations than the stick-slip oscillations.

Figure 6.6 represents the friction force versus velocity presentations for various nodal responses. At velocity near +1 inch/sec, which represents the near sticking state, the steep slope in the friction characteristics is apparent. Since the normal forces are changed by displacements the friction forces exerted on each nodes are not only a velocity dependent, but also position dependent. Large friction forces are observed at rear nodes. Figure 6.7 shows the friction force versus displacement. After some transient motions, which are shown as sparse trajectories, each mass has steady state responses represented as dense trajectories. At node 35 the friction force increases as the displacement increases. On the other hand, at node 11 and 19 the friction forces are decreased linearly with respect to the displacement. At node 27 it apparently looks as if the friction forces are independent of the displacement, shown as flat trajectories. These phenomena result from the coupled effect of the Poisson's ratio between friction force and linear strains. These results are verified by the results in equation (2.2). Figure 6.8 shows the displacement and velocity relation for node 19. The results obtained in this study have qualitatively similar behaviors as those worked by Oden and Martins [117].

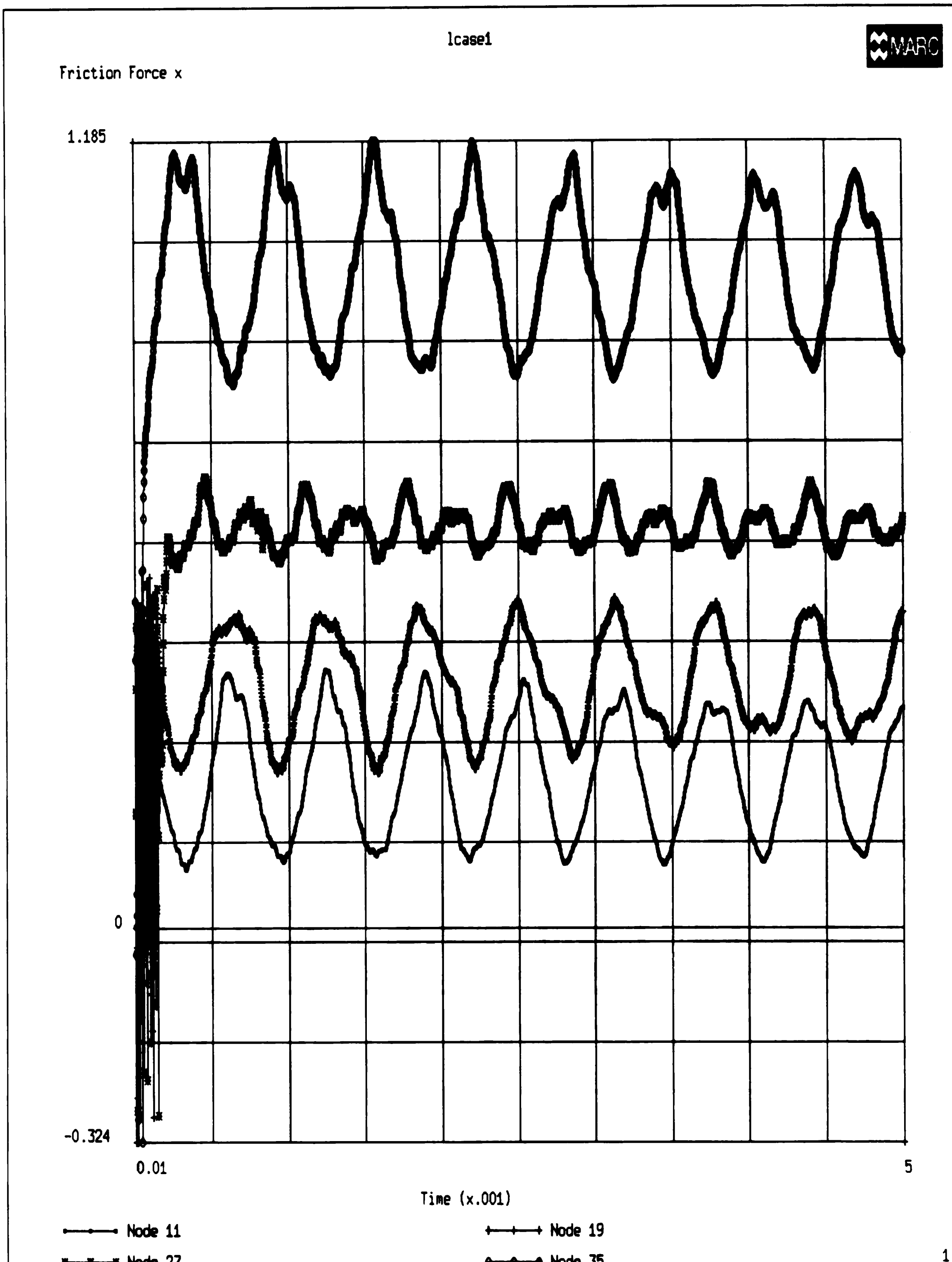

Figure 6.3. The distributions of friction forces versus time at nodes on contact.

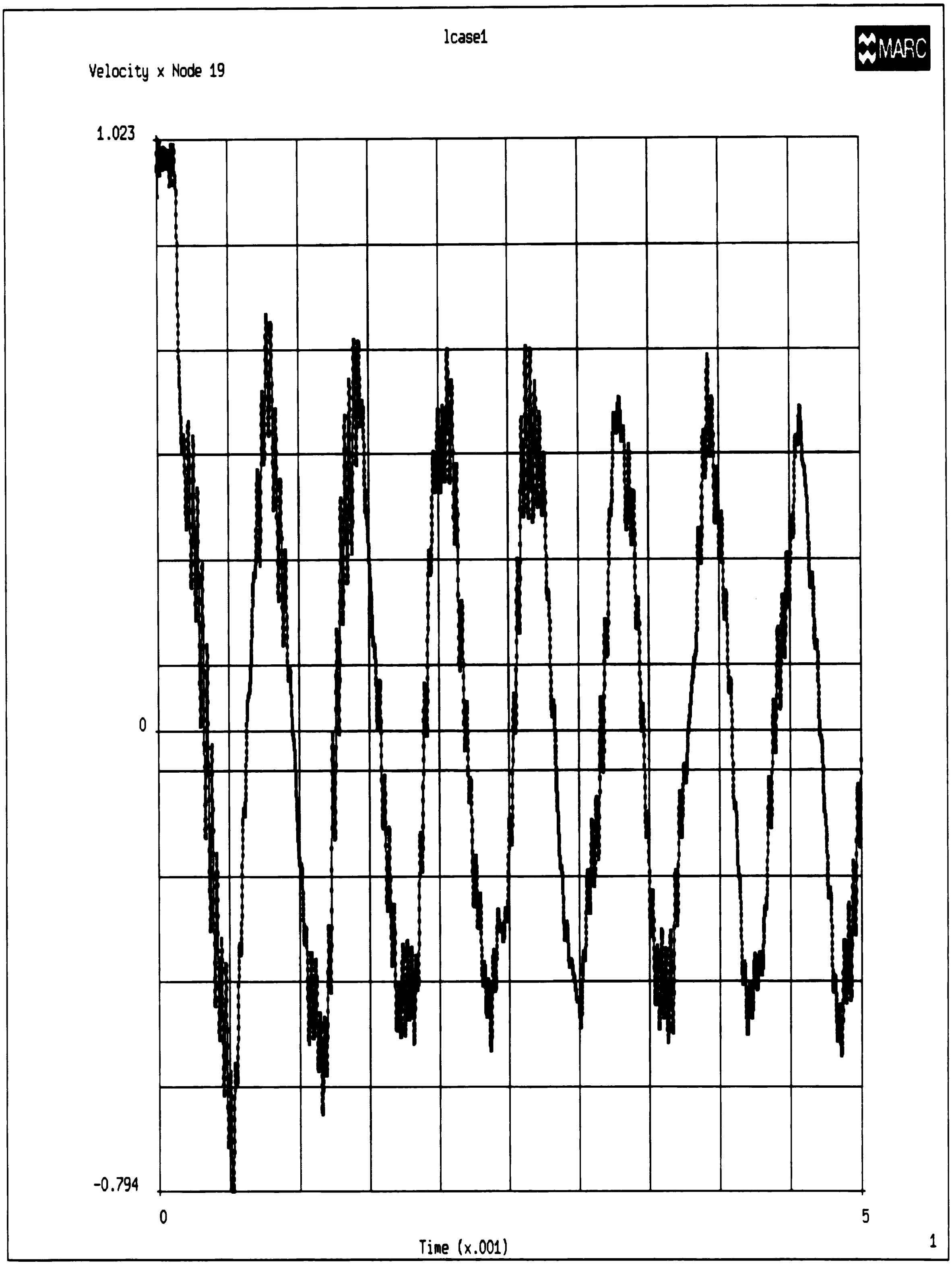

Figure 6.5. Velocity response at node 19.

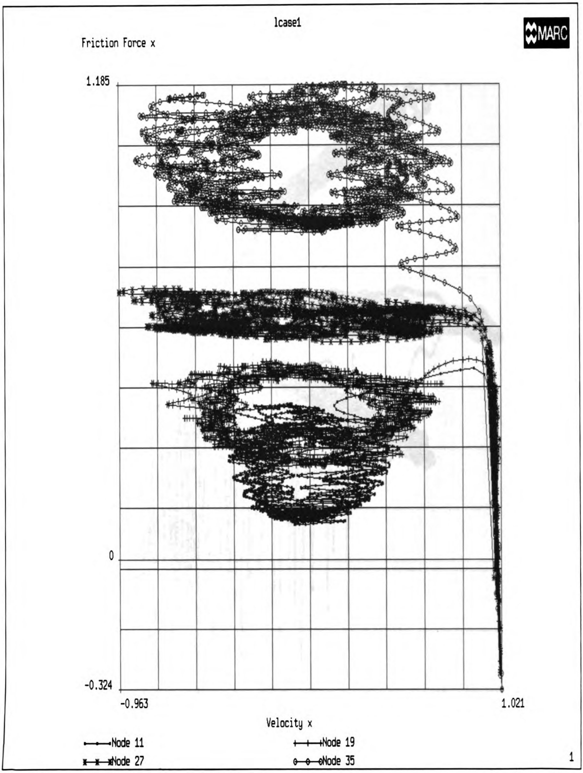

Figure 6.6. Friction force versus velocity at nodes 11, 19, 27, and 35.

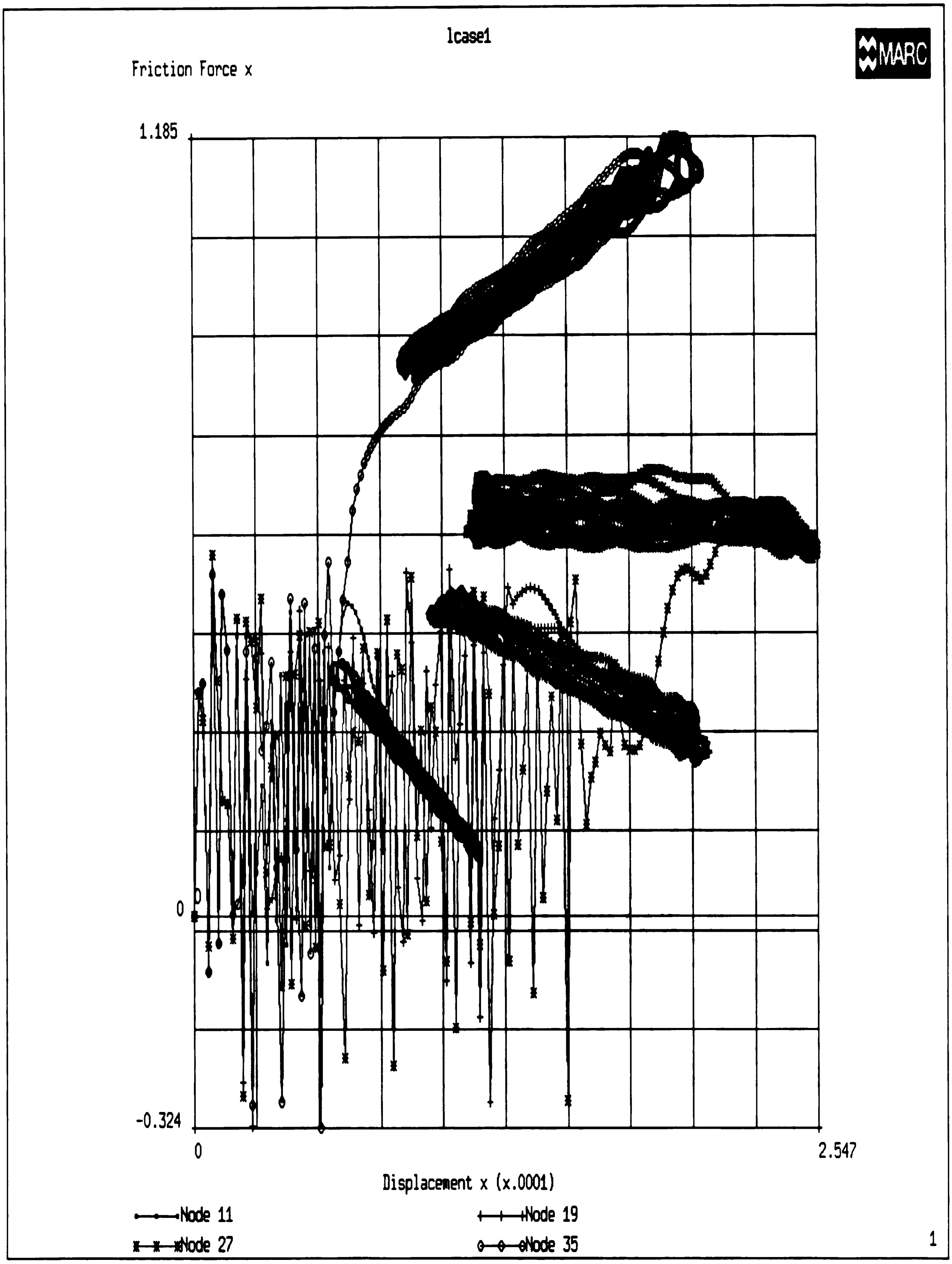

Figure 6.7. Friction force versus displacement at nodes 11, 19, 27, and 35.

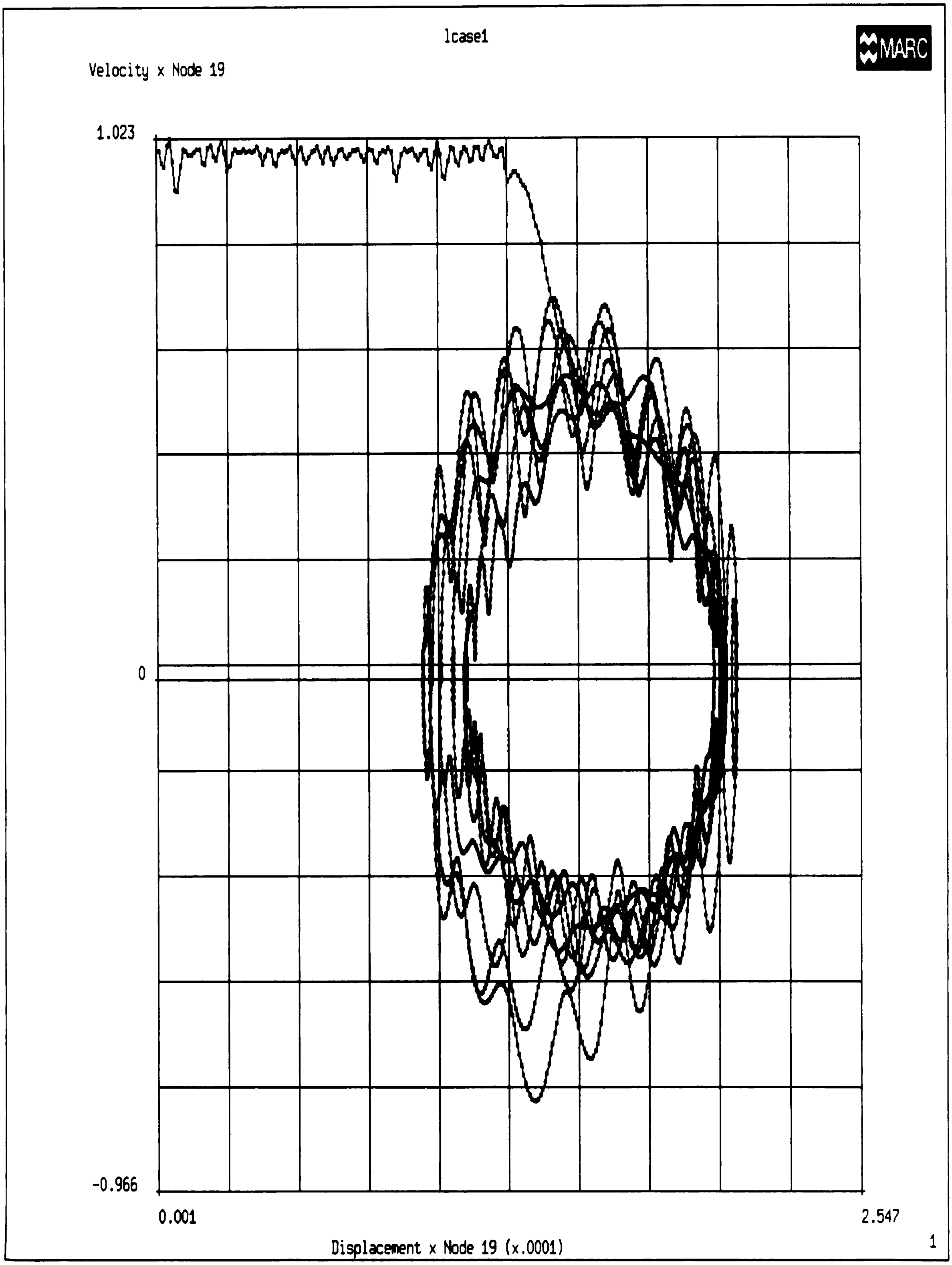

Figure 6.8. Displacement versus velocity at node 19.

6.3 Two-Dimensional System

We investigated the two-dimensional elastic model with periodic boundary conditions in Chapter 3. In this section a two-dimensional elastic medium under distributed contact with fixed boundaries is numerically investigated by applying finite element analysis.

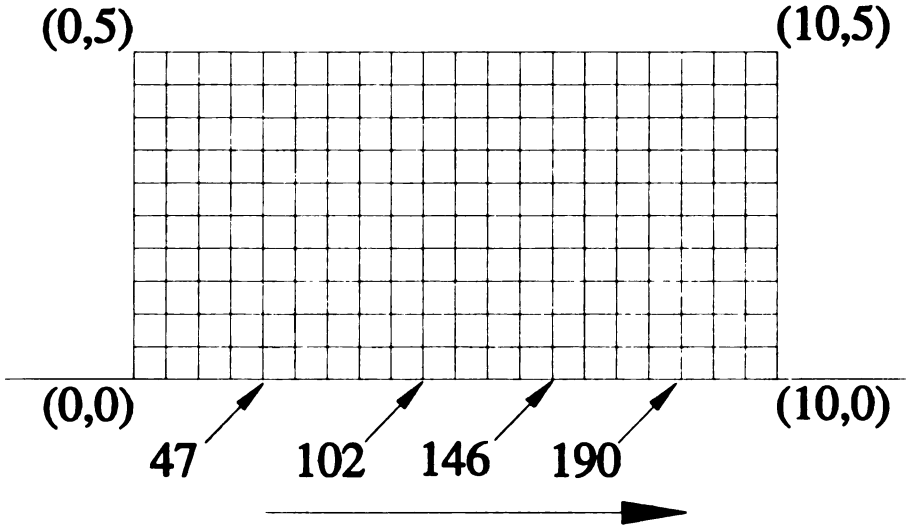

Figure 6.9. A schematic diagram for a two-dimensional elastic medium under distributed contact. The lower rigid body moves at 1 inch/sec to the positive x direction. Selected nodes are shown.

Figure 6.9 shows the schematic diagram for a meshed block. The polyethelen block with dimensions of 10 inches $\times$ 5 inches $\times$ 1 inch is divided into a 20 $\times$ 10 mesh. The lower rigid body moves toward to positive x direction at 1 inch/sec. Here front and rear nodes are defined the nodes positioned in the left- and right-hand sides, respectively. The govern equation of motions for the elastic medium are shown in equation (3.12). The boundary conditions are represented as

$$
\begin{aligned}
u(0,y) = u(10,y) = 0, &\quad \text{for } 0 < y < 5, \\
v(0,y) = v(10,y) = 0, &\quad \text{for } 0 < y < 5, \\
u(x,5) = 0, &\quad \text{for } 0 < x < 10, \\
v(x,5) = 0, &\quad \text{for } 0 < x < 10.
\end{aligned}
\tag{6.10}
$$

The boundary conditions on the contact surface at $y = 0$ are

$$
\begin{aligned}
v(x,0,t) &= 0, \\
\sigma_{yx}(x,0,t) &= \mu\sigma_{yy}(x,0,t),
\end{aligned}
\tag{6.11}
$$

where μ is a coefficient of friction, which is represented in Figure 6.2. The stress-strain relations are $\sigma_{yx} = G(\frac{\partial v}{\partial x} + \frac{\partial u}{\partial y})$, and $\sigma_{yy} = \lambda\frac{\partial u}{\partial x} + (\lambda + 2G)\frac{\partial v}{\partial y}$. (Stability analysis of this two-dimensional system in pure sliding motions will be a furture work.)

Given the sticking initial conditions for all contacting nodes at $y = 0$, the numerical integrations are performed by following the same procedures in the previous section with small time step of $\Delta t = 1 \times 10^{-6}$ sec.

Figures 6.10 shows that the axial stress distributions at specific nodes on contact. The nodes at 47 and 102 oscillate under tensile stresses and the nodes 146 and 190 are under the compressive stresses. Since in two-dimensional system we consider the normal directional motions and include that oscillations to the normal stress in equation (6.11), the system responses are more complicated and strongly coupled by the y-directional motions. The resultant friction forces are shown in Figure 6.11.

The stick-slip oscillations are onbserved in the two-dimensional system even under a condition with a constant coefficient of friction. They are easily expressed by state-space presentations, shown in Figure 6.12. The stick motions are shown as nearly flat trajectories in the state-space presentations. Based on the results of the one-dimensional system studied the previous section the nodes oscillate with quasi-harmonic pure sliding motions without having any stick-slip oscillations under a constant friction coefficient model.

The friction forces versus displacement are shown in Figure 6.13. The responses in friction-displacement are similar to the responses in one-dimensional system in Figure 6.7. However, in the two-dimensional model the variations of friction froces with displacement do not have constant slopes, but include normal oscillations. The importance of the normal vibrations in the stick-slip oscillations have been investigated by several researchers (Tolstoi [48], Sakamoto [49, 50], Tworzydlo and Becker [51], Tworzydlo *et al* [52], Pires and Oden [53]).

According to these numerical responses the near stick-slip oscillations can be observed in the two-dimensional model even under a constant coefficient of friction model.

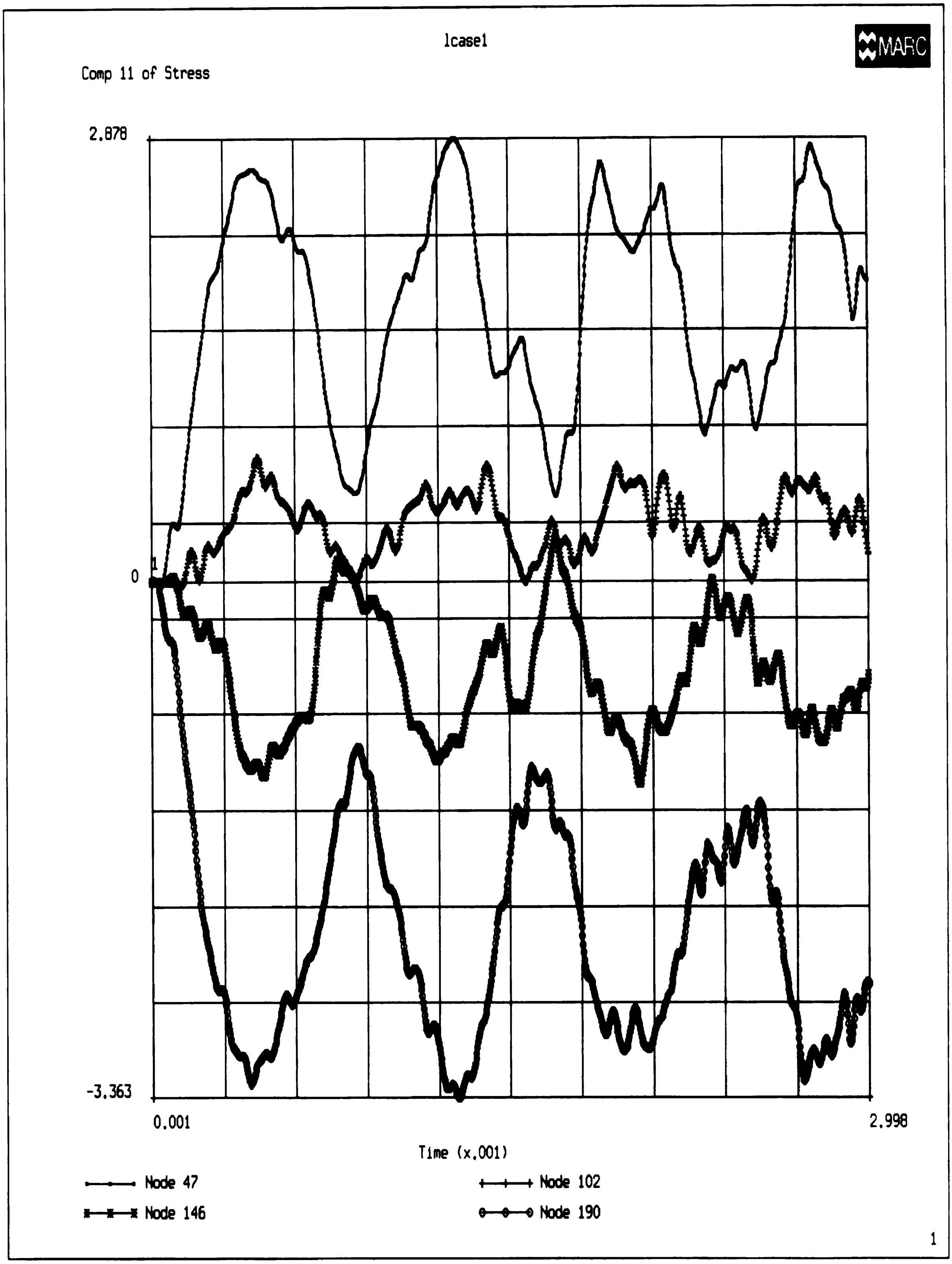

Figure 6.10. Stress distributions (σ_{11}) versus time for nodes at the contact.

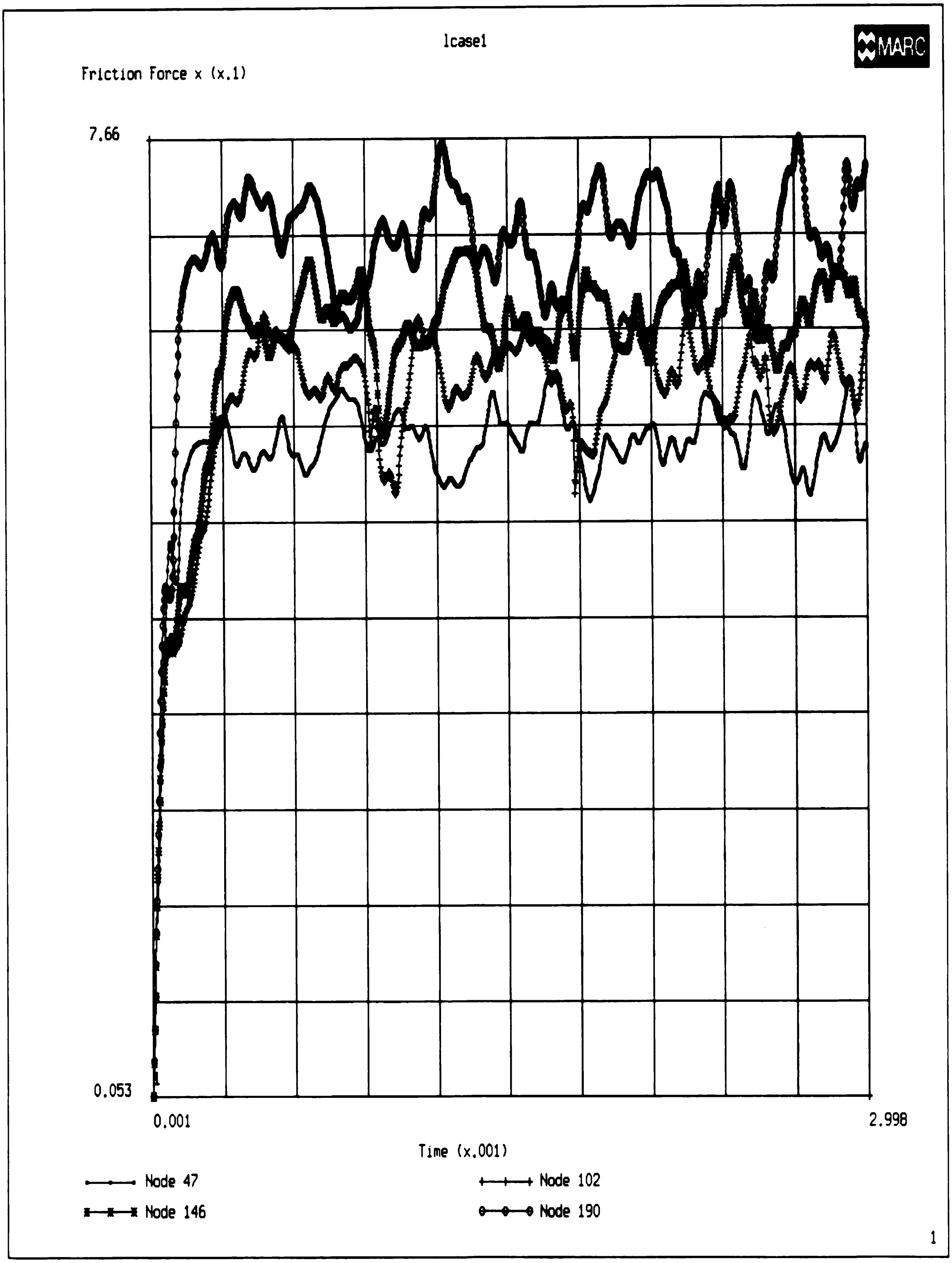

Figure 6.11. Friction forces versus time at nodes on contact.

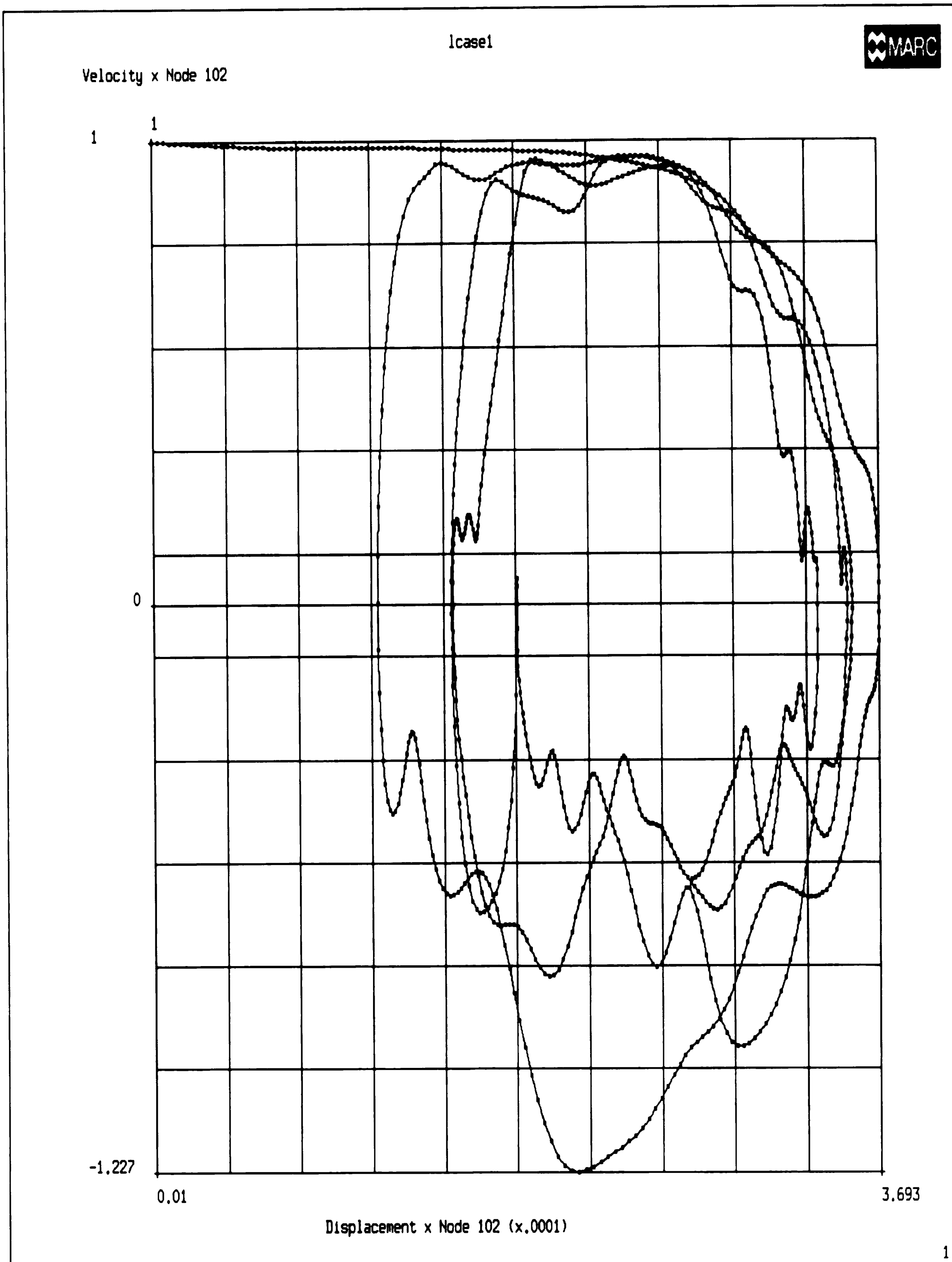

Figure 6.12. Displacement versus velocity at node 102.

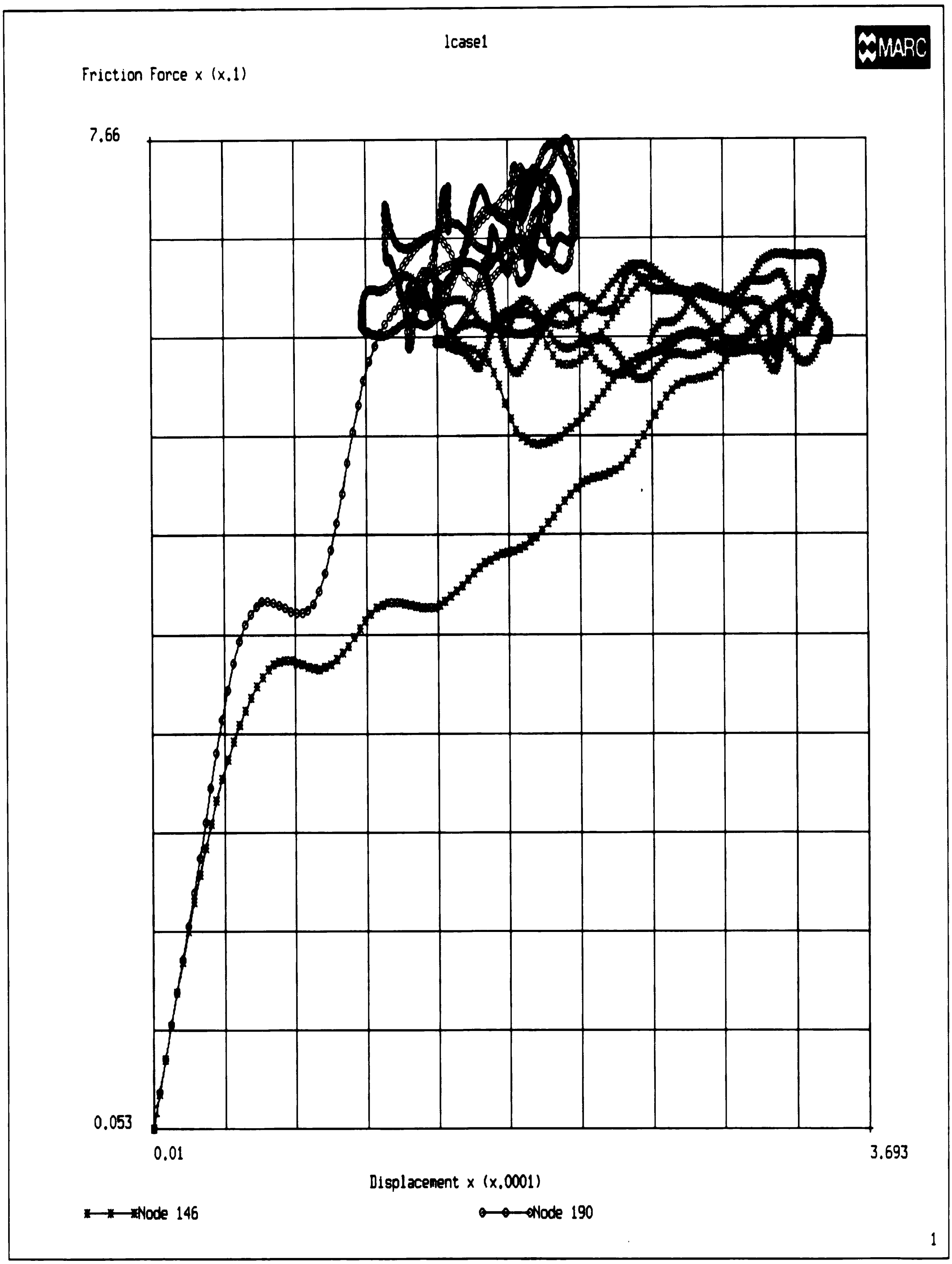

Figure 6.13. Friction force versus displacement at nodes 146 and 190.

6.4 Conclusion

In this chapter we investigated one- and two-dimensional elastic systems under the distributed frictional sliding contact by applying finite element analysis. The system eigenvalues were evaluated and compared to those obtained by the previous studies.

Numerical analyses show that the one-dimensional system undergoes pure sliding oscillations under the condition of same static and dynamic coefficient of friction ($\mu_s = \mu_k$). The relation between friction and displacement shows that the system has properties which depend not only on velocity but also on displacement. Such relations are determined by the Poisson's ratio and the positions of the nodes in the system. The stress and strain have the form of traveling waves in the continuum. In the continuous model the system undergoes quasi-harmonic oscillating motions including high frequency signals.

Through the finite element analysis we demonstrated the possible stick-slip oscillations in a two-dimensional system. According to this investigation it is possible to generate stick-slip oscillations in the two-dimensional system under a constant coefficient of friction condition due to oscillations in the normal degrees of freedom.

CHAPTER 7

CONCLUSIONS AND FUTURE WORKS

In order to investigate dynamic behaviors of an elastic medium under the distributed friction forces we constructed mathematical models and analyzed their dynamic stabilities. The stick-slip phenomena of friction-driven systems were investigated and verified by finite element analysis, lumped-parameter method, and modal projection method. This study yielded the some mechanisms responsible for vibrations, and presumably noise, in the elastic materials and revealed the instability mechanisms of the continuous system under distributed friction.

In Chapter 2, a continuous elastic medium with fixed boundary conditions subjected to the distributed friction was introduced, mathematically modeled, and its exact solutions were provided. The friction made the system non-self-adjoint. The approaches in handling such problems were provided as well. By using the adjoint operator the problem was treated properly. In addition, by projecting through the proper inner product the system was seen to truly be self-adjoint. A contradictory result between the exact solution and an assumed modes approximation in evaluating the eigenvalues was presented as a cautionary example. Consequently, under a constant coefficient of friction ($\mu_s = \mu_k$) the system was shown to be marginally stable. Thus an instability mechanism does not exist under the fixed boundary conditions.

In Chapter 3, the effect of boundary conditions on the system stability was examined. Under periodic boundary conditions the one-dimensional system was destabilized even under a constant friction ($\mu_s = \mu_k$). The destabilizing phenomenon occurred in the form of an unstable traveling wave propagating in the direction of the slider velocity. The effect of internal and external damping were evaluated and they played stabilizing roles in the overall system stability. For a two-dimensional system under periodic boundary conditions the system was destabilized under a condition of a constant coefficient of friction when the system coordinates are strongly coupled by Poisson's effect.

In Chapter 4, the lumped-parameter method was applied to discretize the continuous model which was investigated in the previous chapters. It was shown that the system stability was closely related to the friction characteristics. The negative slope in the friction-velocity curve had a destabilizing effect. By using the lumped-parameter model the previous investigations were verified. Internal and external damping were also proven to be stabilizing factors. Based on consistent results from the lumped-parameter system it was verified that the lumped parameter model provided a convergent discretization.

In Chapter 5, by using the lumped-parameter model which was analyzed in the previous chapter, the stick-slip oscillations under the distributed contact were investigated. For a background study the numerical algorithm for solving the nonlinear stick-slip oscillations of the multi-degree-of-freedom model was provided. Using the typical stick-slip responses the system dynamic characteristics were explained. Stick-slip motions were observed in the form of propagating waves of detachments. The analyses based on the velocity and displacement data were provided. We observed two distinct motions in the stick-slip oscillations: the series of detachment waves sweeping over the whole domain and small-grouped localized stick-slip motions. The detachment waves were ground for the low-frequencies stick-slip oscillations generated on the contact surface. The small-grouped localized stick-slip motions influenced the high frequencies of stick-slip oscillations. Several parameter effects on the stick-slip motions were evaluated. Under high normal loads the frequencies of the sweeping detachment waves were lowered. In addition, high-frequency small-grouped motions prevailed. The high Poisson's ratio increased the natural frequencies of the linear system and stick-slip frequencies as well. It was shown that the Poisson's ratio breaks the symmetry in the stick-slip motions and amplified the irregularity over the stick-slip motions. It was proved that the driving speed was closely related to amplitudes of stick-slip oscillations. The friction characteristics, which had a primary effect on stick-slip motions, were considered. It was observed that the steady state stick-slip oscillations were prevalent when the system is linearly unstable. It is also shown that the system having a discontinuous friction model ($\mu_s > \mu_k$) generates steady state stick-slip oscillations. By applying the modal projection method a possible alternative method in handling the low-dimensional stick-slip oscillations was proposed. The sustained stick-slip oscillations were observed as series of detachments in the busing system.

In Chapter 6, by adopting the finite element analysis the continuous system under distributed friction was numerically analyzed. In case of $\mu_s = \mu_k$, the one-dimensional system underwent steady state pure slipping motions with quasi-harmonic oscillations. On the other hand, for the two-dimensional system it was possible to sustain the stick-slip oscillations even under the $\mu_s = \mu_k$ condition. The influence of the normal directional motions on the stick-slip oscillations were presented .

Conclusions related to the bushing system are listed as follows. Under periodic boundary conditions the bushing system was unstable even with a constant friction coefficient due to the unstable traveling waves (Chapter 3). In addition, the negative slope in friction-speed relation destabilized the system (Chapter 4). The instability led to nonlinear stick-slip oscillations, observed as series of detachments (Chapter 5). Coordinates couplings of the two-dimensional elastic system induced stick-slip oscillations even with a constant coefficient of friction (Chapter 6). These results were verified through the lumped-parameter method (Chapters 4 and 5), the modal projection method (Chapter 5), and finite element analysis (Chapter 6) along with the exact solution (Chapter 2).

The analytical and numerical investigation in this dissertation dealt with complicated friction-induced vibration phenomena. Listed below are the additional specific problems to be investigated in future, which include analytical, numerical, and experimental studies.

- **Material and Friction related Issues**

  In this investigation there is an assumption that the material has linear properties. However under high normal loads the elastic material can undergoes relatively large amplitude stick-slip oscillations. In such case the large oscillations may not result from the linear material properties. The nonlinear material properties in stick-slip oscillations need to be investigated for the one- and two-dimensional systems. When we consider finite radius bushing models coupling effects between radial and circumferential motions need to be investigated.

  All materials have roughness on the surface. Especially in an elastic material, such as rubber, the system roughness and noise generation are closely related (Soom and Kim [42, 43]). Thus including the contact surface roughness is required in the system modeling for more accurate analysis.

  For friction related issues, it has been reported from the experimental studies that the friction force is not a single function dependent on relative velocities. It has hysteresis effects caused from the material intrinsic properties (Martins *et al.*[118]). Moreover friction models including the properties dependent on the load and displacement need to be investigated (Dweib and D'Souza [55, 56]).

  When the friction is involved heat is generated on the contact surface. In real operating conditions huge amounts of heat can not be neglected in system modeling. The system analysis based on the friction-heat relations need to be investigated (Nakai and Yokoi [72]).

- **Load and Boundary Condition related Issues**

It has been reported that when friction is involved, results may not be repeatable even under apparently the same conditions. As investigated by Dweib and D'Souza [56] geometrical misalignments can generate unpredictable results and small mistunings can produce undesirable noise (Bhushan [73]). Sometimes evenly distributed load conditions can not implemented in real situations. In the bushing system uneven load conditions may occur in some operating conditions due to a thrust force on the rotating bar. Effects including uneven loads and external periodic forcing on a system stability need to be investigated.

Stability analysis of pure sliding motions for a two-dimensional elastic system with fixed ends boundary conditions (the model studied in Chapter 6) remains as a future work.

- **System Analysis and Characterization**

  This dissertation has been devoted to the system analysis through analytical and numerical approaches. Experimental verifications should be conducted. However there may be difficulties in sensing the motions and handling huge data sets from the continuous elastic media. The challenging part of the experimental studies would be presentations of motions of the materials caused by the stick-slip oscillations. The finite element analysis including issues described above will also be needed in numerical approaches. The characteristic behaviors of such non-linear phenomena, for example a relation between large fluctuations in slipping group size and spatial self-similarity, called as self-organized criticality (Carlson and Langer [97, 98]), would be a great challenge in analysis of stick-slip oscillations induced by friction.

BIBLIOGRAPHY

BIBLIOGRAPHY

[1] L. Meirovitch and M.K. Kwak 1990 *AIAA Journal* **28**(8), 1509-1516. Convergence of the classical Rayleigh-Rits method and the finite element method.

[2] L. Meirovitch, P. Hagedorn 1994 *Journal of Sound and Vibration* **178**(2), 227-241. A new approach to the modeling of distributed non-self-adjoint systems.

[3] P. Hagedorn 1993 *Journal of Vibration and Acoustics* **115**, 280-284. The Rayleigh-Ritz method with quasi-comparison functions in nonself-adjoint problems.

[4] S.N. Prasad, G. Herrmann 1972 *Int. Journal of Solids Structures* **8**, 29-40. Adjoint variational methods in nonconservative stability problems.

[5] P. Pedersen, A.P. Seyranian 1983 *Int. Journal of Solids Structures* **19**(4), 315-335. Sensitivity analysis for problems of dynamic stability.

[6] R.C. Diprima, R. Sani 1965 *Q. Appli. Math.* **23**, 183-187. The convergence of the Galerkin's method for the Taylor-Dean stability problem.

[7] L.V. Kantorovich and V.I. Krylov 1958 *Approximate Methods of Higher Analysis.* Interscience Publishers, Inc.

[8] E.H. Dowell, H.C. Curtiss Jr., R.H. Scanlan, and F. Sisto 1989 *A Modern Course in Aeroelasticity*, Kluwer Academic Publishers.

[9] K. Higuchi and E.H. Dowell 1989 *Journal of Sound and Vibration* **129**(2), 255-269. Effects of the Poisson ratio and negative thrust on the dynamic stability of a free plate subjected to a follower force.

[10] K. Higuchi and E.H. Dowell 1990 *AIAA Journal* **28**(7), 1300-1305. Dynamic stability of a rectangular plate with four free edges subjected to a follower force.

[11] G. Herrmann and R.W Bungay 1964 *Journal of Applied Mechanics*, 435-440. On the stability of elastic systems subjected to Nonconservative forces.

[12] G. Herrmann and I.C. Jong 1965 *Journal of Applied Mechanics*, 592-597. On the destabilizing effect of damping in nonconservative elastic system.

[13] A.P. Seyranian, P. Pedersen 1993 *ASME Dynamics and Vibration of Time-Varying system and Structures*, 19-31. On interaction of eigenvalue branched in non-conservative multi-parameter problems.

[14] P.B. Beda 1997 *European Journal of Mechanics and Solids* **16**(3), 501-513. Material instability in dynamical systems.

[15] R.H. Plaut 1972 *AIAA Journal Technical Notes*, 967-968. Determining the nature of instability in nonconservative problems.

[16] V.V. Bolotin 1963 *Nonconservative Problems of the Theory of Elastic Stability.* Pergamon Press, Inc.

[17] H. Ziegler 1968 *Principles of Structural Stability.* Blaisdell Publishing Company.

[18] L. Meirovitch 1980 *Computational Methods in Structural Dynamics.* Sijthoff & Noordhoff.

[19] L. Meirovitch 1986 *Elements of Vibration Analysis.* McGraw-Hill Company.

[20] C.R. MacCluer 1994 *Boundary Value Problems and Orthogonal Expansions.* IEEE press.

[21] H. Hochstadt 1963 *Differential Equations.* Dover.

[22] D.L. Powers 1987 *Boundary Value Problems.* Saunders College Publishing.

[23] G.G. Adams 1995 *Journal of Applied Mechanics* **62**, 867-872. Self-excited oscillations of two elastic half-spaces sliding with a constant coefficient of friction.

[24] G.G. Adams 1996 *Journal of Tribology* **118**, 819-823. Self-excited oscillations in sliding with a constant friction coefficient—a simple model.

[25] J.A.C. Martins, L.O. Faria, and J. Guimaraes 1992 *Friction-Induced Vibration, Chatter, Squeal and Chaos, ASME* DE-Vol.49, 33-39. Dynamic surface solutions in linear elasticity with frictional boundary conditions.

[26] A. Schallamach 1971 *Wear* **17**, 301-312. How does rubber slide?

[27] B. Best, P. Meijers and A.R. Savkoor 1981 *Wear* **65**, 385-396. The formation of Schallamach waves.

[28] M. Comninou and J. Dundurs 1977 *Journal of Applied Mechanics*, 222-226. Elastic interface waves involving separation.

[29] D.M. Barnett, S.D. Gavazza, and J. Lothe 1988 *Proc. Royal Society of London* A**415**, 389-419. Slip waves along the interface between two anisotropic elastic half-spaces in sliding contact.

[30] R. Stoneley 1924 *Proceedings of the Royal Society of London* Vol.106, 416-428. Elastic waves at the surface of separation of two solids.

[31] V.A. Palmov, E. Bronmmundt, and A.K. Belyaev 1995 *Dynamics and Stability of Systems* **10**(2), 99-110. Stability analysis of drillstring rotation.

[32] A.K. Belyaev, E. Brommundt 1994 *ZAMM* **74**(4), T53-T55. Influence of the motor and bit characteristics on the stability of drilling rotation.

[33] D.W. Dareing and B.J. Livesay 1968 *Journal of Engineering for Industry*, 671-679. Longitudinal and angular drillstring vibrations with damping.

[34] P.R. Paslay and D.B. Bogy 1963 *Journal of Engineering for Industry* **85**, 187-194. Drill string vibrations due to intermittent contact of bit teeth.

[35] R. Dawson, Y.Q. Lin, P.D. Spanos 1987 *Proceedings of the 1987 SEM Spring Conference on Experimental Mechanics*, 590-595. Drill string stick-slip oscillations.

[36] A.S. Saada 1974 *Elasticity.* Pergamon Press Inc.

[37] Y.C. Fung 1965 *Foundation of Solid Mechanics.* Prentice-Hall Inc.

[38] S.L. Hendricks 1986 *Journal of Applied Mechanics* Vol. 53, 412-416. The effect of viscoelasticity on the vibration of a rotor.

[39] J. Shaw and S.W. Shaw 1989 *Journal of Sound and Vibration* **132**(2), 227-244. Instabilities and bifurcations in a rotating shaft.

[40] D.P Hess and A. Soom 1992 *Journal of Tribology* Vol. 114, 567-578. Normal and angular motions at rough planar contacts during sliding with friction.

[41] A. Soom and J.W. Chen 1986 *Journal of Tribology* **108**, 123-127. Simulation of random surface roughness-induced contact vibrations at Hertzian contacts during steady sliding.

[42] A. Soom and C. Kim 1983 *Journal of Lubrication Technology* **105**, 514-517. Roughness-induced dynamic loading at dry and boundary lubricated sliding contacts.

[43] A. Soom and C. Kim 1983 *Journal of Lubrication Technology* **105**, 221-229. Interaction between dynamic normal and frictional forces during unlubricated sliding.

[44] J.T. Oden and E.B. Pires 1983 *Journal of Applied Mechanics* **50**, 67-76. Nonlocal and nonlinear friction laws and variational principles for contact problems in elasticity.

[45] C. Gao, D. Kuhlmann-Wilsdorf and D. Makel 1993 *Wear* **162-164**, 1139-1149. Fundamentals of stick-slip.

[46] C. Gao, D. Kuhlmann-Wilsdorf and D. Makel 1994 *Wear* **173**, 1-12. The dynamic analysis of stick-slip motion.

[47] S.S. Antoniou, A. Cameron and C.R. Gentle 1976 *Wear* **36**, 235-254. The friction-speed relation from stick-slip data.

[48] D.M. Tolstoi 1967 *Wear* **10**, 199-213. Significant of the normal degree of freedom and natural normal vibrations in contact friction.

[49] T. Sakamoto 1985 *Proceedings of the JSLE International Tribology Conference*, 141-146. Normal displacement of the sliding body in a stick-slip friction process.

[50] T. Sakamoto 1987 *Tribology International* **20**(1), 25-31. Normal displacement and dynamic friction characteristics in a stick-slip process.

[51] W.W. Tworzydlo and E. Becker 1991 *Wear* **143**, 175-196. Influence of forced vibrations on the static coefficient of friction—numerical modeling.

[52] W.W. Tworzydlo, E.B. Becker and J.T. Oden 1992 *Friction-Induced Vibration, Chatter, Squeal and Chaos, ASME*, 13-32. Numerical modeling of friction-induced vibrations and dynamic instabilities.

[53] E.B. Pires and J.T. Oden 1983 *Computer Methods in Applied Mechanics and Engineering* **39**, 337-362. Analysis of contact problems with friction under oscillating loads.

[54] Y. Ichiba and Y. Nagasawa 1993 *SAE paper 930802.* Experimental study on disc brake squeal.

[55] A.H. Dweib and A.F. D'Souza 1990 *Journal of Sound and Vibration* **137**(2), 163-175. Self-excited vibrations induced by dry friction, Part 1: Experimental study.

[56] A.H. Dweib and A.F. D'Souza 1990 *Journal of Sound and Vibration* **137**(2), 163-175. Self-excited vibrations induced by dry friction, Part 2: Stability and limit cycle analysis.

[57] M. Nakai and M, Yokoi 1996 *Journal of Vibration and Acoustics* **118**, 190-197. Band Brake Squeal.

[58] J. Hulten 1995 *SAE paper 951280.* Some drum brake squeal mechanisms.

[59] A.G. Ulsoy, C.D. Mote Jr. 1982 *Journal of Engineering for Industry* **104**, 71-78. Vibration of wide band saw blades.

[60] H.A. Sherif 1993 *SAE paper 933072.* Geometric induced instability in drum brake.

[61] V. Arnov, A.F. D'Souza, S. Kaplakjan and I. Shareef 1983 *Journal of Lubrication Technology* Vol. 105, 206-211. Experimental investigation of the effect of system rigidity on wear and friction-induced vibrations.

[62] V. Arnov, A.F. D'Souza, S. Kaplakjan and I. Shareef 1984 *Journal of Tribology* 54-58. Interactions among friction, wear and system stiffness, Part 1.

[63] V. Arnov, A.F. D'Souza, S. Kaplakjan and I. Shareef 1984 *Journal of Tribology* 59-64. Interactions among friction, wear and system stiffness, Part 2.

[64] V. Arnov, A.F. D'Souza, S. Kaplakjan and I. Shareef 1984 *Journal of Tribology* 65-69. Interactions among friction, wear and system stiffness, Part 3.

[65] C.A. Brockley, R. Cameron, A.F. Potter 1967 *Journal of Lubrication Technology* 101-108. Friction-induced vibration.

[66] C.A. Brockley, P.L. Ko 1970 *Journal of Lubrication Technology*, 551-556. Quasi-harmonic friction-induced vibration.

[67] G. Cockerham and G.R. Symmons 1976 *Wear* **40**, 113-120. Stability criterion for stick-slip motion using a discontinuous dynamic friction model.

[68] T. Majewski 1986 *Journal of Sound and Vibration* **105**(1), 17-25. Audio signal modulation caused by self-excited vibrations of magnetic tape.

[69] T.V. Friesen 1982 *SAE paper 831318.* Chatter in wet brakes.

[70] M.K. Abdelhamid 1995 *SAE paper 95128.* Structural instability test/analysis of brake squeal.

[71] R.J. Black 1995 *Design Engineering Technical Conferences, ASME* **3**A. Self excited multi-mode vibrations of aircraft brakes with nonlinear negative damping.

[72] M. Nakai and M. Yokoi 1990 *Japanese Journal of Tribology* **35**(5), 513-522. Generation mechanism of friction noises in dry friction.

[73] B. Bhushan 1980 *Journal of Lubrication Technology* Vol.102, 201-212. Stick slip induced noise generation in water-lubricated compliant rubber bearings.

[74] T.A. Simpson 1996 *Journal of Vibration and Control* **2**, 87-113. Nonlinear friction-induced vibration in water-lubricated bearings.

[75] A.I. Krauter 1981 *Journal of Lubrication Technology* Vol.103, 406-413. Generation of squeal/chatter in water-lubricated elastomeric bearings.

[76] W.D. Iwan and K.L. Stahl 1973 *Journal of Applied Mechanics*, 445-451. The response of an elastic disk with a moving mass system.

[77] W.D Iwan and T.L. Moeller 1976 *Journal of Applied Mechanics*, 485-490. The stability of a spinning elastic disk with a transverse load system.

[78] K. Popp and P. Stelter 1989 *Nonlinear Dynamics in Engineering Systems, IUTAM Symposium Stuttgart/ Germany*, 233-240. Nonlinear oscillations of structures induced by dry friction.

[79] K. Popp 1992 *Friction-Induced Vibration, Chatter, Squeal, and Chaos, ASME* DE-Vol. 49, 1-12. Some model problems showing stick-slip motion and chaos.

[80] H.I. You and J.H. Hsia 1995 *Journal of Tribology* **117**, 450-455. The influence of friction-speed relation on the occurrence of stick-slip motion.

[81] G. Capone, V. D'Agostino, S.D. Valle and D. Giuda 1992 *Meccanica* **27**, 111-118. Stick-slip instability analysis.

[82] L.C. Bo and D. Pavelescu 1982 *Wear* **8**, 277-289. The friction-speed relation and its influence on the critical velocity of stick-slip motion.

[83] A.K. Banerjee 1968 *Wear* **12**, 107-116. Influence of kinetic friction on the critical velocity of stick-slip motion.

[84] N. Hinrichs, M. Oestreich and K. Popp 1996 *EUROMECH 2nd European Nonlinear Oscillation Conference*, 191-194. Dynamics of a nonsmooth friction oscillator: Comparison of numerical and experimental results.

[85] P. Stelter and W. Sextro 1991 *International Series of Numerical Mathematics* Vol.97, 343-347. Bifurcations in dynamic systems with dry friction.

[86] U. Galvanetto, S.R. Bishop and L. Briseghella 1994 *International Journal of Mechanical Science* **36**(8), 683-698. Stick-slip vibrations of a two degree-of-freedom geophysical fault model.

[87] U. Galvanetto, S.R. Bishop and L. Briseghella 1995 *International Journal of Bifurcation and Chaos* **5**(3), 637-651. Mechanical stick-slip vibrations.

[88] J. Huang and D.L. Turcotte 1990 *Nature* Vol.348, **15**, 234-236. Evidence for chaotic fault interactions in the seismicity of the San Adreas fault and Nankai trough.

[89] J. Awrejcewicz and J. Delfs 1990 *European Journal of Mechanics and Solids* **9**(4), 269-282. Dynamics of a self-excited stick-slip oscillator with two degree of freedom, Part 1.

[90] J. Awrejcewicz and J. Delfs 1990 *European Journal of Mechanics and Solids* **9**(5), 397-418. Dynamics of a self-excited stick-slip oscillator with two degree of freedom, Part 2.

[91] F. Pfeiffer and M. Hajek 1992 *Phil. Trans. R. Soc. Lond. A* **338**, 503-517. Stick-slip motion of turbine blade dampers.

[92] J. C. Schelleng 1973 *Journal of the Acoustical Society of America* **53**(1), 26-41. The bowed string and the player.

[93] R.A. Ibrahim 1992 *Friction-Induced Vibration, Chatter, Squeal and Chaos, ASME*, 107-121. Friction-induced vibration, chatter, squeal and chaos: part1 mechanics of friction.

[94] R.A. Ibrahim 1992 *Friction-Induced Vibration, Chatter, Squeal and Chaos, ASME*, 123-136. Friction-induced vibration, chatter, squeal and chaos: part2 mechanics of friction.

[95] H. Takayasu and M. Matsuzaki 1988 *Physics Letters* Vol.131, No.4,5, 244-247. Dynamical phase transition in threshold elements.

[96] J.M. Carlson, J.S. Langer, B.E. Shaw and C. Tang 1991 *Physical Review A* **44**(2), 884-897. Intrinsic properties of a Burridge-Knopoff model of an earthquake fault.

[97] J.M. Carlson and J.S. Langer 1989 *Physical Review A* **40**(11), 6470-6484. Mechanical model of an earthquake fault.

[98] J.M. Carlson and J.S. Langer 1989 *Physical Review Letters* **62**(22), 2632-2635. Properties of earthquakes generated by fault dynamics.

[99] R.S. De Togni, N.S. Eiss. Jr, and R.A.L Rorrer 1992 *Wear and Friction of Elastomers, ASTM*, 30-49. The role of system dynamics on the behavior of elastomeric friction.

[100] R.A.L Rorrer, N.S. Eiss Jr., and R.S. De Togni 1992 *Wear and Friction of Elastomers*, 50-64. Measurement of frictional stick-slip transitions for various elastomeric materials sliding against hard conunterfaces.

[101] D.P. Vallette and J.P. Gollub 1993 *Physical Review E* **47**(2), 820-827. Spatiotemporal dynamics due to stick-slip friction in an elastic membrane system.

[102] J.P.D. Hartog 1930 *Transactions of the ASME* **53**, 107-115. Forced vibrations with combined coulomb and viscous friction.

[103] G.C.K. Yeh 1966 *Journal of the Acoustical Society of America* **39**, 14-24. Forced vibrations of a two degree of freedom system with combined Coulomb and viscous damping.

[104] M.S. Hundal 1979 *Journal of Sound and Vibration* **64**(3), 371-378. Response of a base excited system with coulomb and viscous friction.

[105] S.W. Shaw 1986 *Journal of Sound and Vibration* **108**(2), 305-325. On the dynamic response of a system with dry friction.

[106] B.F. Feeny 1992 *Physica D* 59, 25-38. A nonsmooth Coulomb friction oscillator.

[107] B.F. Feeny and F.C. Moon 1994 *Journal of Sound and Vibration* **170**(3), 303-323. Chaos in a forced dry-friction oscillator : Experiments and numerical modeling.

[108] B.F. Feeny and J.W. Liang 1995 *Design Engineering Technical Conferences ASME* DE-Vol 84-1, Vol. 3 - Part A, 1049-1059. Phase-space reconstructions of stick-slip systems.

[109] J.W. Liang and B.F. Feeny 1995 *Design Engineering Technical Conferences ASME* DE-Vol.84-1, Vol.3-Part A, 1061-1115. Wavelet analysis of stick-slip in an oscillator with dry friction.

[110] T.K. Pratt and R. Williams 1981 *Journal of Sound and Vibration* **74**(4), 531-542. Non-linear analysis of stick/slip motion.

[111] F. Pfeiffer 1991 *ZAMM* **71**(4), T6-T22. Dynamical systems with time-varying of unsteady structure.

[112] F. Pfeiffer, C. Glocker 1992 *Friction-Induced Vibration, Chatter, Squeal and Chaos, ASME* 65-74. Dynamical system with unsteady process.

[113] C. Glocker and F. Pfeiffer 1992 *Nonlinear Dynamics* **3**, 245-259. Dynamical system with unilateral contacts.

[114] M. Wösle, F. Pfeiffer 1996 *Journal of Vibration and Control* **2**, 161-192. Dynamics of multibody system containing dependent unilateral constraints with friction.

[115] E. Schneider and K. Popp 1988 *Journal of Sound and Vibration* **120**(2), 227-244. Noise generation in railway wheels due to rail-wheel contact forces.

[116] N. Okamoto and M. Nakazawa 1979 *International Journal for Numerical Methods in Engineering* Vol.14, 337-357. Finite element incremental contact analysis with various frictional conditions.

[117] J.T. Oden and J.A.C. Martins 1985 *Computer Methods in Applied Mechanics and Engineering* **52**, 527-634. Models and Computational Methods for Dynamic Friction Phenomena.

[118] J.A.C Martins, J.T. Oden and F.M.F. Simoes 1990 *International Journal of Engineering Science* Vol.28, No.1, 29-92. A study of static and kinetic friction.

[119] T.D. Marusich and M. Ortiz 1995 *Manufacturing Science and Engineering ASME* MED-Vol.2-1/MH-Vol.3-1, 245-258, A finite element study of chip formation in high-speed machining.

[120] MARC Analysis Research Corporation 1997 *MARC/MENTAT Training Guide.* Part Number: CN-3302-04.

[121] G. Strang and G. Fix 1973 *An Analysis of the Finite Element Method.* Prentice-Hall, Inc.